Bayesian Compressive Sensing For Radar Based DoA Estimation Using Sparse Sensor Arrays

Master Thesis

Lucas L. Lamberti

TU Delft

MS3 Microwave Sensing Signals & Systems

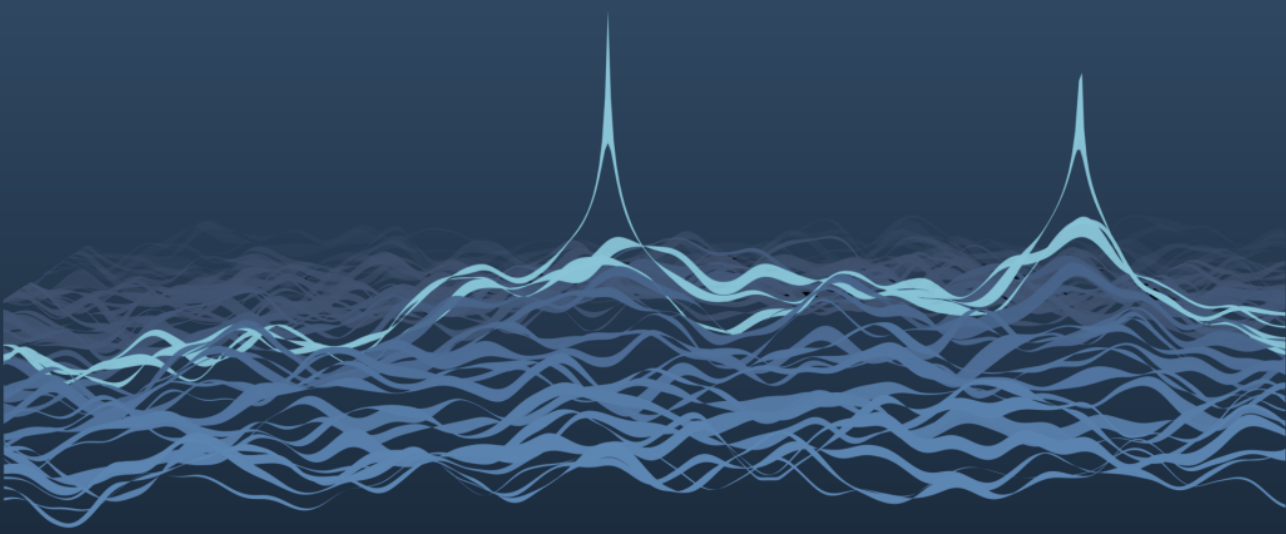

BAYESIAN COMPRESSIVE SENSING FOR RADAR BASED DOA ESTIMATION USING SPARSE SENSOR ARRAYS

MASTER THESIS

Lucas L. LAMBERTI

Student No.: 5369797
Student of Electrical Engineering
Technical University Delft
Department of Microwave Sensing, Signals and Systems

Responsible Professor:	Dr. Francesco Fioranelli
Daily Supervisor:	Ignacio Roldan
Head of Department:	Professor Dr. Alexander Yarovoy
Thesis Committee member:	Dr. Ir. Rob F. Remis
Date of Defence:	23. August 2022

Abstract

Direction of Arrival (DoA) estimation is an important topic in radar application and has significant importance for advanced driver assistant systems in the automotive industry. While there is an increasing need for higher resolution and increased target detection and DoA estimation performance, such improvements often require increased hardware cost, complexity and size. With the increase in computational power of modern systems, Compressive Sensing methods have become more attractive as alternative methods for DoA estimation to the established ones, which often rely on uniform linear arrays (ULA) and the acquisition of multiple snapshots to provide good performance. Compressive Sensing methods have been shown to fit very well into the DoA estimation framework and have the ability to use far fewer snapshots, provide super resolution capabilities and by nature, utilise sparse spatial sampling, i.e. sparse antenna arrays. The latter point is the key incentive of this thesis.

Specifically, Bayesian Compressive Sensing (BCS) which in addition to point estimates also provides measures of uncertainty is used in this thesis, to generate and use sparse linear array structures for DoA estimation. In particular, the entropy of the recovered coefficient vector is reduced in each step. Two array generation algorithms are proposed building on the same concept to generate sensor arrays for the consideration of a uniformly spaced, linear grid of possible sensor locations and for a Multiple In Multiple Out (MIMO) array setup. Utilising sparse arrays with BCS has the potential to reduce the hardware complexity of the circuit board, reduce energy consumption and heat generation, as well as ultimately saving costs in production and operation.

The proposed array generation algorithms are first tested and assessed with simulated Frequency-Modulated Continuous-Waveform (FMCW) radar data, where it is shown that the generated algorithms achieve good estimation and detection performance with a heavily reduced number of sensors compared to their fully filled template arrays. Moreover, they are shown to outperform randomly generated arrays in most cases that have been studied. To add practical insight, the generated antenna arrays are tested with measured data that has been captured in two measurement campaigns with a Texas Instruments Cascade Evaluation board, featuring an 86 element virtual ULA, which has been used as the grid of possible sensor positions for the array generations. The simulated results are affirmed by the measured data, although more sensors tend to be required depending on the clutter present in the scene. It is shown, that BCS can work very well with the proposed, heavily sparse arrays tested on both simulated and measured data, which translates directly to a possible reduction in required hardware antennas. Although in this thesis the possible sensor positions have been confined to a grid of positions spaced by half the wavelength, it is easily possible to extend the procedure to a more finely divided search space.

Acknowledgements

Working on this project has not only given me the opportunity to learn and broaden my horizon in technical aspects, but also to grow as a person. All that would not have been possible without the support and inspiration by the many people that I had the pleasure to be surrounded by.
I would like to thank Prof. Dr. Alexander Yarovoy for his kind and encouraging words and for the very inspiring attitude, as well as for giving me the opportunity of doing my thesis project in the Microwave Sensing, Signals and Systems (MS3) Department. Furthermore, I would like to express my sincere gratitude towards my supervisors Dr. Francesco Fioranelli and Ignacio Roldan, for their tireless and enthusiastic support and countless inspiring discussions. It has been a great pleasure to have you as supervisors.
I am thankful to have had the opportunity to be part of the MS3 research group and to be surrounded by such bright and kind people. Thank you for every little discussion that has given me more insight. Special thanks to Luis and Quentin for helping out during the field experiments. Furthermore, I'd like to thank Dr. Hans Driessen for interesting and insightful conversations about the theory of Bayesian Compressive Sensing.
I would like to thank the friends I made in Delft and at the TU, without whom this journey would only have been half as pleasant in these difficult times and who are among the most inspiring and kindest people that I have met.
Last but not the least, I would like to express my uttermost gratitude for my family, which have always been encouraging and supportive with my undertakings and without whom I would not be where I am today. Thank you, Joshua, for inspiring me with your unyielding will and determination. Special thanks also to Marlene for her inexhaustible support and for bearing with me during my ups and downs.

Lucas L. Lamberti
Delft, August 2022

CONTENTS

Acronyms

ACC Automotive Cruise Control. 3

ADAS Advanced Driver Assistance Systems. 2

ADC Analog to Digital Converter. 21

ARD Automatic Relevance Determination. 7

BCS Bayesian Compressive Sensing. 1, 3, 8, 25, 28

BP Basis Pusuit. 9

CS Compressive Sensing. 2, 4, 25

DoA Direction of Arrival. 2

DOF Degrees of Freedom. 25

EM Expectation Maximisation. 11, 31

ESPRIT Estimation of Signal Parameters via Rotational Invariance Techniques. 2

FFT Fast Fourier Transform. 21

FMCW Frequency-Modulated Continuous-Waveform. v, 21

FOV Field of View. 2, 3

HAD Highly Automated Driving. 2

MAP Maximum a Posteriori. 29

MDL Minimum Description Length. 55

MHA Minimum Hole Array. 11

MIMO Multiple In Multiple Out. v, 3, 20, 24

MRA Minimum Redundancy Array. 11, 15

MT-BCS Multi Task Bayesian Compressive Sensing. 9

MUSIC Multiple Signal Classification. 2, 55

OMP Orthogonal Matching Pursuit. 9

PCA Principal Component Analysis. 33

PDF Probability Density Function. 8, 28

PRF Pulse Repetition Frequency. 22

PRI Pulse Repetition Interval. 21

RIP Restricted Isometry Property. 14, 28

RMSE Root Mean Square Error. 10, 37, 50, 85

ROC Receiver Operating Characteristic. 37, 46

RVM Relevance Vector Machine. 8, 50, 52

SAR Synthetic Aperture Radar. 4

SBL Sparse Bayesian Learning. 3, 7

SNR Signal to Noise Ratio. 2, 10, 23

StOMP Stagewise Orthogonal Matching Pursuit. 9

SVD Singular Value Decomposition. 5, 33

SVM Support Vector Machine. 8

ULA Uniform Linear Array. 9

LIST OF SYMBOLS

A list of symbols used throughout the document. Note that vectors are indicated in boldface as **x**, opposed to scalar values x. Matrices are generally denoted in capital letters.

a	Steering vector
y	Measurement vector (from the sensor array)
$\otimes$	Kronecker Product
Ψ	A general transform basis
x	Vector of target locations that needs to be recovered/estimated
Φ	Sensing matrix
Θ	Compressed transform matrix/ Dictionary matrix
θ	Angle of signal arrival
A	Steering matrix
J	Selection matrix applied to the sensing matrix
K	Number of source signals
M	Number of measurements
N	Number of sensors

List of Figures

List of Tables

1

INTRODUCTION

In this first chapter, the topics of this thesis are introduced and an overview of current literature is given. Starting with the general motivation why DoA estimation with sparse sensor arrays can be desirable and how Bayesian Compressive Sensing (BCS) can be a good method for that, an extensive literature review is followed. The concept of classical compressive sensing is reviewed in 1.2.1 to give a general introduction of the underlying concepts. Then the focus will be shifted to the Bayesian Compressive Sensing literature for DoA estimation in 1.2.2 and a first prospect how it can be applied with sparse sensor arrays in 1.2.6. Finally, the potential gaps that have been worked out from the literature review are formulated into key research objectives for this thesis in section 1.3.

1

1.1. MOTIVATION

ADVANCES in semiconductor manufacturing technology as well as signal processing techniques have opened the field of application for radar (*radio detection and ranging*) technology more and more to consumer technology [1]. A driving branch of such applications is the automotive industry, where vehicles are increasingly equipped with sensor and radar devices to realise Advanced Driver Assistance Systems (ADAS) and push towards Highly Automated Driving (HAD). These radar sensors intend to deliver a good resolution of the observed scene and provide the ability to detect and distinguish different targets as well as to locate them within a given Field of View (FOV). In particular, radar has proven as a valuable sensing technology not only for automotive radar technology, as it can still work reliably under most weather and lighting conditions. Moreover, radar systems can simultaneously provide estimates for range, velocity, and the angle of one or more objects [2]. As the reliability and performance of systems like ADAS is heavily determined by the capabilities of gathering information of the car's surroundings, automotive radar has become a topic of large scientific interest. However, while the need for better performance increases, the cost, and complexity of the required hardware increases as well [1], [3]. Large efforts are made to keep those latter parameters as small as possible.

One of the prominent radar applications is the estimation of angular target locations or direction estimation, called Direction of Arrival (DoA) estimation, since the direction of returning radar pulses is estimated. This is made possible by the use of antenna arrays. The performance of classic DoA estimation is largely influenced by the angular resolution $\Delta\theta$ that the underlying antenna array is able to provide, which is proportional to the utilised wavelength λ and inversely proportional to the array aperture as $\Delta\theta \propto \frac{\lambda}{\text{Aperture}}$. The most basic way of estimating the DoAs of impinging signals is known as classical beamforming spectrum estimation and entails the Fourier transform (FT) of the data vector obtained from the sensor array along the angular (spatial) domain. The angular resolution of this method is bound by the Rayleigh resolution limit, directly related to the array geometry (more precisely its aperture) [3]. Under good Signal to Noise Ratio (SNR) conditions, methods like Multiple Signal Classification (MUSIC) and Estimation of Signal Parameters via Rotational Invariance Techniques (ESPRIT) can achieve higher resolution and resolve even targets within the Rayleigh resolution limit. Such estimator properties are commonly referred to as *super resolution*. However, these methods depend on a sufficient number of snapshots since they need to estimate the covariance matrix of the received data. Furthermore, they often require a priori knowledge about the number of targets to expect [3].

Compressive Sensing (CS) based DoA estimation approaches have shown promising benefits, as they do not show the need for numerous snapshots while still providing super-resolution DoA estimation and are less sensitive to low SNR conditions [4]. In the field of automotive radar, processing time to achieve DoA estimates is a critical factor and this motivates the search for single-snapshot techniques, making the CS framework an interesting candidate.

Another potential benefit of the CS framework is related to the number of measurements that are needed to obtain good estimation results. It has been shown, that the CS framework can provide a way of reducing the needed array elements while maintain-

ing a good angular resolution and guaranteed recovery of the DoAs [5]. To summarise, the CS framework provides two possible benefits to the DoA estimation:

- Requiring fewer, even only a single snapshot to potentially obtain highly resolved DoA estimates with improved robustness against noise [6].
- Reducing the amount of antennas needed in the sensor array while providing high probabilities for proper recovery of target DoAs [5].

While there have been numerous works in the literature investigating the optimal arrangement of sensors for DoA estimation using classical CS recovery methods, the question has not extensively been considered in the view of Bayesian recovery methods. Bayesian Compressive Sensing natively provides additionally to the point estimates also measures of uncertainty, which makes it an option that is worth exploring.
In this thesis, compressive sensing DoA estimation is considered from the Bayesian perspective, known in literature under Bayesian Compressive Sensing (BCS) and building upon the theory of Sparse Bayesian Learning (SBL). Specifically, the goal is to obtain methods to reduce the amount of antennas in a physical ULA and a MIMO array, such that DoAs can still be reliably estimated with the least amount of sensors needed.

In the context of Multiple In Multiple Out (MIMO) Radar, which is extensively applied in automotive technology [1], [3], the number of receive antennas can be virtually increased by combining two arrays of properly spaced transmit and receive antennas and transmitting orthogonal waveforms. The resulting virtual receive antenna array is thus jointly determined by the number of transmit and receive antennas, which needs to be accounted for in possible optimised array arrangements. To properly test the generated sensor arrays, they will be utilised in the BCS-based DoA estimation algorithm (described in chapter 2) with the use of simulated and measured radar data. It will be taken into account, that the desired Field of View (FOV) varies depending on the application. Short-range radar used for example in the parking assistant system typically needs a larger FOV of $\pm 80°$, while long-range radar used in Automotive Cruise Control (ACC) typically needs only a narrow FOV of $\pm 15°$. For this thesis, an FOV of $\pm 40°$ has been used to confine this parameter to a common value for mid-range radar. Furthermore, two frequency bands of $24-29$GHz and $76-81$GHz are commonly used [3], while the latter one is primarily used in most modern systems and therefore also in this thesis.

1.2. LITERATURE REVIEW

1.2.1. CLASSICAL COMPRESSIVE SENSING

Many signals are compressible in a proper representation domain, where the signal can be represented by only a few non-zero coefficients. A common example for such signals are audio signals, which are generally non-sparse in the time domain and have to be sampled at Nyquist-Rate to allow for lossless reconstruction [8]. However, when transforming such signals to the frequency domain e.g. by a Fourier-Transform, only few non-zero frequencies can be enough to fully describe the audio signal. This gave rise to many compression algorithms and formats like mp3 for audio or JPG for image data [9]. It also raises the question, whether there is a way to sparsely sample such signals in the first place, saving the cost and complexity of high sampling rates (or spatial sensors

1

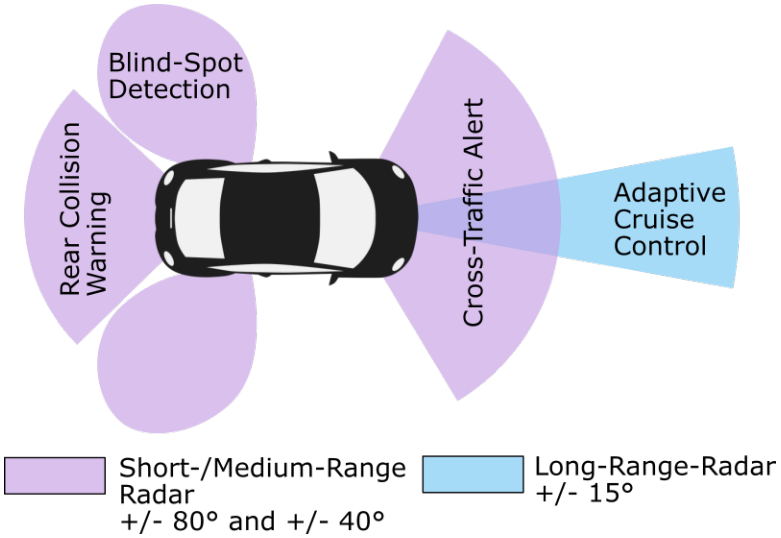

Figure 1.1: Short to long range radar in the automotive industry. Note the use of larger field of views for the short range radar (red) and a rather small field of view for the long range radar (blue). Image derived from [7]

in the case of sensor arrays), instead of throwing away information in the processing. This would allow for the design of less complex and expensive hardware measurement systems, while maintaining high performance. The idea has found great interest in recent literature under the term of Compressive Sensing (CS) [10]–[12]. It is based on the assumption, that the signal of interest is *sparse* in some transform domain, typically denoted by Ψ, and that signals which are sparse in the domain of Ψ must be non-sparse in the domain where they are measured [9]. This latter concept is described under the name of *coherence* and is an important characteristic in CS literature. To fully utilise the CS framework, usually far fewer measurements M are taken, than the dimension of the signal of interest, i.e. $M \ll N$, resulting in an undersampling of the signal and an underdetermined set of equations to solve for the recovery of the original signal [9], [10]. Such a system then does not have a unique solution; however, through efficient computational methods the approximately sparsest solution of them can be found, recovering the coefficients describing the signal [10], [13].
In application to DoA estimation, one faces the problem that the direction of arrival is generally a continuous value, while the classical CS framework works with an overcomplete dictionary of discrete candidate basis functions, corresponding to possible directions (also called atoms). This can lead to errors or uncertainty in the recovered DoA, when a target does not coincide with a DoA grid point of the chosen discretisation. There have been different approaches to deal with these *off-grid* effects and the CS DoA estimation framework can be roughly separated into three methods: On-Grid, Off-Grid and Gridless sparse methods [14]. In this thesis, the applied methods will assume an On-Grid framework.

Since its occurrence, the CS framework has found large interest in different areas of electrical engineering, such as microwave imaging, Synthetic Aperture Radar (SAR), ar-

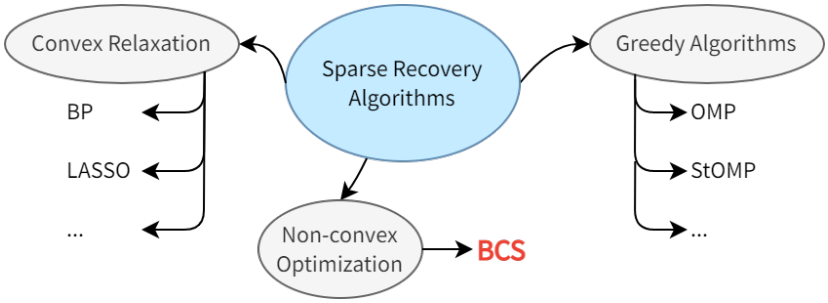

Figure 1.2: Broad subcategories of sparse recovery algorithms and some examples. This thesis is aiming at the Bayesian Compressive Sensing methods marked in red. Graphic based on [16].

ray synthesis or direction-of-arrival (DoA) estimation to name just a few [15]. The focus of this thesis is directed towards 1-Dimensional DoA estimation in automotive radar systems, and this will be kept in mind while reviewing current state-of-the-art literature.
To recover the sparse coefficients that represent the original signal in the sparse basis, a large amount of recovery algorithms have been proposed in literature over the years. They can be grouped into three broad categories [16]:

- Convex Relaxation based: Posed as a convex optimization problem, the solution to the underdetermined system can be computed efficiently with global optimization methods like interior-point methods or gradient descent.
- Non-Convex Optimization based: Often these methods assume a prior knowledge of the signal to recover and aim to compute a full statistical, posterior probability density function, providing not only point estimates but also further statistics about the signal. Compared to the first method, these methods are still suffering from higher computational complexity.
- Greedy Algorithms: These methods utilize an iterative way to recover the signal, selecting local optima in each iteration to finally end at a global optimum.

A graphical overview is given in figure 1.2. Reviewing all sparse recovery methods that have been proposed would break the boundaries of this thesis, and since the emphasis of this thesis is only on one of those methods, the reader is referred to [16] for an extensive review of sparse recovery algorithms. To visualize the relation between the sparse coefficients that have to be estimated, denoted as $\mathbf{s}$, the measurement vector $\mathbf{y}$ and the dictionary matrix Θ, which in the case of this thesis will be a form of the array steering matrix, figure 1.3 aims to provide a first insight. The overcomplete dictionary matrix Θ will be the central element of the array generation procedure. A deeper dive into the compressive sensing theory will, however, be postponed to chapter 2 while this chapter is dedicated to the state-of-the-art literature review.

In [4] it is shown, that the compressive sensing approach applied to source localisation is capable of achieving super-resolution with only a single snapshot. Two interesting processing schemes are introduced, which might be of interest for this work. Firstly, data from multiple snapshots is combined using the Singular Value Decomposition (SVD).

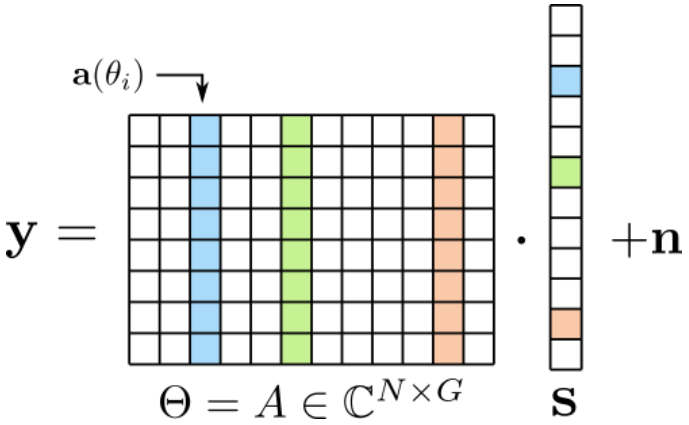

Figure 1.3: Scheme of the central, underdetermined linear equation that CS and BCS tries to solve for the unknown but sparse vector of coefficients **s**. The coloured coefficients in **s** are the unknown, sparse coefficients that have to be recovered. They determine which column of the steering matrix A, which are basis functions of the signal model (in this case the steering vectors $\mathbf{a}(\theta_i)$, are causing the observed signal **y**. Refer to chapter 2 for a more rigorous explanation.

With this method, multiple snapshots can be processed coherently while reducing computational complexity by reducing the dimensionality of the data matrix obtained from multiple snapshots. The data matrix is decomposed into its signal and noise subspace, and only the latter one is kept. [1] Secondly, an iterative grid-refinement strategy is proposed in order to combat off-grid estimation errors. To this end, the grid is refined only in regions around coarsely estimated sources. This idea can be found in another paper building on the Bayesian framework [17], which is described in more detail in section 1.2.2.

The CS framework is extended in [18] to MIMO radar and applied to DoA and range estimation with specific waveform design. This is driven further in [19] to reconstruct target signals in azimuth, range as well as Doppler domain. The importance of the sensing matrix, which is a direct result from the steering matrix of the array geometry, is pointed out. An important trade-off is specified: as the number of columns in the sensing matrix is increased (i.e., increasing the angular grid resolution), the linear system given by the CS equation becomes increasingly underdetermined, resulting in a worse coherence of the sensing matrix. This is due to the fact that neighbouring columns will look more and more alike. This in turn will influence the performance of classical CS recovery methods, and it is not unlikely, that this might be of importance for the Bayesian framework as well.

In [20], [21] and [5], rigorous analysis is done regarding spatial compressive sensing with respect to DoA estimation and MIMO arrays. In [20], mathematical lower bounds on the number of virtual elements resulting from the MIMO architecture are derived and shown

[1] As described in the introductory section, time is viewed as a critical factor and methods that depend on larger amounts of snapshots are less desirable. However, there might be a trade-off between robustness to noise when more than one snapshot is used. Therefore, also multi-snapshot methods could still be a viable option depending on the velocity of the vehicle.

to be dependent on the number of targets in the scene. In [21] these ideas are extended to a multi-snapshot measurement model. Furthermore, the relation between random sensor arrays and the compressive framework is studied, coming to the result that a low number of randomly placed sensors can achieve high angular resolution, offering the possibility to trade off hardware complexity with computational complexity. In [5] the authors further investigate the relation between the mutual coherence property and the steering matrix, resulting from the MIMO array geometry. The insightful link is made between low mutual coherence and sidelobes of the array pattern, offering a more tangible understanding of the property with respect to radar application.
In [22], a mathematical method for coherence reduction in compressive sensing applied to DoA estimation is proposed. To this end, highly coherent columns of the sensing matrix are replaced by Gaussian distributed random matrices, reducing the overall coherence. This method has been derived in a very theoretical way, and the proposed replacement columns might not be realisable by means of placing actual physical sensors.

1.2.2. SPARSE BAYESIAN LEARNING

A different, more statistically flavoured approach to solve the underdetermined systems in compressive sensing problems is closely related to the topic of Sparse Bayesian Learning (SBL), which has its roots in an important property of Bayesian inference and finds vast application in machine learning topics [23]. As it has been pointed out by D.J.C. MacKay in [24], there are two steps involved in inference tasks, namely:

- Model fitting, where the most probable model parameters can be found utilising Bayes rule under a fixed model assumption. The use of Bayesian statistics not only delivers point estimates, but also provides confidence values in the estimated parameters.
- The second task is termed "model comparison", and involves the ranking of models, given the data, with respect to how well they describe the data and, importantly, intrinsically factoring in the model complexity as a penalty.

It is the second task of Bayesian inference which plays a major role in the development of SBL. The ability to rank models against each other allows for model selection among a set of candidates and simultaneously keeping the model complexity as low as possible. Model complexity is an important topic in general linear regression tasks and machine learning, because a too complex model leads to overly parametrised models, which may lead to a modelling of noise and poor generalisation properties [2] [23]. As will be explained in chapter 2, the important information for model selection lies within the normalising denominator in Bayes' rule, often termed *evidence* or *marginal likelihood* [24]. The maximisation of this marginal likelihood lies at the core of the Bayesian compressive sensing framework reviewed next. [3]

[2] A popular adopted term in this regard is the "Occam's razor", which states that simpler models should be preferred to overly complex ones [23], [24]

[3] In the light of sparsity, the selection process via a set of hyperparametrised weights with imposed sparsity (via a prior) is also investigated under the term of Automatic Relevance Determination (ARD) (see for example [25]).

A general sparse Bayesian framework under the name of SBL is introduced by Tipping et al. in [26], [27] to obtain sparse solutions to regression and classification tasks. Although the work of M. Tipping et al. is focused more on SBL in general, and does not only apply to Bayesian Compressive Sensing (BCS), it provides the corner stone on which many following papers base their application of the SBL paradigm to BCS. In [27], the sparsity is promoted by means of prior densities on the model weights which have to be estimated. A popular but analytically more complex choice for sparsity enforcing priors is the Laplace density [28], [29], which concentrates much of its probability density at its centre and along its tails. To ease the analytical complexity, [27] resort to a hierarchical prior based on Gaussian densities which leads to an approximate analytical solution, as it allows for conjugate-exponential analysis [27], [28]. Sparsity is finally obtained, since the posterior PDF of most weights tend to be infinitely peaked around zero and can be pruned away. The remaining non-zero weights are then termed 'relevance' vectors and give the basis functions which are included into the model. The term Relevance Vector Machine (RVM) is thus introduced in [26], [27] which reminds of the Support Vector Machine (SVM). The first proposed iterative algorithm in [27] has later been developed into an efficient, fast RVM algorithm [30], [31] to solve the Bayesian inversion task.
In a later research work [29], the proposed hierarchical prior in [27], [28] has been exchanged by a hierarchical, Laplacian prior. The authors of [29] point out, that Laplace priors act stronger in enforcing sparsity and their method generally outperforms the one in [27] in terms of sparsity and reconstruction error.

1.2.3. THE GENERAL BAYESIAN COMPRESSIVE SENSING FRAMEWORK

Based on the algorithm and framework developed in [27], [31], a general introduction to the BCS framework is given in [28] without a direct link to DoA estimation, yet. The derived signal model follows the same format as in classical compressive sensing literature, the BCS framework merely offers a different method of solving the problem, as visually depicted in figure 1.2. The authors point out the following most important benefits of BSC in agreement with other literature ([32]) about the topic:

- Due to the underlying Bayesian framework, not only point estimates are obtained, but rather a full probability distribution in the form of a posterior density function over the weights. This provides a measure of uncertainty or confidence in the estimation.
- The additional confidence metric, termed "error-bars", also provide a way to determine if a sufficient number of measurements has been taken. This is exploited in [28] to optimise the measurements and reduce uncertainty with every new measurement.
- The proposed framework inherently accounts for additive measurement noise and can yield an estimate of its variance.

As in the classical CS framework, the proposed scheme assumes compressibility of the signal of interest or, equivalently, sparsity in a proper transform basis. Given compressive measurements and a known basis in which the signal can be represented via a sparse set of coefficients, the objective is to recover those coefficients or weight values. The

speciality and distinguishing factor to classical CS methods is the estimation of those weights by means of a full posterior density function, providing not only point estimates but also confidence values in the estimated weights [28]. The authors of [28], [33] provide an implementation of the RVM algorithm that has been proposed in [31], adapted to the BCS task. In addition to the pure estimation of the unknown sparse coefficients, the BCS framework is utilised to show a way for adaptive optimisation of the projections onto the sparse basis, which has been introduced by the same authors in a previous paper [34]. In contrast to random projections, optimised projections might be facilitated in the design of sensing systems [28], [34], an aspect which will be important in the search for optimised antenna arrays. The authors compare the BCS method to classical CS inversion methods like Basis Pusuit (BP), Orthogonal Matching Pursuit (OMP), and Stagewise Orthogonal Matching Pursuit (StOMP). The BCS reconstruction is shown to be cleaner than the BP reconstruction, while additionally providing confidence metrics and outperforming BP in terms of computation time. In [33], Ji et al. extend their work by developing a method that incorporates statistical dependencies in the sparseness of consecutive snapshots to improve performance of the inversion. The shared sparseness is exploited by placing a shared prior over the hyperparameters, which is influenced by all the used snapshots (tasks). This method has been generally termed Multi Task Bayesian Compressive Sensing (MT-BCS). Another follow-up contribution in [35] extends the multitask method to work directly with complex valued input, thus exploiting joint sparsity between the real and imaginary parts of input signals and better preserving phase information. However, the developed algorithm is not working with the fast update equations that have been worked out in [31] and subsequently used in [33], making it slower and less stable.

1.2.4. BCS FOR DOA ESTIMATION

In [36], a narrowband DOA estimation method based on a minor extension to the BCS framework in [28] is proposed. The array manifold matrix of a Uniform Linear Array (ULA) is discretised into an over complete manifold matrix over the potential range of DoAs, casting the problem into a grid-based CS problem, very similar to the classical CS approaches reviewed earlier. The proposed signal model is derived to incorporate multiple snapshots. The likelihood function (its logarithm in practice) that is to be maximised is then computed by summing the likelihoods of all snapshots together. This is a different approach as compared to the multitasking approach proposed in [33].
A following, more rigorous application to DOA estimation building upon [36] has been done in [32], [37], where a similar expansion for the use of complex values is done as in [38], first introduced in [39]. Both a single-snapshot and multi-snapshot framework is provided, based on [28] and [33], respectively. In contrast to [36], they make use of the multitasking strategy, where correlation between snapshots is exploited to facilitate the estimation procedure. They show that their method is able to yield accurate DoA estimation without prior knowledge about the number of targets in the scene (i.e., the number of non-zero coefficients). Moreover, the accuracy and robustness to noise is increased with the multi-snapshot method, since correlations between snapshots can be exploited.
Another multitask BCS approach has been proposed by Carlin et al. in application to the

DOA estimation problem in [40], building upon their earlier works in [32]. Here again a grid-based discretisation of the steering matrix is considered. The work is compared against the established techniques of ROOT MUSIC and ESPRIT under varying number of snapshots, target spacings and Signal to Noise Ratio (SNR). The used performance metric is the Root Mean Square Error (RMSE) of the estimated DoA. As it has already previously been stated, the two traditional methods require a priori knowledge of the number of targets, which BCS methods do not. With respect to the RMSE, the mutli-task BCS approach outperforms the two traditional as well as the singletask BCS approach in all aspects. It might be worth pointing out, that in the case of varying target spacing (in azimuth), the singletask BCS seems to perform better than the multitask one under very closely located targets. However, it is proved in [40], that the multitask BCS approach efficiently exploits correlations between snapshots to arrive at an overall better performance.

In [17], two new aspects are introduced, being the coupling between the antenna array elements and a method of grid-refinement to locally increase the angular resolution where targets have been estimated under a more coarse angular grid (Similar as introduced by [4] in the classical CS scheme). To achieve the multi-scaling procedure, the confidence values in the estimated weights, which are readily yielded by the BCS inversion, are utilised. This is one option to deal with the off-grid estimation errors, induced by targets that do not fall onto the discretised grid of DoAs. In this approach, only single-snapshot processing is considered, and the sensor arrangement is a ULA but this time with non-ideal dipole antennas including mutual coupling and polarisation mismatch. The iterative refinement strategy is based on the confidence level of an initial coarse angle estimation, and a defined number of “zooming” iterations is performed into designated areas of interest ("ARoIs"). This allows for a selective grid refinement while maintaining a coarser grid outside those regions, saving computational burden. The refinement strategy provides a good way of “checking” again at angular sections and improving the certainty of target presence. It is shown by means of the angular RMSE, that the refinement iterations reduce the RMSE to almost 0 after only 3 zooming steps. Interestingly, the authors show that the multi-scaling BCS approach outperforms the single scale BCS approach even when this one is used with a very fine angular grid, while even the computational time has been lower in the multi-scaling approach. Finally, a very useful performance assessment provided in [17] is that the zooming strategy efficiently corrects for falsely located targets. If in the initial coarse prediction 10 target DoAs are estimated, but only 6 targets are present, following iterations are able to reduce the number of estimations to the correct value.

In [41] an off-grid approach to the DoA estimation problem is proposed by considering a first order approximation of the array steering matrix. Following the sparse Bayesian inference framework as in [27], however considering a complex valued dictionary matrix, a reconstruction algorithm is proposed. In a further step, the algorithm is modified by utilising the SVD in order to reduce the computational burden as well as the noise sensitivity. The proposed algorithm can be utilised for both single- and multiple snapshot data. Through simulations, the authors show, that their algorithm is not only more precise than ℓ_1-based classical CS methods, but is also able to resolve closely spaced targets where classical methods like MUSIC fail.

Extending upon the idea presented in [41], Dai et al. propose a scheme in [42] to improve the computational efficiency of the grid refinement to mitigate the off-grid errors. To this end, they employ the Expectation Maximisation (EM) algorithm to iteratively perform the grid refinement, where they relate each update to a root-finding problem of a specific polynomial. To deal with outlier measurements, Dai et al. in [43] propose a DoA estimation algorithm, again derived similarly as in [27] and [41]. They resort to a grid refinement as introduced before in [42] to deal with off-grid effects.
Another modification to the SBL model of [27], inspired by the use of a Laplacian prior as in [29] is done in [44], where explicit attention is laid on the non-negativity of the sparse weights (i.e. the target locations). To include this proposition into the SBL model, the Laplacian prior as in [29] is adopted to yield only non-negative values. Similar derivations are then performed as in [27] and [29], yielding an algorithm based on the EM procedure, which is shown to outperform previous methods (including the one proposed in [29]). An interesting addition is that the authors do not use ULAs, but instead evaluate their method using a Minimum Redundancy Array (MRA).

Such array types can be generally grouped into the research category of sparse or non-uniform arrays. One of the earlier works in this field by A.T. Moffet introduced the concepts of Minimum Redundancy Array (MRA)s and Minimum Hole Array (MHA)s, which are linear arrays with as few redundant inter element spacings as possible to achieve maximum resolution capabilities [45]. This idea was extended to the MIMO array concept in [46]. Another type of such arrays is termed Co-prime arrays, which contrary to the MRA and MHA geometries have closed form expressions for the sensor locations [47]. Following up, as an improvement to co-prime arrays, nested arrays and super-nested arrays were introduced which also have closed form solutions for the antenna positions [48], [49]. There are many other variations to these array geometries, and reviewing those would go beyond the scope of this thesis. Generally, these array types offer one way to reduce the antenna elements utilized within an antenna array, by getting rid of redundant information [49], and have shown to improve the DOA estimation performance using subspace based methods like MUSIC estimation [50]–[52]. Moreover, using these array structures has offered the ability to estimate more targets DOAs than there are physical sensors in the array, which has been demonstrated for example using nested arrays in [47]. These array structures have also been applied to DOA estimation in conjunction with sparse Bayesian learning methods. In [53], [54], coprime and nested arrays are used. Another two papers using coprime arrays and nested arrays can be found in [55] and [56], respectively.

Up until now, the discussed literature based their models on the assumption of narrowband signals. In [57], the authors extend the multi-scaling BCS DOA estimation approach in [37] to work with wideband signals instead, working with single snapshot data. The DoA estimation is facilitated and improved by exploiting correlations between different frequencies instead of different snapshots. Moreover, frequency contents of the impinging signals can be estimated. Similarly to previous methods, the azimuth angle domain is discretised, resulting in a grid-based method. It is shown in a small numerical evaluation, that with this “spectral correlation”, multitask BCS method estimates both DoA and signal bandwidth correctly. In a follow-up work [58], the authors extend their

strategy to also incorporate multiple snapshots in time in order to improve the estimation under low SNR conditions. However, since in the MIMO radar case the signals are available only after the matched-filter processing, we might not have such wideband-based opportunities.

Concluding this section, a collection of the main reviewed literature dealing with BCS based DoA estimation is provided in table 1.1. It has become evident that most literature utilises fully filled receiver array architectures within the Bayesian CS framework, leaving the potential for reduction in sensor elements mostly untouched.

Reference	Snapshots	Method	Grid-based	Sensors
[36]	single	[28]	yes	ULA (full)
[37]	single/multi	[27], [28]	yes	ULA (full)
[40]	multi	[33]	yes	ULA (full)
[59]	multi	[37]	yes (refined)	ULA (full)
[17]	single	[28]	yes (refined)	ULA (full)
[57]	single	[37]	yes	ULA (full)
[58]	multi	[57]	yes	ULA (full)
[41]	multi	[41] similar to [27], [29]	Off-Grid	ULA (full)
[43]	multi	[43] similar to [27], [29]	yes (refined)	ULA (full)
[42], [43]	multi	[41], [42]	yes (refined)	ULA (full)
[44]	single	[29]	yes	MRA

Table 1.1: List of major BCS based DoA estimation methods. The works of S. Ji and L. Carin in [28], [33] as well as the work surrounding M. Carlin et al. in [37], [40], [59] form a central contribution to the related literature. Some methods build upon the Laplace prior as introduced in [29], while others build upon the Gaussian prior model from the original paper of Tipping [27]

1.2.5. BCS APPLIED TO MIMO RADAR

To the best of the author's knowledge, only few resources could be found that apply the BCS scheme to MIMO Radar.

In [60], the BCS framework is applied to DoA estimation with MIMO radar. A grid of possible DoAs is considered, discretising the angular domain and neglecting possible off-grid errors. The discretised and known steering matrix obtained from the transmitting and receiving steering vectors is used as the dictionary matrix in the sparse inversion problem, where the task is to find the non-zero support, corresponding to the directions of impinging signals. The complex valued data is extended to yield real valued vectors and matrices similar to [17], [38]. In the proposed measurement model, the DoAs correspond to the non-zero coefficients in a weight vector applied to the dictionary matrix. To retrieve this weight vector, the RVM scheme is adopted, similar to [28], [31].

Another study in [61] aims to extend the MIMO DoA estimation framework using sparse SBL to arbitrary transmit waveforms. Those waveforms are iteratively optimised to reduce the DoA estimation error. To perform the DoA estimation, the measurement model is cast into the BCS framework similar to [60]. Finally, they show that the optimised waveforms perform better in terms of estimation error compared to classical orthogonal waveforms [61].

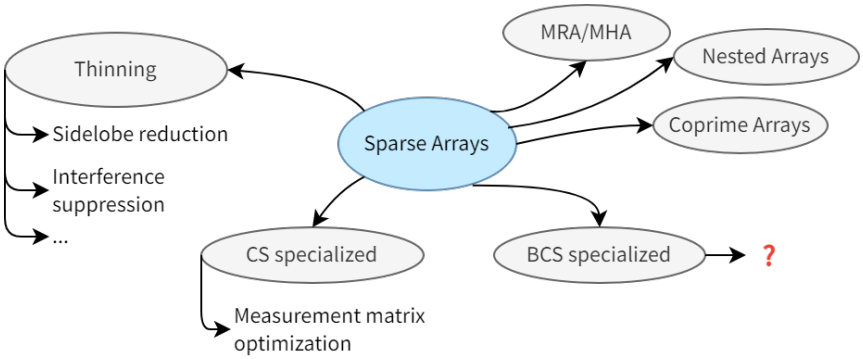

Figure 1.4: Overview of sparse array configurations that have been proposed throughout literature for different purposes

In [62], the SBL framework is applied to MIMO radar DoA estimation under consideration of unknown non-uniform noise. However, they assume a MIMO array with redundant elements and include methods of reducing the data obtained by such redundant elements. Dealing with imperfect waveforms that may not be perfectly orthogonal in MIMO radar is considered in another off-grid DoA Estimation method utilizing sparse Bayesian learning in [63], where similar to [62], the complexity stemming from redundant virtual sensors is reduced via a reduced-complexity framework. Finally, a combination of sparse Bayesian learning and MUSIC is proposed in [64] for direction of arrival and direction of departure estimation in MIMO radar. Again, the virtual sensor array generated by the MIMO setup is considered to have a lot of overlapping elements causing redundant measurements, which are removed by a dimensionality reduction.

1.2.6. PROSPECT ON ARRAY OPTIMISATION

The literature reviewed so far and the methods therein have been proposed and tested largely based on fully filled uniform receive arrays. It has been investigated and shown, that the sensing matrix plays a major role in the performance of compressive sensing algorithms and there exist different possible realisations [65]. This section is dedicated to literature that specifically aims to find sparse sensing matrices under realisation of antenna arrays. Optimality in this sense is understood with respect to the estimation performance and/or with respect to the least amount of elements needed for robust DoA estimation, specifically in the CS and BCS framework. It is important to note that there is a wide range of sparse array types, but this thesis aims to use a specific characteristic of the BCS method to find sparse arrays that work well specifically for BCS DoA estimation methods. Refer to figure 1.4 for a first overview and orientation.

In the classical CS literature, many efforts have been made to optimise the measurement matrix or, equivalently, the sensor placement in the DoA estimation context. One of the metrics often found for this purpose is the mutual coherence [9], [66], a well established criterion for successful recovery of the sparse weights, which has been related to low sidelobes in the array pattern for all looking directions in [5]. The optimisation with respect to the mutual coherence of the sensing matrix or its average has been the

subject of previous literature [67]–[71]. In [72] the sensor placement in a MIMO setup is considered with respect to minimising the mutual coherence of the sensing matrix and to improve the CS recovery performance over randomly placed elements as proposed in e.g. [5]. They formulate the problem into an iterative algorithm and compute probabilities of sensor placement. Finally, they show by means of numerical simulation that their antenna arrays perform better than randomly placed ones. Those positive results motivate the search for a similar optimisation in the BCS framework. It is important to point out, that the mutual coherence is a recovery condition derived in the classical CS framework [9]. It is a property imposed on the measurement matrix that gives certain guarantees for the existence of unique solutions [73].

To the best of the author's knowledge, similar metrics directly related to the success of the sparse Bayesian recovery have not been rigorously developed for the Bayesian CS framework with regard to antenna arrays yet (which has also been stated in literature [74]). Moreover, it has been explicitly stated that in BCS, the sensing matrix does not need to fulfil recovery guaranteeing properties as for example the Restricted Isometry Property (RIP) like classical CS inversion methods need to do [32], [74]. However, the theory behind the sparse reconstruction follows a similar thought in the Bayesian approach, and thus array/sensing matrix optimisation might add valuable benefits to the BCS field as well. It has been hinted at in [34] that the readily provided uncertainty measurements in the BCS framework might be utilised to select measurement projections which add the most new information. To this end, they propose the *differential entropy* as a possible performance metric. This method is picked up in [75], [76] and viewed under the more general term of *Bayesian experimental design*[4], however, using a different approach to SBL. In fact, the design of measurements that yield the most new information in a Bayesian setting has been a general subject of research [24], [78]. This idea has been applied in the fields of sonar sensing for the optimal creation of uniform linear sensor arrays [74]. However, this technique has not yet been applied to the radar sensing application and not under the MIMO radar setup. Moreover, it has not been tested with real measured radar data yet, which could provide valuable new inside about the performance of these techniques. This motivates the work of this thesis and its major research questions, which will be described in the following section.

1.3. THESIS OBJECTIVE AND NOVELTY

After reviewing a large body of research concerning both the classical and the Bayesian compressive sensing framework applied to DoA estimation, it has become clear that those methods form promising and established new alternatives to classic DoA estimation methods. They provide recognisable benefits such as super-resolution, reduced number of snapshots, noise robustness and a reduced number of antenna elements (leading to possible reduction in hardware cost and complexity), which make these methods worth investigating further. While impressive results have been obtained in the classic CS literature, the Bayesian framework offers several benefits, such as providing uncertainty metrics, and has emerged as an attractive statistical alternative to the classic CS literature. The reduction in sensor elements or, equivalently, the thinning of sensor

[4] It is also found under the term *active learning* in the machine learning field (see [77] for an overview)

arrays has been investigated for classic CS methods, where the most popular choice of metric for the thinning procedure is the mutual coherence of the dictionary matrix (i.e. the array steering matrix). This mutual coherence is directly related to mathematical theorems, in this case the *restricted isometry property (RIP)*, which have been derived for CS. However, in the Bayesian counterpart of CS, it has been claimed that such properties do not exist or have not been derived yet [32], [74]. Furthermore, it is said, that in BCS, the steering matrix does not need to fulfil the mutual coherence property. The question arises, to what extent and by what methodology, arrays could be thinned in order to reduce hardware complexity, cost and computational load due to high amounts of collected data. Besides rather rigid architectures like Minimum Redundancy Array (MRA), to the best of the author's knowledge, no such methods have been proposed for radar antenna arrays yet. This thesis makes use of the uncertainty measures provided by the BCS method to propose a method for generating thinned sensor arrays for both the ULA and the MIMO array architecture. A pipeline is developed, that aids in the generation and performance assessment of thinned arrays when used for BCS-based DoA estimation. It is shown, that the generated arrays are able to perform well in terms of ROC curves, even when targets are spaced closer than the native resolution of the array aperture and the number of sensors is heavily reduced.

Moreover, after reviewing related literature, there have not been many tests of the BCS framework applied to radar DoA estimation with real measured data. Most literature uses simulated data to test the proposed methods. In this thesis, the generated arrays are tested also with real data, captured with the Texas Instruments cascade evaluation board, which uses a MIMO array architecture providing 86 unique virtual sensors. Due to this fact, the proposed array thinning methods are tailored towards this array architecture, such that the generated arrays can be tested with the available hardware. However, the proposed methods rely on a very general measure (the provided uncertainty) and can easily be extended and adjusted for different hardware.

Lastly, the BCS framework relies on the concept of sparsity in the signal of interest. Most literature deals with simulated data that features point like targets. This thesis will test the BCS method when targets, like a human body, are not point like.

To the best of the author's knowledge, except for a single paper in SONAR technology [74], the utilisation of the uncertainty measures inherently provided by the BCS method have not been studied in the literature for sensor placement in radar systems. This thesis provides an algorithm exploiting the intrinsic characteristics of the Bayesian CS framework to achieve a reduction in sensor elements used for DoA estimation with radar technology. Two methods are proposed based on the same underlying concept to generate sparse arrays with a physical ULA based architecture and a MIMO array architecture. The proposed algorithms are tailored towards the available hardware in order to test the arrays with captured data, adding further contribution to this field of literature. Due to the available hardware, the algorithms are bound to work with sensor arrays that are confined to an underlying grid of ULA positions with a sensor spacing of $\frac{\lambda}{2}$. However, the concepts used in the proposed methods are easily extendable to other boundary conditions.

Considering the given boundary conditions and parameter choices in this thesis, the resulting arrays perform well in terms of ROC curves and RMSE with a heavy reduced

number of sensors. It is proven by real world measurements, that Bayesian Compressive Sensing has the potential to be used in conjunction with sparse sensor arrays and achieve good detection and estimation performance. For the MIMO case, this directly translates to the possibility of removing or deactivating complete RF chips on the TI cascade evaluation board, leading to reduced hardware complexity, energy consumption and lower amounts of data to process.

Summarising the main contributions of this thesis:

- The inherently provided uncertainty measures by the BCS method in the form of a covariance matrix for the estimated DoA coefficients are utilised to iteratively fill an empty base-array by adding the most informative new sensor position at each step. Two algorithms are proposed, for the physical ULA and MIMO array architecture.
- Through simulation and measured data, the sensor arrays resulting from the proposed method are shown to outperform randomly generated arrays in terms of the ROC curves and are able to achieve good detection and estimation performance with a reduced number of sensors.
- Valuable insight is gained by testing the generated sparse array structures in conjunction with the BCS DoA estimation method with real-world measurements of point-like targets and an extended target.

The results obtained in this thesis are being written up for submission in a journal paper to IEEE Transactions on Aerospace and Electronic Systems.

2

THEORY

The preceding literature review has shown that the BCS framework has been applied for DoA estimation with promising results. Possible questions that are yet to be answered have been worked out and will be tackled in this thesis. This chapter is dedicated to review the theoretical foundation for the methods that are used. First, the commonly used signal model for DoA estimation as well as the concepts behind MIMO antennas are introduced in sections 2.1 and 2.3, respectively. Following that, the theory behind the Bayesian compressive sensing framework and its principal derivation is described in section 2.5. It will be explained, how the DoA signal model can readily be cast into the BCS framework under some small assumptions that are common practice throughout the literature. Important relations between classical and Bayesian compressive sensing will be pointed out, to give a good understanding of the common goal that both frameworks attempt to achieve, and how they differ in achieving this goal. Finally, section 2.6 is dedicated to the generation of the sensor arrays.

2.1. DIRECTION OF ARRIVAL ESTIMATION SIGNAL MODEL

DIRECTION of Arrival estimation has already been a topic of large interest for a long time. Different methods have emerged throughout literature, and this thesis will only focus into one branch of them, namely *sparse reconstruction based* methods, which is at its core a method of spectral estimation [79]. For a brief overview of the broader methods, refer to figure 2.1.

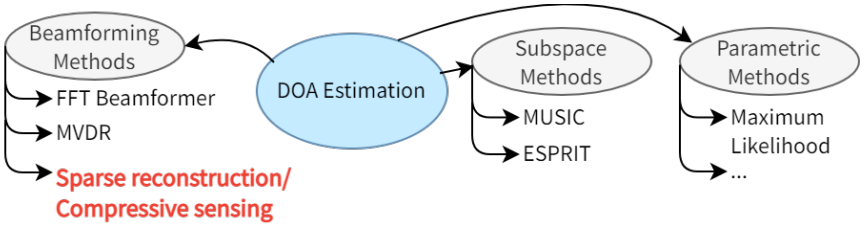

Figure 2.1: Broad overview of major DOA estimation categories, grouped by the way they approach the problem. Methods can be found in more detail in [79]

To describe the signal model that will be used for the DoA task using compressive sensing methodology, some assumptions will be adopted that are commonly encountered in related literature. Firstly, the signal sources (or reflecting targets) are considered to be positioned in the far field of the antenna array. This allows the simplification of the incoming wavefronts to be plane waves, and the time delays of the signal arriving at each sensor in the array can be easily derived. Secondly, the signals arriving at the sensor array are assumed to be narrowband signals, which holds when $B \cdot \Delta T \ll 1$, where B denotes the signal bandwidth and ΔT the signal's maximum travel time between two antennas in the array.

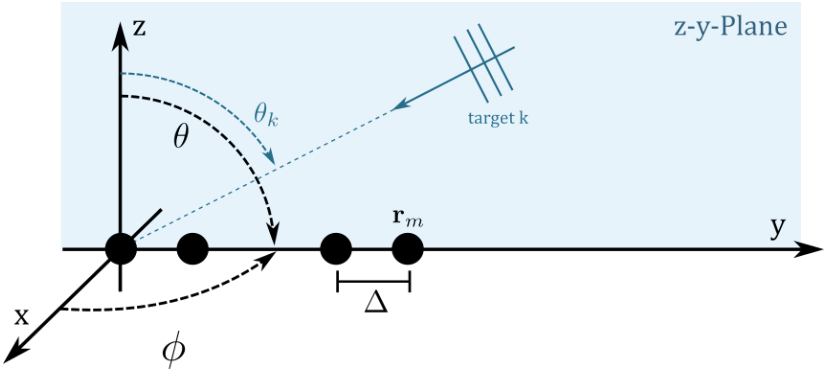

Figure 2.2: Incident plane of target return signals and sensor placement into a linear array. An exemplary target is shown with its incident angle denoted as θ_k

Let K be the number of sources present in the scene. In general, for an antenna array consisting of M antennas, the received signal at a specific antenna $m = 1, \ldots, M$ in the antenna array is given by the sum of all impinging signals with a time delay τ_{mk}

and a noise term n_m. The time delay τ_{mk} is taken with respect to the first element of the antenna array, which is often considered coinciding with the origin of the reference system and this is adopted here as well [79]:

$$y_m(t) = \sum_{k=1}^{K} s_p(t - \tau_{mk}) + n_m(t) \tag{2.1}$$

Now taking into account the far-field assumption resulting in incoming plane wave signals, the time delay τ_{mk} can be expressed as $\tau_{mk} = \mathbf{k}^T \mathbf{r}_m$ [79]. Here, $\mathbf{r}_m$ is the position of the m'th antenna in three-dimensional space and $\mathbf{k}$ denotes the propagation direction expressed depending on the angles of arrival ϕ, θ, of azimuth and elevation, respectively:

$$\mathbf{k} = \begin{bmatrix} \sin\phi_k \cos\theta_k \\ \sin\phi_k \sin\theta_k \\ \cos\theta_k \end{bmatrix} \tag{2.2}$$

Within the scope of this work, linear, 1-dimensional arrays are considered, which will simplify the expressions a bit. To this end, the elements are formally placed along the y-axis of the coordinate system (see figure 2.2). Reducing the DoA estimation problem to a one-dimensional angle estimation problem, let $\phi = 90^\circ = \pi/2$ such that the plane of incidence for incoming signals becomes the z-y-plane as depicted in figure 2.2, and the propagation direction reduces to

$$\mathbf{k} = \begin{bmatrix} \cos\theta_k \\ \sin\theta_k \\ 0 \end{bmatrix} \tag{2.3}$$

With the sensor elements placed along the y-axis at positions spaced by Δ, the position vectors become

$$\mathbf{r}_m = \begin{bmatrix} 0 \\ (m-1)\Delta \\ 0 \end{bmatrix} \tag{2.4}$$

As a result, the expression for the time delays simplifies to

$$\tau_{mk} = \mathbf{k}^T \mathbf{r}_m = k(m-1)\Delta \sin\theta \tag{2.5}$$

where $k = \frac{2\pi}{\lambda}$ is the propagation constant in free space. By furthermore expressing the sensor spacing in units of wavelength as $d = \Delta/\lambda$, the incurred time delay at each sensor can be expressed as $\tau_{mk} = 2\pi d(m-1)\sin\theta$.

The signal vector received by the antenna array is obtained by stacking each array output into a vector as $\mathbf{y} = [y_1(t), \ldots, y_M(t)]$. Performing the Fourier transform on this array output, due to the well known shift property of the Fourier transform and the plane wave assumption, the time delays τ_{mp} become phase shift terms as $e^{-j\omega\tau_{mp}}$. Expressing this for the $M \times 1$ data vector $\mathbf{y}$ leads to the commonly found model for the received data:

$$\mathbf{y} = \sum_{k=1}^{K} \mathbf{a}(\theta_k) s_k + \mathbf{n} \tag{2.6}$$

where the phase shifts for each element have been stacked into the *steering vector* [79] $\mathbf{a}(\theta_k) \in \mathbb{C}^M$ as

$$\mathbf{a}(\theta_k) = \begin{bmatrix} 1 \\ e^{j2\pi d sin(\theta_k)} \\ \vdots \\ e^{j2\pi(M-1)d sin(\theta_k)} \end{bmatrix} \tag{2.7}$$

Further combining the steering vectors for each source K into a $M \times K$ matrix as $\hat{A} = [\mathbf{a}(\theta_1), \ldots, \mathbf{a}(\theta_K)] \in \mathbb{C}^{M \times K}$, referred to as *steering matrix* [79], equation 2.6 can be compactly expressed as

$$\mathbf{y} = \hat{A}\mathbf{s} + \mathbf{n} \tag{2.8}$$

with $\mathbf{s} \in \mathbb{C}^K$ now indicating the amplitudes of the K source signals and $\mathbf{n}$ accounts for measurement noise in each sensor.

It should be pointed out that the problem given in equation 2.8 is not linear in the unknown DoA parameters θ_k, since they are located in the exponents of the steering matrix $\hat{A}$ [37]. A common approach is therefore adopted here, which then also enables the application of the BCS framework to this type of problem. The angular range over all possible θ is discretised into a grid of G equally spaced angles $\hat{\theta}$. The steering matrix can then be generated as an over complete dictionary matrix $A \in \mathbb{C}^{M \times G}$ where each column is a steering vector $\mathbf{a}_g = \mathbf{a}(\theta_g)$ with $g = 1, \ldots, G$ corresponding to each possible source direction. Furthermore, since the number of sources K is typically not known, the vector of signal coefficients $\mathbf{s} \in \mathbb{C}^K$ is now expanded into a sparse vector $\mathbf{x} \in \mathbb{C}^G$ with unknown support $\mathbf{s}$, corresponding to actually present targets at those angles. The resulting data model is denoted as

$$\mathbf{y} = A\mathbf{x} + \mathbf{n} \tag{2.9}$$

This overcomplete dictionary matrix $A \in \mathbb{C}^{M \times G}$ can now directly be used in the CS framework, abiding to an on-grid method. As a consequence of this angular discretisation, target DoAs which do no fall exactly onto one of the G angles will lead to different degrees of estimation inaccuracies, depending on the resolution of the angular grid. To complete the signal model and prepare it to be used with the BCS algorithm in [28], the complex valued representation given in equation 2.9 is expanded into a real valued equation as proposed in [37]:

$$\begin{bmatrix} \Re(\mathbf{y}) \\ \Im(\mathbf{y}) \end{bmatrix} = \begin{bmatrix} \Re(A) & -\Im(A) \\ \Im(A) & \Re(A) \end{bmatrix} \begin{bmatrix} \Re(\mathbf{x}) \\ \Im(\mathbf{x}) \end{bmatrix} + \begin{bmatrix} \Re(\mathbf{n}) \\ \Im(\mathbf{n}) \end{bmatrix} \tag{2.10}$$

where $\Re(\cdot)$ and $\Im(\cdot)$ denote the real and imaginary part, respectively. Using this expansion, the dimensions of the involved quantities are doubled.

2.2. MIMO DATA MODEL

The use of radar has become a key ingredient in current generations of automotive technology and the ones to come. In this sector of technology, radar devices are typically of small size, have a considerably lower range, lower power consumption and lower cost than their counterparts in military or airborne applications [80]. Among the alternatives, Multiple In Multiple Out (MIMO) technology has received a lot of attention among

automotive radar manufacturers as it is able to provide a high angular resolution by synthesising a larger amount of virtual antennas with only a few physical transmit and receive antennas as described in section 2.3. Autonomous radar typically operates in the frequency bands at 24GHz and 77GHz, while the latter one is preferred in newer generations [80]. The common choice of waveform is the Frequency-Modulated Continuous-Waveform (FMCW) waveform (chirp), which is a complex sinusoidal signal with its frequency modulated over a certain modulation time period. In this thesis, a **linear FMCW chirp** is considered, where the chirp frequency f_T is linearly modulated along a certain bandwidth B over a time interval T as:

$$f_T(t) = f_c + \frac{B}{T}t \tag{2.11}$$

where f_c denotes the central carrier frequency and $t \in [0, T]$. This is continuously repeated with a period T_{PRI} called Pulse Repetition Interval (PRI) [80]. After transmission in the high-frequency band and reflection at the target, the signal received back at the radar receive antennas resembles a delayed and attenuated copy of the transmitted, linear FMCW chirp signal. Considering a target moving with a radial speed v at a radial distance R, the delay induced in the receive-signal can be described as

$$\tau = 2\frac{R + vt}{c} \tag{2.12}$$

In the receiver, the received signal is mixed [1] with the transmitted signal (also called *dechirped* [81]) and low-pass filtered, which yields a complex valued, sinusoidal signal called *beat signal* and has a frequency of $f_b = f_R + f_D$ called *beat frequency*. The two components in f_b are the frequency corresponding to the target's range:

$$f_R = 2\frac{RB}{Tc} \tag{2.13}$$

and the Doppler frequency induced by radial movement

$$f_D = 2\frac{f_c v}{c} \tag{2.14}$$

The beat signal is converted to the digital domain by means of an Analog to Digital Converter (ADC). The dechirped and digitised time-domain echo signal is collected into a signal vector of N_r samples. This time period of one chirp signal is commonly termed *fast time*. When multiple such chirps are collected, e.g. N_c, the time along which this is done is termed *slow time*. Furthermore, considering an array of N_{Rx} receiver antennas or channels, the well known *Radar Datacube* can be assembled as shown in figure 2.3.

To obtain the range information from the collected beat signals, a Fast Fourier Transform (FFT) is performed along the fast time, yielding an estimate of the beat frequency f_R of the beat signal, from which the target range can be calculated as [80]

$$R = \frac{f_R c T}{2B} \tag{2.15}$$

[1] Mixing entails the multiplication of two signals. This operation is typically done in the analogue part of the RF-Frontend.

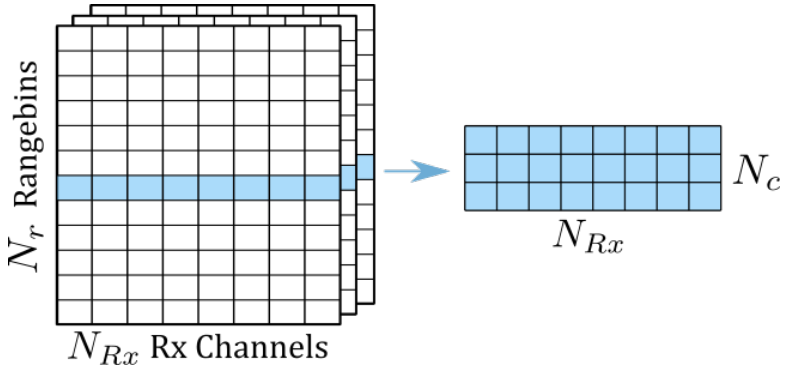

Figure 2.3: Radar Datacube on the left and the extracted range bin information (in blue). The different layers of the data cube indicate the data captured from N_c consecutive chirps (in slow time). The x-Axis shows the data for the different receiver channels, which are denoted here as N_{Rx} and can be either formed by a physical or a virtual array.

This is possible, since under automotive conditions, $f_D \ll f_R$ and f_D can be assumed constant within a chirp [80]. An important aspect of the FMCW technology is, that for signals with a *time-bandwidth product* satisfying $T \cdot B > 10$, the range resolution is described by $\Delta R = \frac{c}{2B}$, which does not depend on the sweep length but only on the modulation bandwidth. This decouples the dilemma faced in pulsed radar, where for a finer range resolution, shorter pulse lengths are required, leading to a diminished overall signal power [81].

Since the target range is obtained via the beat frequency of a target's return signal, which in turn is calculated by means of an FFT, it can be related to the number of points N_{FFT} used in the FFT as [82]:

$$R = \frac{f_R T c}{2B} = \frac{N_{FFT} c}{4B} \tag{2.16}$$

The desired maximum distance R_{max} directly corresponds to the maximum beat frequency $f_{R,max} = \frac{2R_{max}B}{Tc}$ which determines the bandwidth of the beat signal (or IF signal). As the maximum beat frequency, $f_{R,max}$, is capped by the sampling rate f_s of the ADC in the receiver chain, the maximum range of an FMCW system before ambiguities arise is given by [82]

$$R_{max} = \frac{f_s c T}{2B} \tag{2.17}$$

Similarly, as with the range information, Doppler information can be extracted by performing the FFT along the slow time, while the range frequency f_R is considered fixed across the slow time (this depends on the length of the processing interval). Transmitting pulses with a PRI of T_{PRI}, the reciprocal measure is called Pulse Repetition Frequency (PRF) and is given as $f_{PRF} = \frac{1}{T_{PRI}}$. It has to satisfy $f_{PRF} \geq 2 f_D$ to avoid that targets with a speed within the speeds of interest fold back onto the opposite of the velocity spectrum, leading to ambiguities in the radial velocity estimation. The maximum radial velocity without ambiguities is therefore given as $v_{max} = \frac{c}{4 f_c T_{PRI}}$ [80].

By performing the FFTs over fast-time (range) and slow-time (Doppler), a processing

gain is introduced, which improves the SNR and further facilitates the DOA estimation thereafter. This processing gain in units of dB can be described by [80]

$$G_{FFT} = 10\log_{10}(N_{FFT}) \tag{2.18}$$

To generate FMCW MIMO radar signals, the wideband, baseband model derived in [83] is used, and its most important aspects are reviewed here. The baseband receive signal $z_i^{(l)}(m,t')$ of the m'th pulse, reflected from a target i, arriving at the l'th array element after the dechirping operation, is described according to [83] as:

$$\begin{aligned} z_i^{(l)}(m,t') &= r_i^{(l)}(m,t') \times s^*(m,t') \\ &\approx \alpha_i \exp\left(-j2\pi(f_0+\mu t')\frac{ld}{c}\sin\theta_i\right) \\ &\quad \times \exp\left(-j2\pi(f_0\frac{2v_i}{c}Tm+\mu\gamma_i t')\right) \\ &\quad \times \exp\left(-j2\pi\mu\frac{2v_i}{c}Tmt'\right) \end{aligned} \tag{2.19}$$

where $t' = t - mT$ describes the fast-time domain with $m = \lfloor \frac{t}{T} \rfloor$. The frequency modulation rate[2] during a modulation period T_0 over a bandwidth of B is described by $\mu = \frac{B}{T_0}$. The initial round trip delay of a scattering target i is denoted as $\gamma_i = \frac{2R_i}{c} \ll T_0$. In equation 2.19, the first exponential term describes the phase shifts introduced by the displacement of the antenna elements, while the second one describes the phase shifts induced by the target's range. The last exponential is a residual coupling term between fast and slow-time. It is worth to point out, that this signal model has been derived in [83] for a wideband investigation. In this thesis, however, the signals are assumed narrowband, thus the model might be more complex than actually needed.
A typical, simplified FMCW radar block diagram is displayed in figure 2.4 where the simulated signal is indicated to give an orientation of the procedure.

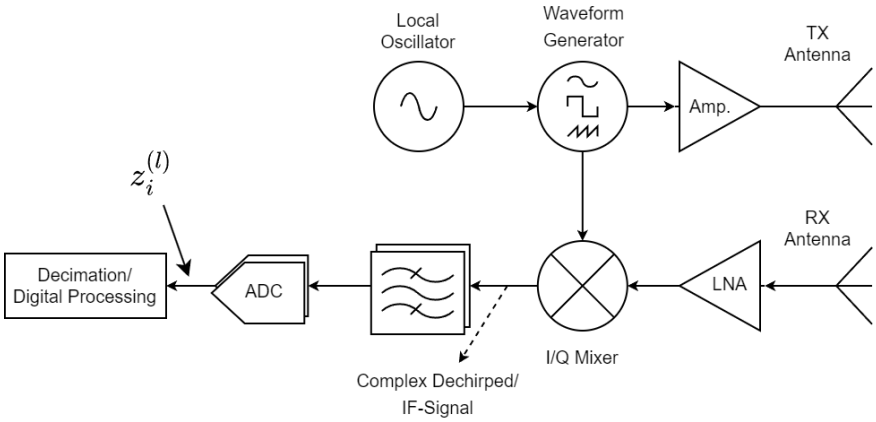

Figure 2.4: Simplified example block diagram of a FMCW transmit and receive frontend. Based on [81], [82]

[2] Also called ramp-rate or slope [81]

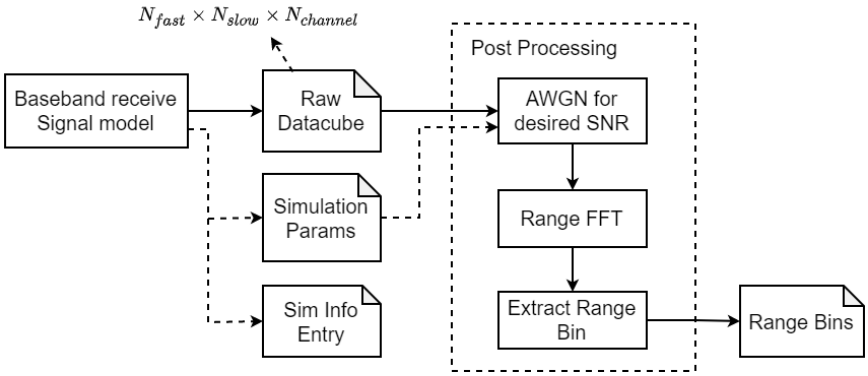

Figure 2.5: Block diagram of the simulation used in this thesis for received FMCW MIMO baseband signals based on the model that has been described in this chapter.

Based on equation 2.19, raw FMCW data is generated without any noise in the block "Baseband receive Signal model" shown in figure 2.5. Parameters are set according to the desired radar, simulation and array parameters. The data cube of dimensions $N_{fast} \times N_{slow} \times N_{channel}$ is then stored, to be loaded in a subsequent step for noise adding and extraction of the range bin of interest, as shown in the steps in figure 2.5. Specifically, additive Gaussian noise is added in the time domain to the raw receive signal. Then the range FFT is performed over the fast time domain and the range bin where the targets are located is found by a peak search. This range bin data is then extracted for all receive channels and slow-time chirps. Since the noise is added additively before the range FFT is performed, it is important to keep in mind that the range FFT induces a processing gain, described by equation 2.18. Since the range FFT is calculated with 256 samples, the resulting processing gain amounts to ≈ 24.1dB.

Finally, a matrix of dimension $N_{slow} \times N_{channel}$, containing the array data for the selected range bin of each chirp, is stored for each simulated target scene. The generated data by this pipeline is used in the remainder of this thesis for the array generation and performance evaluation.

2.3. MIMO ARRAY ARCHITECTURE

Since in this thesis a Multiple In Multiple Out (MIMO) radar is considered, the architecture of the MIMO antenna array will be described in this section. In general, MIMO radar consists of an array of $N_t \geq 2$ transmit antennas and an array of $N_r \geq 2$ receive antennas. The transmitting antennas are assumed to radiate uncorrelated signals, such that they can be distinguished in the receiver chain. Ideally, the signals radiated by each individual transmit antenna are orthogonal, which can be achieved for example by frequency division or time division multiplexing and the latter one is assumed for this thesis. Moreover, in this thesis a *colocated* MIMO architecture is considered where the transmitter and receiver array elements are closely spaced such that the target response can be assumed equal for each pair of transmitting antenna and receiving array (i.e. they have the same

viewing angle of the target). This MIMO architecture results in a virtual array, which is generated by a convolution of transmitter and receiver sensor locations. If the antenna positions of the two sub-arrays are well-designed, the resulting virtual array can have a much larger aperture than the sub-arrays and therefore offer a higher angular resolution [84]. The transmitted signal from the n_t'th transmit antenna will arrive at each receive antenna n_r with a time delay relative to their origins as $\tau_{n_t,n_r} = \tau_{n_t} + \tau_{n_r}$ [85]. Recalling the general steering vector given in equation 2.7, individual steering vectors for the transmitter and receiver arrays can be defined. Again, the sensor elements are placed linearly along the y-axis as shown in figure 2.2 and their positions in units of wavelengths are denoted as [72]:

$$y_{t,i} = (i-1)d \quad i = 1,\dots,N_t \tag{2.20}$$

$$y_{r,j} = (j-1)d \quad j = 1,\dots,N_r \tag{2.21}$$

where again $d = \lambda/\Delta$. Then the individual steering vectors for the transmitter and receiver array can be written similar to equation 2.7 as [72], [85]

$$\mathbf{a}_t(\theta) = [e^{-j2\pi y_{t,1}\sin(\theta)},\dots,e^{-j2\pi y_{t,N_t}\sin(\theta)}] \tag{2.22}$$

$$\mathbf{a}_r(\theta) = [e^{-j2\pi y_{r,1}\sin(\theta)},\dots,e^{-j2\pi y_{r,N_r}\sin(\theta)}] \tag{2.23}$$

The resulting virtual array is then given by the Kronecker product of the two steering vectors [85]:

$$\begin{aligned}\mathbf{a}_v &= \mathbf{a}_t \otimes \mathbf{a}_r \\ &= [e^{-j2\pi(y_{t,1}+y_{r,1})\sin(\theta)},\dots,e^{-j2\pi(y_{t,1}+y_{r,N_r})\sin(\theta)},\dots,e^{-j2\pi(y_{t,N_t}+y_{r,N_r})\sin(\theta)}]\end{aligned} \tag{2.24}$$

When the elements of both receiver and transmitter arrays are placed linearly along the y-axis of the reference system (refer to figure 2.2), the time delays τ_{r,n_r} and τ_{t,n_t} follow the same expression as given in equation 2.5. Therefore, the positioning of the antennas is very important for the resulting virtual array structure. This is illustrated with two examples for a 2×2 MIMO array in figure 2.6. Observe how the spacing between transmitter elements can create overlapping elements when chosen smaller than $\Delta \times N_{Rx}$. The placement of transmitter and receiver elements offers a certain amount of Degrees of Freedom (DOF) to create desired virtual arrays.

Taking into account the new steering vector given in equation 2.24, the steering matrix introduced in section 2.1 is now constituted of rows given by equation 2.24. Taking again $\theta = \theta_g$ and $g = 1,\dots,G$ for each possible look direction, the overcomplete dictionary matrix $A_v \in \mathbb{C}^{N_v \times G}$ can be defined, where the first dimension results from the number of virtual array elements given as $N_v = N_t \cdot N_r$. The resulting data model can then again be written as shown in equation 2.9.

2.4. COMPRESSIVE SENSING FRAMEWORK

The general Bayesian Compressive Sensing (BCS) framework is very similar to the classical Compressive Sensing (CS) framework in terms of its linear model, the sparseness requirements and the goal of the reconstruction. To give a consistent introduction to the

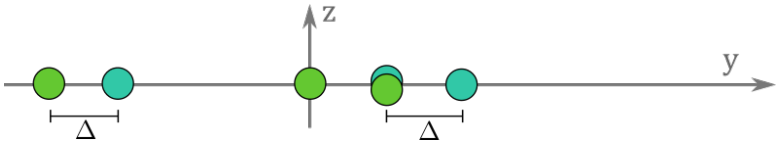

(a) Example 1: The spacing between the transmitter elements (left) creates overlapping virtual receiver elements (right).

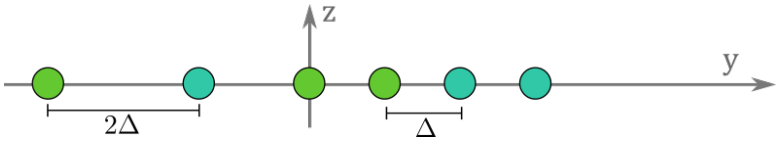

(b) Example 2: The spacing between transmitter elements is now equal to the spacing of the receiver elements multiplied by their number, in this case 2. The resulting virtual array has now all-unique element positions.

Figure 2.6: Two examples showing the concept of the MIMO array. It visualises the design choices regarding the placement of the sensors.

theory, the classical CS framework is briefly described, before turning to the Bayesian perspective.

It has been shown in literature [10], that a lot of natural signals that are non-sparse in one representation space, e.g. time, can be represented equivalently using only a few coefficients and a corresponding transform basis. An example of such a basis is the wavelet transform basis, which enables the representation of signals in terms of a dictionary of frequencies. Those frequency components are often sparse and thus offer a way of compression for such signals. This has been driven further, exploiting the compressibility of a signal, in order to take fewer measurements (compressive measurements) of a signal in the first place, offering a potential to save cost and complexity in the sensing hardware system [10], [86]. Specifically, a signal vector $\mathbf{x}$ may be represented in terms of a set of basis vectors which are multiplied by corresponding weights [86]:

$$\mathbf{x} = \sum_{n=1}^{N} s_n \psi_n = \Psi \mathbf{s} \tag{2.25}$$

with $\mathbf{s}$ a $N \times 1$ vector containing those weights or coefficients of the signal in the basis, which is defined by a set of orthonormal basis vectors $\Psi = [\psi_1, \psi_2, \ldots, \psi_N]$ [3]. If a generally non-sparse signal vector $\mathbf{x}$ can be expressed in a basis that results in a sparse vector $\mathbf{s}$, the signal is said to be compressible [86]. With increasing redundancy in the signal information contained in $\mathbf{x}$, the coefficient vector $\mathbf{s}$ contains fewer $K \ll N$ significant coefficients, i.e. having few values considerably larger than zero, and is called "K-sparse". Values in $\mathbf{s}$ can be seen as projections of the coefficients in $\mathbf{x}$ onto the basis vectors in Ψ as $s = \Psi^T \mathbf{x}$ [4]. This scheme requires the signal in its original basis to be non-sparse,

[3] In the DoA estimation problem, the signal of interest, namely the angular energy distribution, is already sparse and Ψ is therefore taken to be a "spike" base as $\Psi = \mathbf{I}_N$. Therefore, $\mathbf{x} = \mathbf{s}$

[4] Consider Ψ^T to be a Fourier transform matrix, to see the analogy of few Fourier coefficients for a non-sparse time signal

which is linked to the requirement of incoherence. Incoherence in this context refers to the relation between the original and the sparse domain of the signal. If the two are incoherent, the signal vector $\mathbf{x}$ will be non-sparse in one domain, while being sparse in the other [9], [86]. To generalise the CS scheme to arbitrary signals, an intermediate transform domain is introduced [86]:

$$y = \Phi\mathbf{x} \tag{2.26}$$

where Φ denotes the $M \times N$ "sensing matrix" with columns ϕ_n, $n = 1, \ldots, N$, being the basis vectors of the intermediate domain and $\mathbf{y}$ now being the $M \times 1$ compressed measurement vector. A common choice for this intermediate transform matrix, i.e. the sensing matrix, is a random transform domain, which has been shown to satisfy the incoherence requirement with high probability [9]. Having this sensing matrix available for design, it can be implemented on a hardware level, allowing for sub-Nyquist sampling [86]. For this thesis, Φ will be constituted from the steering vectors of the antenna array, yielding the steering matrix A, as it is this matrix that is used to "sense" the spatial signals.

One of the quests for this thesis entails the search for a good "design" of the sensor array. This will amount to activate or deactivate sensors at certain locations, which can directly lead to a reduction in hardware complexity, cost and energy consumption. The process can be included into the model equations via a matrix $J = \text{diag}(w_1, \ldots, w_M)$, called selection matrix hereafter. The diagonal elements w_m will determine whether the corresponding sensor is included or excluded from the measurement. Combining equations 2.25, 2.26 and the selection matrix, the three described matrices (Ψ, Φ and J) can be collected into one $M \times N$ compressed transform matrix Θ:

$$\mathbf{y} = J\Phi\mathbf{x} = J\Phi\Psi\mathbf{s} = \Theta\mathbf{s} \tag{2.27}$$

The final goal becomes that of inverting 2.27 to recover the coefficients $\mathbf{s}$, which since problem 2.27 is an underdetermined system of equations, is ill-posed. Only by utilising the assumed sparsity property, a unique solution can be found, namely the sparsest one. The straightforward formulation of the reconstruction problem is by means of an ℓ_0-pseudo norm optimisation problem, which can theoretically recover the sparse $\mathbf{s}$ exactly. However, as this combinatorial search problem is computationally intractable, the most popular relaxation via the ℓ_1-norm has led to the convex optimisation problem [87]:

$$\hat{\mathbf{s}} = \arg\min_{\mathbf{s}} \|\mathbf{s}\|_1 \quad \text{subject to} \quad \Theta\mathbf{s} = \mathbf{y} \tag{2.28}$$

which is also commonly known as Basis Pursuit (BP) [87]. Another, very similar found formulation, which also accounts for noise in the measurements is known as least absolute shrinkage and selection operator (LASSO), formulated as [9]:

$$\hat{\mathbf{s}} = \arg\min_{\mathbf{s}} \|\mathbf{s}\|_1 \quad \text{subject to} \quad \|\Theta\mathbf{s} - \mathbf{y}\|_2 \leq \epsilon \tag{2.29}$$

where ϵ is a parameter that has to be carefully, heuristically determined to bound the noise in the data [9]. Yet another version of the above problem form is the ℓ_1 regularised formulation by use of Lagrangian multipliers, given as [28]:

$$\hat{\mathbf{s}} = \arg\min_{\mathbf{s}} \|\mathbf{y} - \Theta\mathbf{s}\|_2^2 - \rho\|\mathbf{s}\|_1 \tag{2.30}$$

which is given here as a reference for later, since it allows for an insightful comparison with the BCS framework, introduced in section 2.5.
In the classical compressive sensing literature, properties of the matrix Θ have been worked out to guarantee recoverability. Specifically, it is required that Θ has a sufficient degree of linear independence to guarantee robustness in the underlying inversion problem, which has been expressed by the Restricted Isometry Property (RIP) [13], [88].

This RIP condition has been further elaborated and a more computationally feasible condition which approximates the RIP has been developed under the name of "Mutual Coherence" regarding the matrix Θ [66]. It has been observed, that under selection of the sensing matrix Φ to be a random matrix, good RIP as well as the mutual coherence properties can be obtained [87]. It is worth noting here, that those requirements are only valid for the classical, deterministic CS recovery. The focus will later be turned towards a statistical approach with the Bayesian Compressive Sensing (BCS) framework, where those requirements have, to the best of the author's knowledge, not been developed yet [74].

2.5. BAYESIAN COMPRESSIVE SENSING (BCS) FRAMEWORK

Based on the works of Tipping *et al.* in [27], [30], [31], the BCS framework has been generally introduced in [28] and [33]. It will be briefly introduced here, before making the connection to the DoA estimation problem.

The Bayesian aspect comes into play, when the inversion or recovery of the sparse weights $\mathbf{s}$ is performed. As it is typical in Bayesian statistics, a prior belief is formulated in terms of a Probability Density Function (PDF), that in the transform basis Ψ the vector of weights $\mathbf{s}$ is sparse. It is then aimed to compute a posterior PDF about this vector $\mathbf{s}$. Due to this full posterior PDF, also confidence metrics about the estimates are provided, as well as an estimate for the noise variance.
At this point it is again important to note, that in the DoA estimation framework, the transform matrix Ψ is taken to be a spike basis, i.e. $\Psi = \mathbf{I}_N$ with $\mathbf{I}_N$ being an identity matrix, since our signal of interest is already sparse. This will give from equation 2.25 that $\mathbf{x} = \Psi\mathbf{s} = \mathbf{I}_N\mathbf{s} = \mathbf{s}$. The signal of interest, i.e. the sparse vector of coefficients indicating the DoA of targets present in the scene, is denoted simply as $\mathbf{x}$ from now on. Consequently, the sensing matrix will be denoted as $\Theta = J\Phi$, yielding the following notation of the system of linear equations:

$$\mathbf{y} = J\Phi\mathbf{x} = \Theta\mathbf{x} \tag{2.31}$$

Finally note, that for the sake of readability, the sampling matrix J is omitted for this section, indicating that the full sensor array, i.e. full Φ is utilised. It will be reintroduced, when array generation is discussed in chapter 3.
Following the assumption of sparsity of $\mathbf{x}$, the $N \times 1$ vector can be split into two vectors of equal size $N \times 1$. One containing all zero entries except for the largest coefficients in $\mathbf{x}$, termed $\mathbf{x}_s$, the other one with all zero entries except for the smallest entries in $\mathbf{x}$, termed $\mathbf{x}_e$. The CS measurement equation introduced earlier in equation 2.26 can be reformulated as [28]:

$$\mathbf{y} = \Phi\mathbf{x}_s + \Phi\mathbf{x}_e = \Phi\mathbf{x}_s + \mathbf{n}_e + \mathbf{n}_m = \Phi\mathbf{x}_s + \mathbf{n} \tag{2.32}$$

where in the last step of equation 2.32, the influence of $\mathbf{x}_e$ has been concluded as noise $\mathbf{n}_e$ and measurement noise has been introduced as $\mathbf{n}_m$ [5]. Both noise contributions are assumed to be Gaussian distributed and are summarised into the Gaussian noise vector $\mathbf{n}$ with zero-mean and unknown variance σ^2. The Gaussian assumption for the noise will now result in the likelihood model [28]:

$$p(\mathbf{y}|\mathbf{x},\sigma^2) = \frac{1}{(2\pi\sigma^2)^{K/2}} \exp\left\{-\frac{1}{2\sigma^2}\|\mathbf{y}-\Phi\mathbf{x}\|_2^2\right\} \tag{2.33}$$

A full posterior PDF is now sought for $\mathbf{x}$ and σ^2, while the matrix Φ and the CS measurement vector $\mathbf{y}$ are known. To enforce sparsity onto the weights $\mathbf{x}$, a sparsity promoting prior probability is imposed, similar to the selection of a sparsity promoting norm in the standard CS inversion. A popular choice for such a prior is the Laplace PDF [28]. Under such a choice and the likelihood in 2.33, point estimates for $\mathbf{x}$ could be obtained by using the Maximum a Posteriori (MAP) estimate, which would correspond to the result given by the ℓ_1-regularised problem in equation 2.30 [28]. To obtain a full posterior density for the weights $\mathbf{x}$, however, the full Bayesian formulation has to be evaluated. Since the Laplace PDF is not conjugate prior to the Gaussian likelihood, the posterior cannot readily be evaluated in closed form [23], [28]. The adopted method in [27], [28] is therefore to utilise a hierarchical prior, which has similar sparsity promoting characteristics but results in closed form expressions. To this end, a zero-mean Gaussian density is defined as the prior probability on each element in $\mathbf{x}$:

$$p(\mathbf{x}|\alpha) = \prod_{i=1}^{N} \mathcal{N}(x_i|0,\alpha_i^{-1}) \tag{2.34}$$

where $\alpha = [\alpha_1,\ldots,\alpha_N]$ is the precision of each Gaussian density, and $\alpha_i^{-1} = \sigma_i^2$ the *variance* of each distribution for x_i. Now *hyperpriors* are imposed upon the *hyperparameters* α and the noise variance σ^2, where its precision is denoted by $\beta = 1/\sigma^2$ [27]. Since the hyperparameters resemble *scale* parameters, the hyperpriors are chosen to be Gamma distributions, as they feature only positive values [27]:

$$p(\alpha) = \prod_{i=0}^{N} \Gamma(\alpha_i|a,b) \tag{2.35}$$

$$p(\beta) = \Gamma(\beta|c,d) \tag{2.36}$$

In [27], the hyperparameters a, b, c and d are all set to zero. That way, uniform or "improper" hyperpriors are obtained, which provide the property that results will not depend on the unit of measurement and furthermore will simplify the derivations later on. Moreover, this enables the posterior probability to accumulate more at very large values at some hyperparameters α. The posterior of the corresponding weights will then peak around zero, "turning-off" those weight inputs and their associated basis functions (columns in Φ). This elimination process is causing the sparsity properties, and the remaining weights are termed "relevant" vectors. As a visual example of the effects of sparsity promoting prior distributions, see figure 2.7

[5] Since the interest always lies in the sparse weight solutions, the subscript s is dropped in what follows

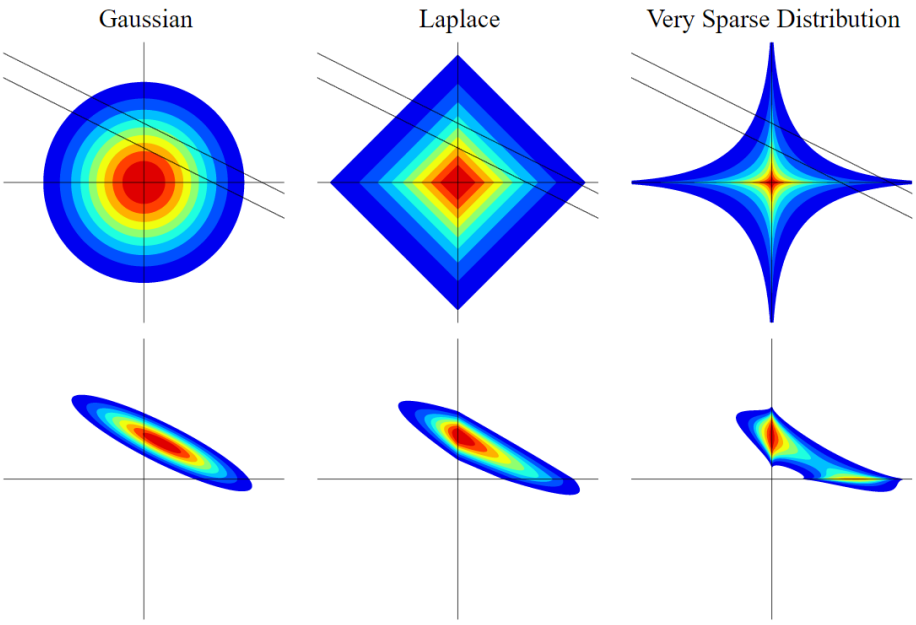

Figure 2.7: Upper row: Contour plots of a Gaussian, Laplace and a very sparse distribution $P(a_i) \propto \exp(-T|a_i|^{0.4})$ Lower row: Contour plots of the posterior distributions. It can be seen, how the probability mass is dragged onto the axes by the sparsity promoting priors, while for the Gaussian prior the majority of the probability mass lies somewhere off-axis. Note the similarity of the Laplace prior distribution and the ℓ_1-norm. Figure from [75]

The ultimate quantity of interest is the full posterior density describing all unknown parameters $\mathbf{x}, \alpha$ and σ^2 and can be expressed as:

$$p(\mathbf{x}, \alpha, \sigma^2|\mathbf{y}) = \frac{p(\mathbf{y}|\mathbf{x}, \alpha, \sigma^2)\, p(\mathbf{x}, \alpha, \sigma^2)}{p(\mathbf{y})} \tag{2.37}$$

Since the normalising constant in equation 2.37 cannot be calculated in closed form, the posterior is decomposed into [27]:

$$p(\mathbf{x}, \alpha, \sigma^2|\mathbf{y}) = p(\mathbf{x}|\mathbf{y}, \alpha, \sigma^2)\, p(\alpha, \sigma^2|\mathbf{y}) \tag{2.38}$$

In this form, the posterior over the weights $p(\mathbf{x}|\mathbf{y}, \alpha, \sigma^2)$ can be evaluated in closed form (because the likelihood and prior in 2.39 are Gaussian) as a multivariate Gaussian distribution [27], using Bayes' equation:

$$p(\mathbf{x}|\mathbf{y}, \alpha, \sigma^2) = \frac{p(\mathbf{y}|\mathbf{x}, \sigma^2)\, p(\mathbf{x}|\alpha)}{p(\mathbf{y}|\alpha, \sigma^2)} \tag{2.39}$$

$$= \frac{1}{(2\pi)^{(N+1)/2}|\Sigma|^{1/2}} \exp\left\{-\frac{1}{2}\|\mathbf{x} - \mu\|^2_{\Sigma^{-1}}\right\} \tag{2.40}$$

with mean and covariance given as:

$$\Sigma = (\sigma^{-2}\Phi^T\Phi + A)^{-1} \tag{2.41}$$

$$\mu = \sigma^{-2}\Sigma\Phi^T\mathbf{y} \tag{2.42}$$

and the definition $A = \text{diag}(\alpha_0, \alpha_1, \ldots, \alpha_N)$. Note here the dependence on the unknown hyperparameters α as well as on β. The second term in equation 2.38, namely the hyperparameter prior $p(\alpha, \sigma^2|\mathbf{y})$ is approximated as [27]:

$$p(\alpha, \sigma^2|\mathbf{y}) \propto p(\mathbf{y}|\alpha, \sigma^2)p(\alpha)p(\sigma^2) \tag{2.43}$$

and this equation 2.43 is to be maximised with respect to α and β, where under the previously made choice of uniform hyperpriors ($a = b = c = d = 0$), only the first term on the right-hand-side of equation 2.43 remains. By marginalising ("integrating out") over the unknown weights $\mathbf{x}$, a closed form solution is obtained as [27] [6]:

$$p(\mathbf{y}|\alpha, \sigma^2) = \int p(\mathbf{y}|\mathbf{x}, \sigma^2)p(\mathbf{x}|\alpha)d\mathbf{x} \tag{2.44}$$

$$= \frac{1}{(2\pi)^{N/2}|C|^{1/2}} \exp\left\{-\frac{1}{2}\mathbf{y}^T C^{-1}\mathbf{y}\right\} \tag{2.45}$$

with $C = \sigma^2\mathbf{I} + \Phi A^{-1}\Phi^T$. This expression is known as the marginal likelihood or "evidence function" for the hyperparameters [23], [24], [27]. The process of its maximisation, or more commonly its logarithm:

$$\mathscr{L}(\alpha) = \log p(\mathbf{y}|\alpha, \sigma^2) \tag{2.46}$$

$$= -\frac{1}{2}\left[Nlog(2\pi) + log(|C|) + \mathbf{y}^T C^{-1}\mathbf{y}\right] \tag{2.47}$$

is termed as *type-II maximum likelihood* or "evidence procedure" [27]. Since the maximising α and σ^2 for equation 2.44 cannot be acquired in closed form, it might be done in an iterative fashion by the Expectation Maximisation (EM) algorithm, a popular tool when it comes to maximisation when multiple unknown hyperparameters are involved [23]. The type-II ML procedure estimates α and β as point estimates [23], [28]. In [27] and [30], an efficient iterative algorithm is derived. During the iteration process, most of the hyperparameters α_i (representing the precision) tend to infinity and peak very sharply, following that the posterior distribution of those corresponding weights, $p(x_i|\mathbf{y}, \alpha, \sigma^2)$ will peak infinitely high at zero. Therefore, after taking observed data, namely the CS measurements $\mathbf{y}$ into account, there is a high certainty that those weights are zero and can be pruned away, hence realising the sparsity property [27]. Building upon the analysis in [30], an efficient algorithm for the RVM inversion is provided in [31], which starts with an empty model and iteratively adds or removes basis functions. Those basis functions are ultimately columns in Φ, each corresponding to the steering vector of a possible signal DoA. The deletion process distinguishes it from other CS algorithms like OMP and StOMP, where added basis functions are not removed. This likely explains the improved sparsity of this algorithm, as it has been investigated in [28].

[6] This marginal likelihood is found in the denominator of equation 2.39 and its maximisation amounts to the well known model selection in Bayesian inference [89].

2.5.1. MULTI-TASK BCS - EXPLOITING STATISTICAL INTERRELATION

The BCS framework described in the previous section represents the most popular formulation, which can be found in many publications working with this topic. However, this framework usually performs the regression task with only one CS measurement of the data (one CS measurement refers to one vector of samples). Even if a set of L measurements $\{\mathbf{y}_i\}_{i=1,\dots,L}$ has been obtained, the original BCS framework would be utilized in a way that it performs the inversion tasks individually for each $\mathbf{y}_i$. However, if the measurements $\mathbf{y}_i$ are statistically related, there can be a benefit if the algorithm takes this into account by sharing information between the regression tasks during the inversion process. Such cases can be, for example, when the underlying measured signal is not changing rapidly, such that L consecutive measurements may be combined. This can be assumed for example in radar applications, where the target scene is nearly constant between L consecutive chirps. A BCS algorithm that takes such statistical interrelation into account has been developed in [33], based on prior work in [33] and [31]. Again, a hierarchical Bayesian model is derived, only this time each regression task, working locally with its own single CS measurement vector $\mathbf{y}_i$, shares information with other tasks via a common prior density function, used and learned by all L tasks. Placing this common or global prior is the means by which tasks share information, and it is a popular method for information sharing in learning and regression literature [33]. Describing the full derivative steps here would not add a lot of valuable information to this thesis, so the reader is referred to [33] for detailed derivations. For this thesis, only the most important key points of this modified method will be summarized.

- The use of the common prior, which has been introduced for the single task method in equation 2.34, also means that the hyperparameters α are now shared and used by all L regression tasks. Conversely, these hyperparameters and therefore the common prior is learned in a combined manner by the information of all the L individual tasks. This way, the information of each CS measurement vector $\mathbf{y}_i \in \{\mathbf{y}_i\}_{i=1,\dots,L}$ is influencing the learning of both the common prior, and the individual learning tasks.

- It is important to note at this point, that if the CS measurements in $\{\mathbf{y}_i\}_{i=1,\dots,L}$ have no or only little statistical relation (for example when the radar scene has changed dramatically), then there can be no benefit in sharing the information. This has been validated in [33], leading to the fact that in such cases, single-task learning even outperforms the multi-task one.

- In a further modification to the algorithm, Ji et al. integrate out the noise variance parameter α_0, thus avoiding the need to estimate it, relaxing the Gaussian assumption for the noise and improving robustness.

Ji et al. provide a fast iterative scheme for their new algorithm in [33] very similar to the one developed in [31] and provide their code online, which can be found here: `https://github.com/shihaoji/bcs`. This version of the algorithm has been used throughout this thesis. It is referred to simply as BCS whenever it is used with a single snapshot (single task) and as MT-BCS when multiple snapshots have been used (multi-task).

2.6. PROJECTION OPTIMISATION

Recapping the important underlying assumption in compressive sensing, it is generally assumed that measurements are taken randomly. The measurement or sensing matrix Φ, which generates the CS measurements (refer to equation 2.27), is under this assumption constituted of M rows as $\Phi = [\mathbf{r}_1, \ldots, \mathbf{r}_K]^T \in \mathbb{C}^{M \times G}$, with G denoting the number of discretised steering directions. The question to ask is now, what new measurements could be added to a set of initial measurements (i.e. new rows in the sensing matrix), such that they optimally facilitate the DoA estimation process using the RVM/BCS method. This question has been addressed for a general BCS use case in [34]. The key part and major novelty in the BCS framework compared to other compressive sensing techniques is the availability of uncertainty measures in the form of the covariance matrix, as in equation 2.41.

Running the inversion algorithm once, estimates of the weight's mean values μ_x and their covariances Σ_x are obtained. The estimated DoA is obtained by the index of the non-zero coefficients (or mean values). The decisive information lies in the covariance Σ_x. By having this information available, the computation of the *differential entropy* of the reconstructed signal is proposed as [34]:

$$\begin{aligned} h(\mathbf{x}) &= \frac{1}{2}\log|B\Sigma_x B^T| + c \\ &= \frac{1}{2}\log|\Sigma_x| + c \\ &= -\frac{1}{2}\log|A + \alpha_0 \Phi^T \Phi| + c \end{aligned} \tag{2.48}$$

where $A = diag(\alpha_1, \ldots, \alpha_N)$. The differential entropy corresponds to the Shannon entropy of a continuous random variable, which can be understood as the minimum descriptive complexity of a random variable or a measure of its average uncertainty [90]. This function constitutes what is referred to as a *utility function* in the literature of Bayesian Experimental Design. Optimising the measurements with respect to the entropy, specifically, is called *D-Optimality* [78].

The goal is now to select a new measurement, or in our case a new sensor position, which would be optimal in the sense of minimizing the differential entropy, i.e. the average uncertainty of the variable. The new measurement must be designed such that it adds the most informative new information, or the data which has been most uncertain. In [34], it is proposed to add new measurement projections based on the Eigenvalue analysis of the covariance matrix Σ, which has similarity with the topics of Principal Component Analysis (PCA) and the Singular Value Decomposition (SVD). It is therefore worth exploring these connections to gain more intuitive understanding.

Performing the eigenvalue decomposition of Σ yields a factorisation of the form

$$\begin{aligned} \Sigma &= Q\Lambda Q^{-1} \\ &= Q\Lambda Q^H \end{aligned} \tag{2.49}$$

where Q denotes a square, unitary and orthonormal matrix of eigenvectors with the corresponding eigenvalues placed accordingly in the diagonal matrix Λ. By definition, such

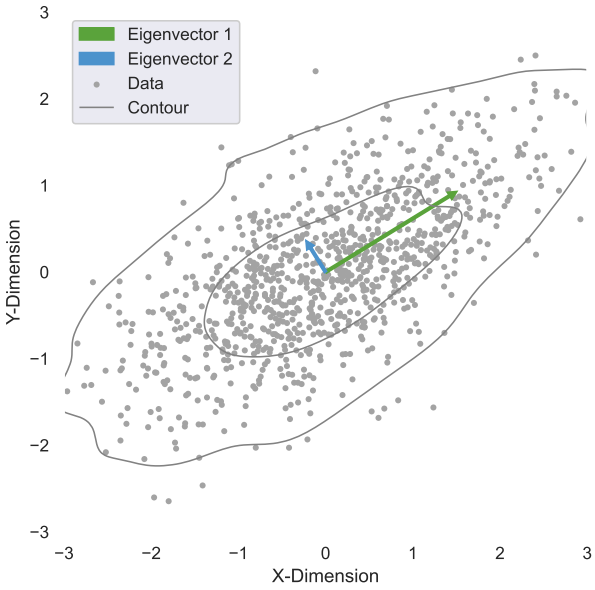

Figure 2.8: Visual example for a two-dimensional dataset and the eigenvectors of its covariance matrix. Observe how the largest eigenvector points into the direction of most variance.

a decomposition can always be obtained for a covariance matrix [91]. The covariance matrix can be interpreted as defining the variance or "spread" of the data, as well as the orientation of the data. Following this point of view, the eigenvectors of the covariance matrix point in the directions of uncertainty or variance, while the eigenvalues give information about the degree of uncertainty, i.e. the spread. This allows to find the "direction" of maximum uncertainty, by selecting the eigenvector with the largest corresponding eigenvalue. This is illustrated in figure 2.8 for a 2D case, where the largest eigenvector (green) points into the direction of the largest spread of the data points. In [34], this geometrical interpretation is used to generate the new projection or measurement (new row in the sensing/dictionary matrix), which is taken to be exactly that eigenvector.

Another intuitive, geometric observation can be made. The goal is to reduce the entropy, which is a measure of average uncertainty and directly related to the determinant of Σ_x (see equation 2.48). Since the determinant can be interpreted as a measure of volume spanned by a matrix [92], the goal is to reduce this volume. Equivalently, the determinant of the eigenvectors scaled by their eigenvalues should be minimised along with the entropy, which would correspond to the multidimensional volume spanned by the degrees of uncertainty, expressed by the eigenvectors.

However, in our model for the radar DoA estimation, the sensing matrix is not a random matrix, but rather the array manifold matrix with columns obtained from discretised steering directions. Each row is directly related to an analogue antenna position.

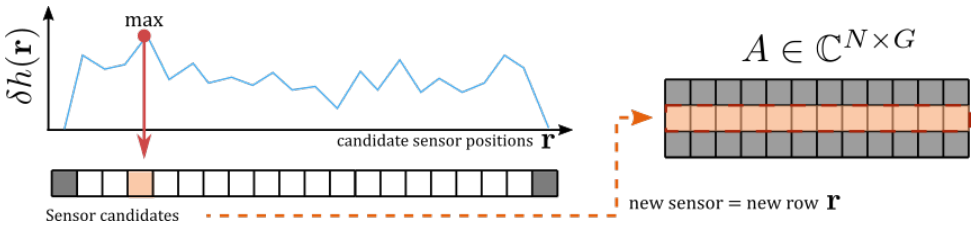

Figure 2.9: Visualisation of the concept of checking each candidate sensor location and adding the one which achieves max δh.

Taking the eigenvector of Σ_x with maximum eigenvalue as a new measurement, is not realisable in terms of antenna array geometry. The differential entropy therefore has to be minimised in another way. To this end, each new candidate sensor location along a search space has to be evaluated in terms of how including this measurement would benefit the minimisation of the entropy. In [34], an update equation is proposed which allows testing a new candidate row for how much it reduces the entropy if it is included into the sensing matrix:

$$h_{new} = h_{old} - \frac{1}{2}\log(1 + \alpha_0 \mathbf{r}_{new} \hat{\Sigma}_x \mathbf{r}_{new}^H) \tag{2.50}$$

Here, α_0 denotes the noise variance, $\hat{\Sigma}_x$ is the estimate of the covariance matrix obtained in the previous run of the BCS algorithm and $\mathbf{r}_{new}$ denotes a new candidate row of the sensing matrix Φ, which in the radar case is equivalent to a row of the steering matrix. Therefore, adding a new candidate row amounts to including a new candidate sensor location. It is at this point important to remember, that the steering matrix has been expanded to real values as shown in equation 2.10. The estimated covariance matrix $\hat{\Sigma}_x$ therefore also abides to this expansion. This has to be taken into account and is further discussed in chapter 3. The important term is the second one in equation 2.50. In order to minimize the entropy with each new sensor as much as possible, the second term has to be maximized for each new candidate. This term is defined as [34], [74]:

$$\delta h(\mathbf{r}_{new}) = \log(1 + \alpha_0 \mathbf{r}_{new} \hat{\Sigma}_x \mathbf{r}_{new}^H) \tag{2.51}$$

where the nomenclature δh is borrowed from [74], where this has been recently applied to sonar technology. The procedure is visualised in figure 2.9. This idea, which is a very general concept for no specific application, is in this thesis adopted to radar antenna arrays in order to realize a sparse spatial sampling in the angular domain. The developed algorithms for ULA and MIMO antennas, based on 2.48 and 2.51, are described in chapter 3.

2.7. SYSTEM ASSUMPTIONS WITHIN THIS THESIS

RADAR based DoA estimation, (Bayesian) compressive sensing and sparse array architectures are all large areas of research on its own. However, the scope of this thesis is specifically focused on the generation of sparse array structures for one-dimensional DoA estimation with the use of Bayesian compressive sensing. Sparse array structures can deliver several benefits, such as reduced hardware cost, complexity and energy consumption. The assumptions and boundary conditions to confine the scope of this thesis are clearly summarised in this section.

- The targets are considered to be placed in the far field of the radar. This is also reflected in the data model and the used data simulation framework.
- An On-Grid BCS framework is used within this thesis. The grid size of the dictionary matrix (the steering matrix in practice) is chosen appropriately for the expected target's angular separation.
- The aperture of the sensor arrays that are generated is fixed to the maximum aperture that is provided by the TI cascade evaluation board. This is done by fixing the two sensors at the outermost edges of the sensor array to be always included. This way, the array generation problem is confined by the available hardware, however it can easily be adjusted for different preferences. More detail about the used hardware as well as the radar parameters that are used in the TI cascade evaluation board is given in chapter 4.
- The possible sensor locations are fixed to a grid which is based on a ULA with 86 sensors and spacing of $\frac{\lambda}{2}$. This is done, again, to be able to use the generated arrays with the available hardware. The proposed method, however, can also be applied to other design guidelines.
- The DoA estimation is considered for a one-dimensional angular domain (azimuth DoA estimation)
- The simulated and measured targets have been placed at the same radial distance to the radar, such that they are in the same range bin. To reduce unnecessary computational load in empty range bins, the DoA estimation is only performed on the range bin where the targets are present.
- An estimated number of 1 to 5 targets in one range bin has been chosen to represent example scenarios.
- Based on typical applications in automotive radar, an FOV of $\pm 40°$ corresponding to mid-range radar has been considered [39]. This is the FOV region where targets are considered and placed in both simulation and measurement setup.
- The MIMO array architecture relies on orthogonality of the transmitting waveforms. In this thesis, this orthogonality is achieved in time by activating one transmitter after the other. The waveform that is modelled and used in practice is a linear FMCW chirp.

3

Proposed, Entropy-based, Sparse Array Generation

It is pointless to do with more what can be done with fewer.

William of Ockham

Based on section 2.6 in the previous chapter, it will be described now how the theory is applied to sensor arrays in order to reduce the number of sensors utilized, starting from a full ULA (either physical or virtual by means of a MIMO architecture). This will be investigated separately for the physical ULA in section 3.2 and the MIMO case in section 3.3. Since the project was planned with the aim in mind, that these arrays should be tested with real, measured data, some simulation and array parameters are fixed to match those of the available hardware (namely the Texas Instruments AWR2243 Cascade evaluation board, whose parameters will be described in chapter 4). The resulting, sparse arrays will then be further investigated and evaluated with respect to their performance using data simulated with the model described in chapter 2 and then with real measured data. To access the performance, the metrics of Root Mean Square Error (RMSE) of the angle estimates, the Receiver Operating Characteristic (ROC) curves and the Jaccard index (intersection over union) will be used. How these metrics have been computed is described in more detail in the appendix B. These metrics provide a means for the engineer to finally pick a level of array sparsity with feasible performance. It is shown, that the entropy based sensor-placement can reduce the overall uncertainty faster than randomly added sensor positions. Furthermore, it is shown with different case studies that this method can generate sparse arrays which outperform random ones, and can successfully detect and estimate target DoAs with very few sensors.

3.1. PRELIMINARIES

BEFORE describing the algorithms in detail, a few important initializations will be noted here. Referring back to the introduction of the compressive sensing framework in chapter 2, recall the selection matrix used to activate or deactivate certain sensor locations (corresponding to rows in the sensing matrix Φ), denoted as $J = \text{diag}(w_1, \ldots, w_M)$. In this case, for the physical ULA array arrangement, each weight $w_i \in \{w_1, w_2, \ldots, w_M\} \equiv W_{ULA}$ will take on a value of either zero or one, corresponding to either excluding or including this sensor location into the array, respectively. To keep a fixed aperture, and therefore a fixed native angular resolution of the array, the two elements at the borders of the array w_1 and w_M will be set to one (included) and not be changed during the algorithm.

In the MIMO case, the weights are separated into the weights for the Tx and Rx elements as $w_i^{Tx} \in \{w_i\}_{i=1,\ldots,M_{Tx}}$ and $w_i^{Rx} \in \{w_i\}_{i=1,\ldots,M_{Rx}}$, respectively. Their combination results in a set of virtual weights, denoted as w_i^{Vx}. To ensure, again, that the largest possible aperture is obtained, the border elements of both Tx and Rx weights are set to one as $w_1^{Tx} = w_{M_{Tx}}^{Tx} = 1$ and $w_1^{Rx} = w_{M_{Rx}}^{Rx} = 1$.

The algorithm can also be understood as a thinning algorithm working backwards. Considering a fully filled physical ULA with 86 sensor elements (or a MIMO array with the same number of virtual receivers), the algorithm starts with all but 2 sensors (for maximum aperture) deactivated and subsequently reactivates sensors that lead to most improvement with respect to the uncertainty in the recovered signal (which is measured via the entropy). The resulting thinned array is not expected to have a better performance than the fully filled array. It will be rather the question of how few sensors are enough, to achieve an acceptable performance. Optimisation in this scenario means, that the number of antennas is reduced, while the included antennas are placed in a way that they reduce the uncertainty in the inversion (as assessed via the Entropy) as good as possible. Table 3.1 shows important global parameters, that are set for the ULA and the MIMO algorithm versions in this thesis. Notice, that the base grid which gives the possible sensor locations consists of 86 elements. In the MIMO case, this refers to the number of unique virtual receiver-sensor locations. This number has been chosen to correspond with the resulting number of virtual sensors provided by the Texas Instruments cascade evaluation board, but it could also be applied to any other one dimensional sensor arrangement. This way, the generated antenna arrays can directly be tested with real captured data. Furthermore, targets are placed within a field of view region of $\pm 40°$, according to mid-range radar [3]. It is noted here that the observation has been made, that a larger field of view leads to generally more required sensors.

As the proposed algorithm needs to run the (MT-)BCS algorithm in order to obtain an estimate of the covariance matrix, the method will inherently also be dependent on the input data it is given. This will be the extracted range bins of simulated FMCW data for different scenarios. After simulation of the FMCW receive data and addition of white, Gaussian noise, a range FFT is performed to acquire the beat frequency bins and finally the range of the simulated point targets. These are all placed on the same range bin to obtain single, spatial measurement vectors with the dimension equivalent to the number of sensors (in this thesis 86). The range bin is then cut out and stacked into a matrix for each simulated FMCW chirp (refer to figure 2.3 in chapter 2). This data will be used

Parameter	Value
No. of positions (ULA/virt.)	86
Sensor Spacing	$\lambda/2$
SNR (before range FFT)	15dB
Grid-Spacing	0.5° or 1.0°
FOV	± 40°
No. of Training Scenes	100
Target Range	30m
Target RCS	1 (fixed for all)

Table 3.1: Parameters for the entropy-based sensor placement algorithm confined to a ULA sensor grid

Simulation ID	No. of targets	Description
S1	2	Separation < 1.33° (≈ 0.5°)
S2	5	Separation ≫ 1.33°
S3	5	Mixed separations
S4	2	Separation > 1.33°

Table 3.2: Summary of the simulated data for the subsequent performance assessments. The targets have been placed in FOV region of ±40° for all simulations.

as input to the proposed array generation algorithm, as well as the subsequent performance assessment. Different scenarios have been simulated, where targets are spaced closer or further apart in the angular domain than the resolution limit of 1.33°. Note that in all cases, targets are not placed on the DoA grid that is used for the BCS based estimation, which will inevitably induce off-grid errors but provides a more realistic scenario. A reference table of the main simulated scenarios is given in table 3.2.

3.2. ALGORITHM: IMPLEMENTATION FOR PHYSICAL ULA

This version of the algorithm is considering a physical ULA, placing one new sensor at each iteration until a fully filled, physical ULA is obtained. At its core, it runs the (MT-)BCS algorithm to obtain an estimate of the covariance matrix Σ and is therefore reliant on a set of training scenes. This estimate of Σ, which gives an estimate of uncertainty of the recovered, sparse vector of coefficients, which directly relates to the DoA estimates, is then used to compute the update equation 2.51 in order to find the next row that should be added to the steering matrix. The algorithm repeats these steps in an iterative manner, until all possible sensor locations have been included. After this procedure, further analysis can aid in deciding a level of array sparsity which achieves sufficient performance in terms of detecting the targets and estimating the angles. The block diagram in figure 3.1 describes the high-level procedure for adding new sensor elements to an initially empty uniform linear array. A more mathematical formulation of the algorithm is provided in the appendix A.1.

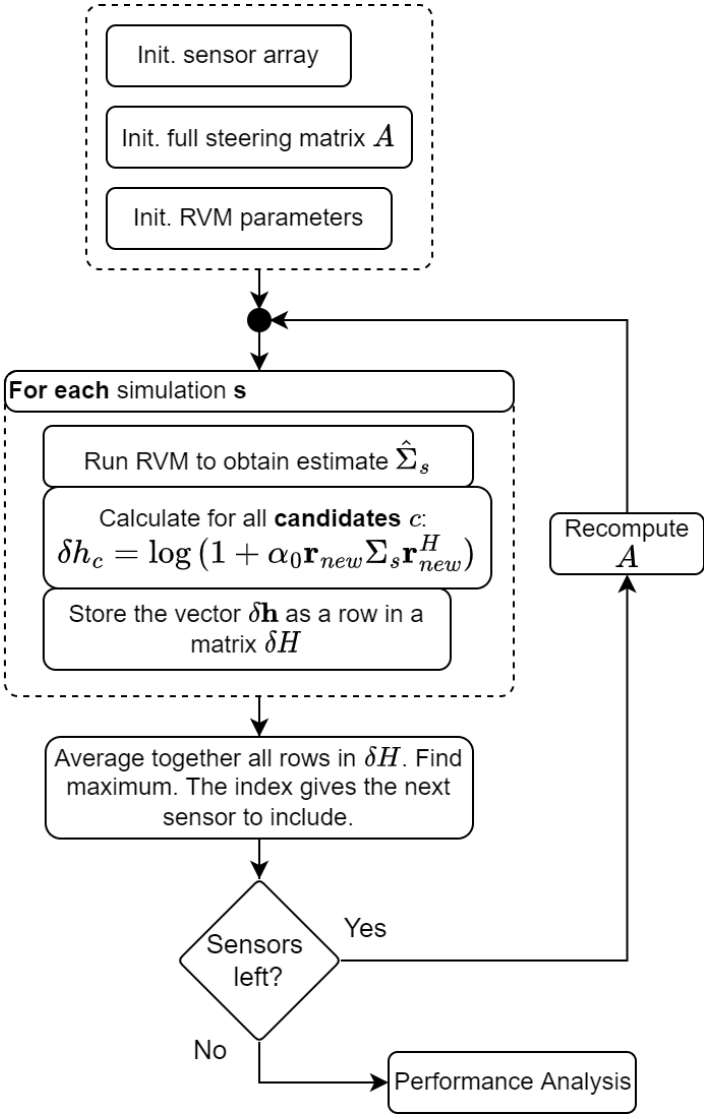

Figure 3.1: Overview block diagram of the entropy based sensor inclusion algorithm for the ULA case. It is important to note, that the algorithm will run until all possible sensor positions are included. A stopping criterion (i.e. maximum number of antennas) could be added depending on the use case.

The central part that is generated by the algorithm is a reduced steering matrix along its rows, which serves as the dictionary matrix given to the (MT-)BCS algorithm. The columns of the steering matrix, which correspond to possible target locations (basis functions), are not altered during the process and depend on the angular grid resolution that has been chosen. Since the steering matrix is a complex-valued matrix but the used (MT-)BCS algorithm has been developed for real valued input data, a few extra

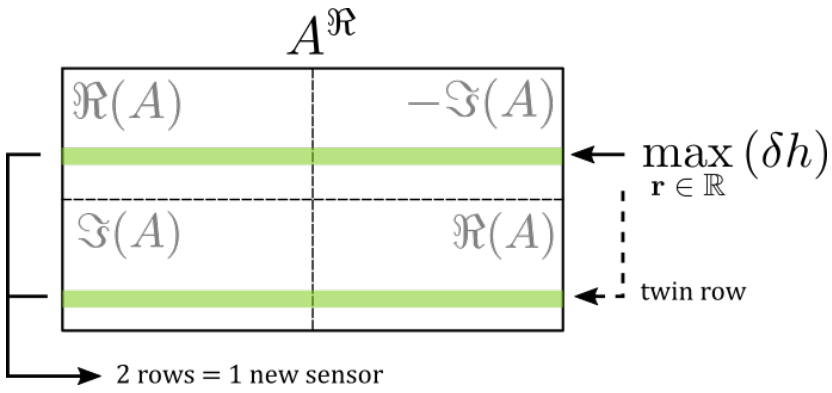

Figure 3.2: Conceptual visualization of the relationship between sensor elements and rows in the expanded steering matrix. The upper row is the one for which the entropy update equation achieves a maximum. However, adding the corresponding sensor will add the lower row as well due to the matrix expansion from a complex to a real valued one.

steps are necessary. In chapter 2, equation 2.10 it has been described, how the steering matrix is expanded to obtain a real valued matrix as input for the RVM. The algorithm described in this chapter therefore needs to take this into account, since it is looking for a new row to add to the steering matrix (corresponding to a new sensor). However, as the steering matrix is split, each sensor corresponds to two rows in the expanded steering matrix. Therefore, when the algorithm selects the row from the expanded steering matrix that achieves the highest score for δh, also its twin-row resulting from the expansion will be included, to represent correctly the new sensor location. It is observed, that the secondary row does generally not score a high value for δh. It is argued that this will most likely not result in a performance degradation, as with each new sensors, two rows and therefore more information is added to the system. However, it should be noted that the proposed update equation given in 2.51 has been derived for only one single new measurement (i.e. row). Figure 3.2 visualizes the described relation.

During the procedure, at each iteration, the entropy calculated with equation 2.48 is tracked. The resulting progression plot gives insight into how the uncertainty is reduced with each new sensor, and might give a first indication about the minimum number of sensors needed to be included into the array. As an example case, figure 3.3 shows how the entropy is reduced with each new included sensor when using the entropy based method and compared to the entropy achieved by a randomly filled array.

It has been observed, that the elbow change in the entropy progression marks a point at which the estimation algorithm (the RVM) is able to recover the true targets and their DoAs. Before that point, too few sensors and therefore spatial measurements are provided, and the algorithm generates target estimates rather randomly. After the elbow point, the correct targets can be recovered and adding more sensors leads to further reduction of uncertainty. This observation leads to the expectation, that from a certain number of included sensors, the algorithm could achieve acceptable performance and the corresponding sparse array can be picked out. During testing, the algorithm has been run with different training scenes, resulting in different behaviour of the entropy

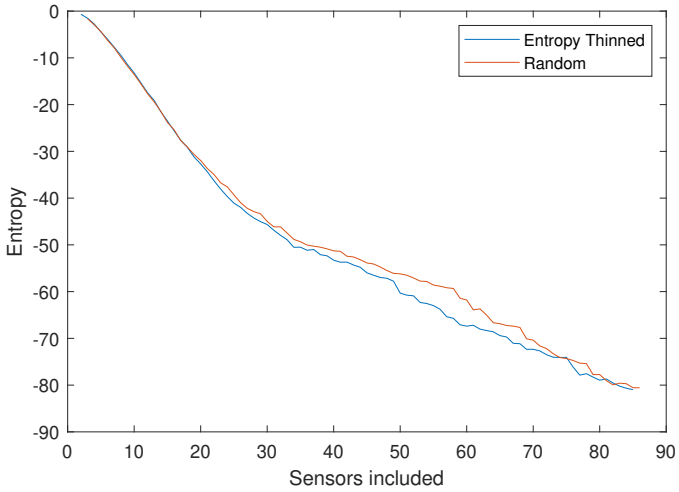

Figure 3.3: Example entropy progression when 5 targets are present in the training scenes. Note the slight elbow-like change in entropy at about 30 included sensors, when the array reaches a certain number of included sensor positions.

while more sensors are added:

- Increasing the number of targets: When fewer targets are present in the training scenes, the elbow-like change is more pronounced than with increasing number of targets.
- Reducing the step size of angular discretization: The RVM needs a matrix of basis vectors, which is provided by the steering matrix. To compute the steering matrix, the angular domain has to be discretized with a certain grid size. Making the grid finer has shown to also lead to a more pronounced elbow-like change in the entropy plot.

However, this elbow point is not always as pronounced, further performance assessment of the array in conjunction with the RVM should be done to guide the array-sparsity choice. This is described in section 3.4.

3.3. ALGORITHM: IMPLEMENTATION FOR MIMO ARRAY

The procedure described before for the physical ULA has been extended for the MIMO radar case. The MIMO array architecture naturally provides a more challenging scenario, since the resulting virtual receiver array that is used in the DoA estimation is the result of two separate arrays, the physical transmitter and receiver array. Running the algorithm for the virtual array, thereby treating it as a ULA, will lead to the problem of factorizing this array into a transmitter and receiver array afterwards. This is not a trivial task, and it might be, that this factorization cannot be found (especially when overlapping virtual elements are considered). In this thesis, an iterative approach is taken, where at each iteration a new element is added to either the transmitter or the receiver array. The decision, again, is made based on the entropy but of the resulting virtual array. This way guarantees, that no virtual arrays are obtained that cannot be realised in terms of transmitter and receiver arrays. The procedure is described schematically in 3.4 and a more mathematical description is provided in the appendix, A.2.

Due to the MIMO architecture, adding a new sensor element to either of the two arrays, might lead to more than one new element in the virtual array. The method therefore has fewer degrees of freedom for placing new sensors than in the ULA case. For this thesis, the array layout of the TI cascade evaluation board has been adopted as noted in section 2.7. As many of the resulting virtual receiver sensors occupy the same spatial position, the relation between added physical sensors and resulting virtual sensors changes from the typical MIMO layout case. The array layout of the TI board is described in chapter 4. Due to the expansion of the steering matrix to real values, each of the new virtual sensors leads to two new rows in the expanded matrix, similar as in the physical ULA case. In total, this can cause the addition of a multitude of rows to the steering matrix, which is illustrated in figure 3.5.

There are some challenges with this MIMO version of the algorithm that have been observed:

- The algorithm seems to add a lot of physical transmitter elements early during the filling process. This could be due to the fact, that adding a new transmitter sensor amounts to more added virtual receiver sensors, which are also more distributed across the whole span of the array. Since transmitter elements are typically more expensive from a hardware and energy consumption point of view, a higher cost within the algorithm could be added to the addition of transmitter elements in a future version of the algorithm.

- The entropy update equation which is used (equation 2.51) is based on the theory for adding one single new measurement [93] (i.e. adding one row to the steering matrix). With one added measurement, the covariance matrix should be re-estimated and then a next measurement position can be sought. In the MIMO case, this is unfortunately not possible, due to the addition of multiple virtual sensors at each step (which correspond to the added measurements). It is therefore hard to access, whether the entropy is maximally reduced with each step. Furthermore, it cannot be prevented that also those virtual sensors that add only little new information are added to the array.

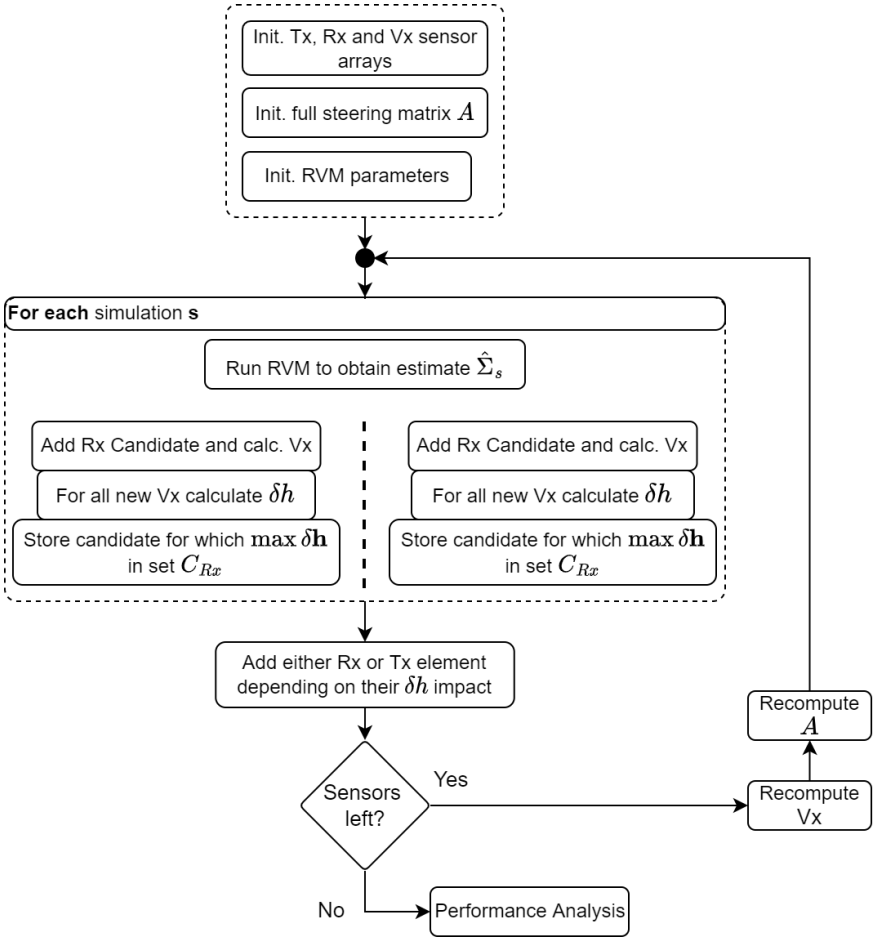

Figure 3.4: Overview block diagram of the entropy based sensor inclusion algorithm for the MIMO case.

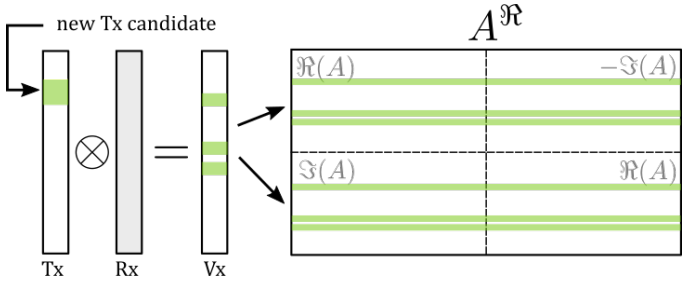

Figure 3.5: Exemplary illustration of the relation between new sensors in the Tx MIMO array, resulting new sensors in the virtual array and finally new rows in the expanded steering matrix. The Rx MIMO array is considered unchanged in this example.

3.4. EVALUATING THE DETECTION AND ESTIMATION METRICS

The described algorithms can deliver different arrays, depending on when it is decided to stop the addition of new elements. It is important to note, that this method is not intended to provide *the one best array* to work in all application scenarios. It is rather intended to provide a pipeline that can help to reduce the number of elements in a controlled manner (via the entropy), which yields sparse/thinned arrays that perform well on average in certain scenarios. Nevertheless, a criterion is needed to estimate a feasible level of sparsity. As a first measure, the progression of the entropy is analysed. This progression is the result of the thinning process as described in sections 3.2 and 3.3, by storing the current entropy value for each iteration.

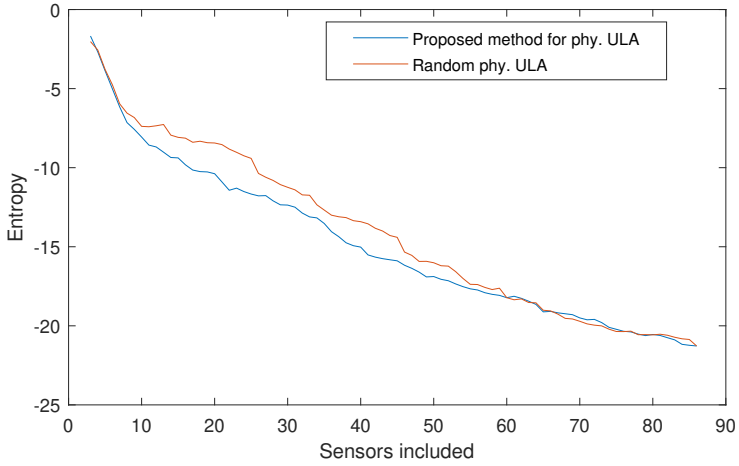

Figure 3.6: Example for the entropy progression in the physical ULA case, when running on scenes with 2 targets. For each step on the x-Axis, a new sensor location has been added to the ULA based on the best improvement of Entropy.

An exemplary entropy-plot is shown in figure 3.6 for a sparse ULA (section 3.2) and training scenes with 2 targets. It is compared against a purely randomized addition of new sensor locations. As can be seen, the entropy based method shows a faster and more stable reduction in entropy, until an elbow-like change happens. It can therefore be argued, that compared to randomly generated sparse arrays, the proposed algorithm offers a method that searches for the next sensor that decreases the uncertainty the most, and therefore leads to a faster and more stable entropy reduction. Although this elbow-like change is not always as pronounced as in this case (e.g. a higher number of targets has been observed to soften this elbow), it is worth to investigate. It has been observed, that before the point of this elbow, which in figure 3.6 appears between 10 and 20 elements, the RVM algorithm is not able to reconstruct the correct coefficients and the result is rather random. From the elbow onwards, however, the algorithm converges to a result that includes the correct coefficients with very high probability. Including even more sensors from this point further reduces the remaining uncertainty (as measured

by the Entropy). It is therefore argued, that the entropy progression might serve as a first indicator and rough estimate of the least number of sensors that is required for the MT-BCS method to work. The same observation is made for the MIMO case.

As has been mentioned, the entropy progression might serve as a first indicator of when the least amount of sensors has been reached, but is not always as prominent as shown in the example cases. Furthermore, the MT-BCS method is acting like an estimator and a detector at the same time. The resulting vector of coefficients returned from the (MT-)BCS method is sparse and as such already acting like a kind of detector. At the same time, the detected or non-zero coefficient's locations within the return vector are the angle estimate. In order to deal with coefficients that are non-zero only by a small amount, a method of thresholding needs to be implemented, common to detector problems. Therefore, a second stage of evaluation is proposed, which will look at the Receiver Operating Characteristic (ROC) when the arrays of different sparseness are used. In addition to that, a metric called the *Jaccard Index* will be utilized similar to [74], since it includes the number of true positives (TP), false positives (FP) and false negatives (FN) in one, scalar value. This allows the comparison of the detector performance summarised in the Jaccard index against a range of possible candidate thresholds. As used in [74], the Jaccard index is defined as

$$\text{Jaccard} = \frac{\text{TP}}{TP + FP + FN} \tag{3.1}$$

As a first step, each array stage along the sensor addition process is utilised in the MT-BCS method. For each array, a range of thresholds is used, providing a matrix of array versus threshold data. The data that is stored for each point on this matrix are the number of false positives (FP), number of false negatives (FN), number of true positives (TP) and the Jaccard index calculated from the three. A two-dimensional map of array sparsity vs threshold can be plotted, indicating the Jaccard index by the colour values. This way, a parameter pair that scores the best performance in terms of the Jaccard index can be selected. Lastly, the ROC curves are plotted for a selected set of array-sparsity stages. To summarise, three stages are proposed to select a sparse array that performs well on average with respect to detection and estimation metrics:

- Entropy progression, providing first insight into the least amount of sensors needed. Depending on the training simulations, the described elbow might not be as pronounced.
- Jaccard index, enabling the combined performance analysis for the two parameters of array sparsity and detection threshold.
- ROC curves for a closer look, after the first rough parameter region has been determined by the former two methods.
- Lastly, the DoA estimation error is assessed via the RMSE.

For a better visual overview, the steps are shown in the block diagram shown in figure 3.7.

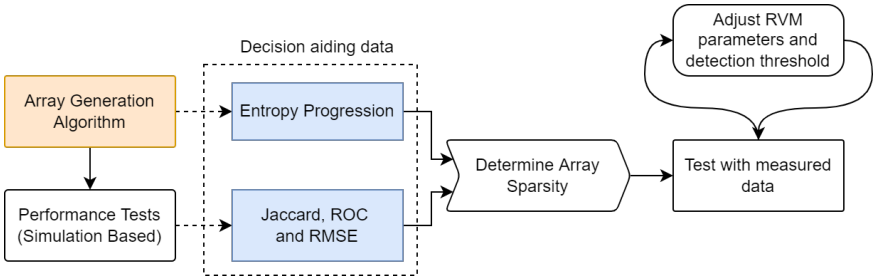

Figure 3.7: Visual block diagram of the array generation procedure proposed in this thesis.

In the next section, generated arrays are tested with simulated data for three different case studies:

1. 5 targets that are separated in azimuth by more than the array resolution (the resolution using a ULA). This is to test the general estimation and detection performance of the algorithm without looking at the super-resolution capabilities.

2. 2 targets that are spaced closer than the native array resolution, specifically to test the super resolution capabilities of the arrays.

3. Scenes with 5 targets and mixed angular separations (can also be closer than the array resolution).

3.5. CASE STUDY 1: 5 TARGETS WELL SEPARATED

For the first case study, the generated arrays are tested with simulated scenes that feature 5 targets placed in a field of view region of $\pm 40°$. The minimal distance between two targets in this case is never closer than the Rayleigh resolution limit of the underlying array aperture, which in this case of $86 \cdot \frac{\lambda}{2} \approx 16.96$cm is $\Delta\theta \approx 1.33°$. The steering matrix that is input to the BCS method and determines the angular resolution capabilities is therefore set to 1°, which will be sufficient for each simulation in this case. The BCS method is used as a single-task method using only one snapshot. It will be pointed out, where applicable when more than one snapshot has been used and the method is referred to as MT-BCS (multi-task BCS). Figure 3.8 shows the entropy progressions for the physical ULA and the MIMO cases, that have been tracked during the array generation procedure. It is visible, that the proposed algorithm successfully achieves a faster reduction in entropy for both ULA and MIMO, with each new sensor that is added, when compared to a randomly generated array.

The next step is to look at the Jaccard index, as it gives an indication at what point the number of correctly detected targets (true positives) is greater than the number of false positives and false negatives. The scenes used for testing are again generated with 5 targets, but noise has been added to achieve an SNR of between 15dB and -20dB, such that the method can be tested under good SNR conditions and rather bad ones. It is important to recall that the noise is added as additive Gaussian noise before performing the range FFT. Through the range FFT, there is an additional FFT gain of about 25dB

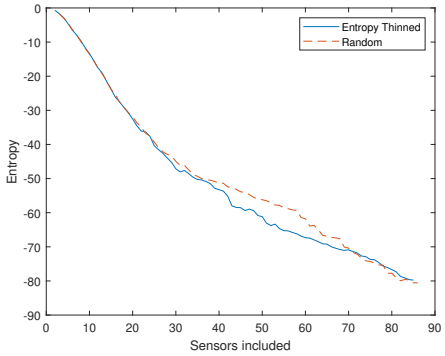

(a) Entropy progression of the ULA algorithm

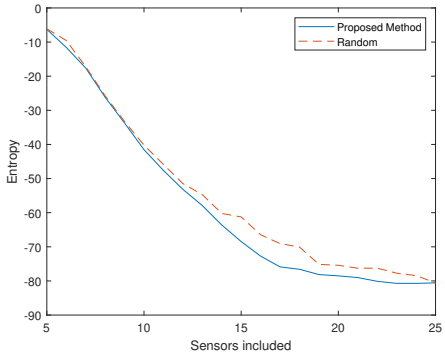

(b) Entropy progression of the MIMO algorithm

Figure 3.8: Entropy progressions for the ULA (left) and MIMO (right) architectures during the array generation process.

(refer to equation 2.18), leading to improved SNR conditions. Using the Jaccard index allows plotting it against a threshold used for the target detection.

The two plots in figure 3.9 show, how the Jaccard index is used as a metric to get insight into how many sensor elements might be sufficient for good detector performance. The Jaccard index is plotted for the physical ULA, as more sensor elements are included (x-Axis) and the detector threshold is swept (y-Axis). Bright yellow values indicate a Jaccard index closer to 1, which implies that there are very few false negatives and false positives (refer to equation 3.1). Comparing the right and the left side in figure 3.9 it can be seen how the SNR heavily influences the performance and increases the amount of sensors that have to be included in order to obtain higher Jaccard index values. While for the high SNR case, around 20 sensors start to achieve good performance, in the low SNR case as many as 40 sensors are needed. This condition can be improved to an extent by utilizing more snapshots in the MT-BCS method, leading again to a slight reduction in required sensors. Since the MIMO array has very similar plots, they are not shown here, to not overfill this chapter with too many plots.

Considering the observations made in figure 3.9, the ROC curves are plotted for exemplary, reasonable sparsity levels in figure 3.10 for both physical ULA and MIMO. It can be seen, that the proposed thinning method achieves better performance with fewer elements than if the sensors would have just been added randomly. This shows that the entropy based methods indeed provide a level of improvement (coinciding with the results in [74] from the sonar literature). Note that in the MIMO array case, shown in figure 3.10 on the right, the number of sensors, given with 9 and 10, refers to the physical Tx and Rx sensors that would constitute the resulting virtual arrays with 20 and 25 sensors, respectively. To have a fair comparison, the stages of virtual array sparsity have been matched to the randomly generated MIMO array. Furthermore, it can be observed in some instances, that the performance of the random array in terms of ROC curves comes closer to the array that has been thinned with the proposed method. It has been observed, however, that this is not always the case and there is no guarantee that a ran-

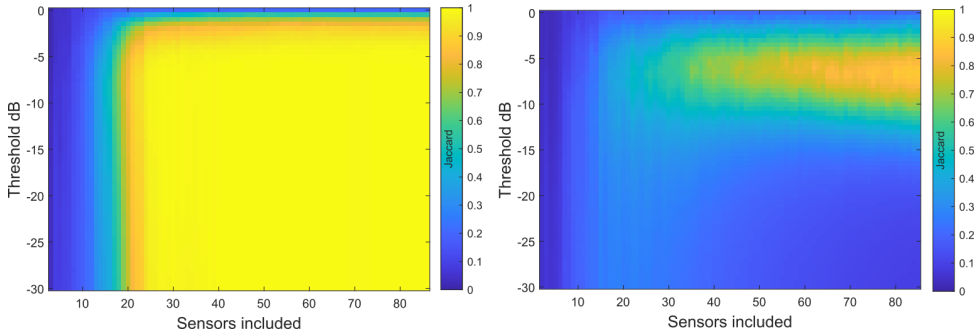

Figure 3.9: The Jaccard index plotted over the detection threshold and the number of sensors in the array. Plots shown for the physical ULA case, with SNR of 15dB (+ range FFT gain) on the left and -20dB (+ range FFT gain) on the right.

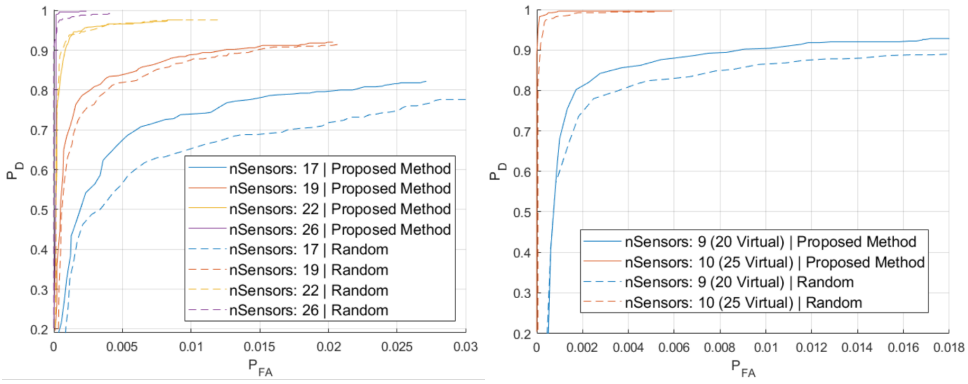

Figure 3.10: ROC curves shown for the ULA (left) and the MIMO array (right). The solid line represents the array generated by the proposed method, compared to the random one shown by the dashed line.

dom generated array will always perform similarly well as the designed one.

To give a better feeling of the potential improvement, a zoomed in version of figure 3.10 is provided in figure 3.11. For an exemplary number of 25 sensors included into the sensor array, the improvement in terms of the ROC curves is indicated for a constant false alarm probability. For the physical ULA case in figure 3.10 on the left, it amounts to an improvement of 1.4% for this study. Similarly, for the MIMO array on the right-hand side in figure 3.10, where an improvement of 1.6% is observed. With 25 sensors utilised in the array and assuming a fully filled physical ULA with 86 sensors has been the starting point, this would amount to a reduction of ≈70% of sensors.

Considering the MIMO array setup as a base, the 25 virtual sensors are constituted from 5 transmitter and 5 receiver antennas. Transferring this to the TI board, which provides 3 transmit antennas and 4 receive antennas per chip, two such chips would be necessary to realise the sparse array. This would directly translate to a reduction of 50% of the utilised chips, as two of the four implemented chips could be removed. Of course, the removal of these chips would necessitate the rearrangement of the antenna layout

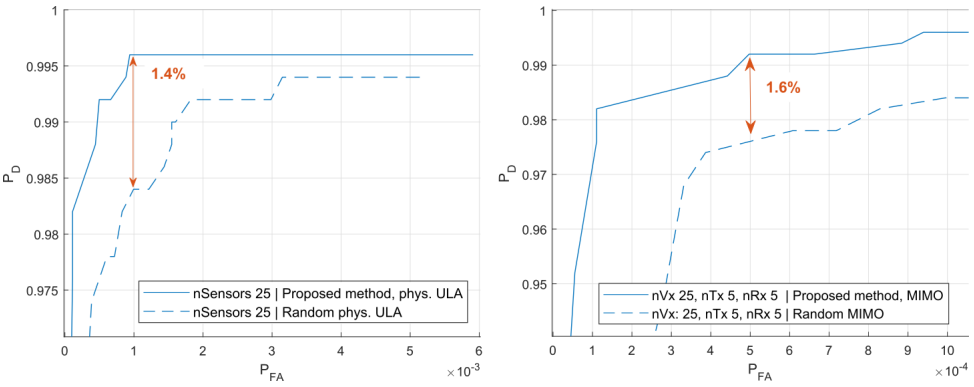

Figure 3.11: ROC curves shown for the ULA (left) and the MIMO array (right).

and the corresponding feeding circuitry. Other effects might come into play, but their assessment is not part of this thesis.

Key-Observation: In this case study of 5 targets, a possible reduction of sensors by around 70% could be achieved when a physical linear array is considered. For the MIMO case and the example of the TI board which has 4 transceiver chips, 2 of them could be removed, leading to a hardware reduction of 50%.

To assess the estimation performance, the Root Mean Square Error (RMSE) is computed for the angle estimates with respect to the known ground truth. The computation of the RMSE is described in the appendix chapter B. Figure 3.12 shows the RMSE for the physical ULA case and both levels of SNR. Again, the values and general observations for the MIMO array are very similar and therefore not included as well. It has been observed, that up to the point where the least amount of sensors is included such that the BCS can properly recover the targets, the RMSE values are very high or unrealistically low. It is however important to keep in mind, that the BCS estimation algorithm produces random estimates and often no ground truth can be associated to an estimation. The RMSE that is shown becomes meaningful only when the least amount of sensors is added, such that the BCS estimator is able to roughly recover the correct number of targets. To avoid confusion, the RMSE values are plotted from this point onwards.

Especially in the high SNR case (blue in figure 3.12), the addition of further sensors seems to have no great impact on the estimation error. Moreover, also the proposed sensor adding method does not seem to have a consistent effect on the estimation error, hinting that the array sparsity might play a more dominant role for the detection capabilities.

As a final investigation for this case study, the computation time that is needed by the BCS method (more specifically, the Relevance Vector Machine (RVM) that lies at its core) is assessed by keeping track of the iterations that are needed until the BCS algorithm converges to a reconstruction. By keeping track of the iterations rather than the exact

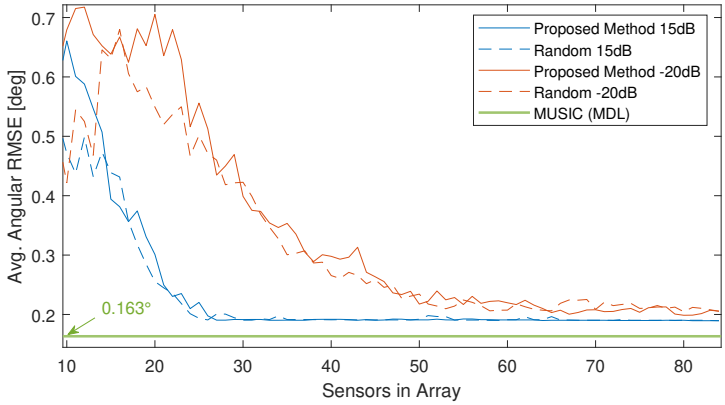

Figure 3.12: Plot of the RMSE in the angular estimation assessed with 15dB and -20dB SNR in the testing data. The MUSIC algorithm has been shown as a comparison for 15dB SNR, as it does not show a significant difference for -20dB. It is plotted as a constant line, since it always uses all 86 antennas.

time, the assessment is less dependent on the machine the algorithm has been run on, and other background tasks that could not have been controlled properly. To this end, figure 3.13 shows the number of iterations for the two inspected SNR cases. It can be seen, that for the high SNR case (blue), the number of iterations does not increase or decrease, when more sensors are added. However, for the low SNR case (red), the number of iterations increases dramatically with more sensor elements. It is argued, therefore, that for good SNR levels, the use of thinned down antenna arrays does not negatively impact the computation time of the BCS method. For low SNR levels, the sparse arrays may save iterations, but it has to be carefully checked that the arrays are equipped with enough sensors to achieve the desired detection and estimation performances.

3.6. CASE STUDY 2: 2 TARGETS WITH SUB-RAYLEIGH ANGULAR SEPARATION

A challenging scenario for DoA estimation problems is the case when targets are separated in the angular domain by less than the native resolution limit, which is provided by the array (more specifically by its aperture). This scenario is tested here for the array, that has been generated with the 5 targets in the scenes, as in the previous section. Different to the previous case study, the steering matrix for the BCS estimation is generated with an angular step-size of 0.5° to give the BCS algorithm better resolution capabilities when tested with the testing data. Through multiple simulations it has been observed, that the entropy based thinning method does not work very well in low SNR conditions when it is trained with simulated scenes, in which the two targets are very close together. Nevertheless, it is shown, that also in this case study, heavily thinned arrays are able to achieve good detector performance when used with the BCS DoA estimation method.

The array that has been generated with the target scenes, as in case study 1, is now tested against scenes where two targets are separated in the angular domain only by

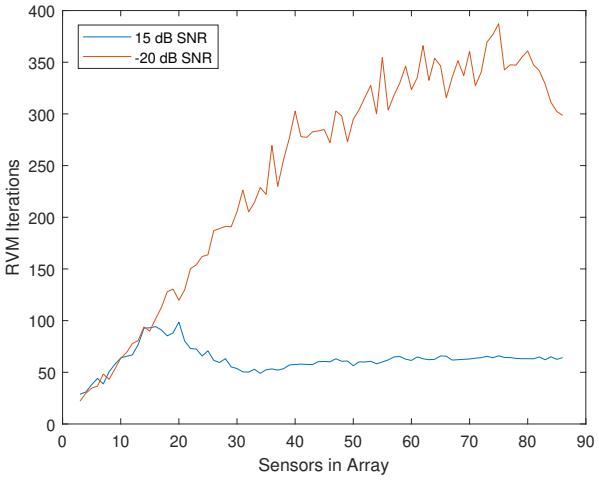

Figure 3.13: Iterations of the Relevance Vector Machine (RVM) used in the BCS method that are needed at each step of array sparsity until the convergence criterion is fulfilled.

1°. This is below the potential native array resolution of around 1.33° at boresight and will therefore test the super resolution capabilities of the array. At this angular distance, the FFT beamformer utilizing the data of all 86 sensors is not able to discriminate the two simulated targets, as can be seen in figure 3.14. However, the BCS method has the capability of detecting both targets, which is shown by the red dots, indicating the BCS angle estimates.

The steps to assess the array would be the same as before, looking at the Jaccard index to locate the point from which on the array has enough sensors included and then closer inspect it by means of the ROC curves. Repeating this for each scenario would flood this thesis with plots that are all very similar. Since the whole procedure has been shown once for the first case study, here only selected plots of interest will be shown. In comparison to the scenes with 5 targets, it is shown that the array can be much more sparse, when only two targets are present. This is shown by means of the ROC curves for the thinned physical ULA and the thinned MIMO virtual ULA in figure 3.15. Note, how the physical ULA is able to discriminate the two closely spaced targets with only 17 sensor elements and a proper threshold quite well on average, as compared to the 23 sensor elements needed when 5 targets are present. Although it has been claimed that for the BCS DoA estimation method there does not exist a mathematical formulation on the minimum number of sensors needed to detect a certain number of targets, there is clearly a relation between the number of targets and the needed amount of sensors, as the sparsity of the scene is also changed.

For this experiment, the angular step size of the dictionary (steering) matrix has been set to 0.5°. This is an important parameter to set for the BCS method in this scenario of closely spaced targets. Its connection to the steering matrix has been described in chapter 2. Since the targets are spaced only 1° apart, a step size of 1° would lead to problems

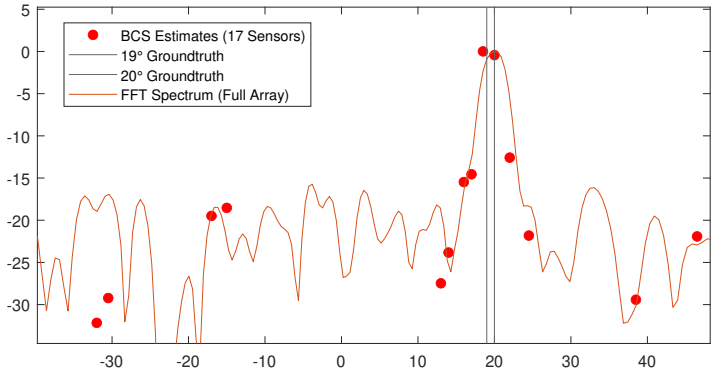

Figure 3.14: Example simulation scene with 2 targets that are 1° separated in angular domain. The FFT is not able to discriminate the two targets and sees them as one.

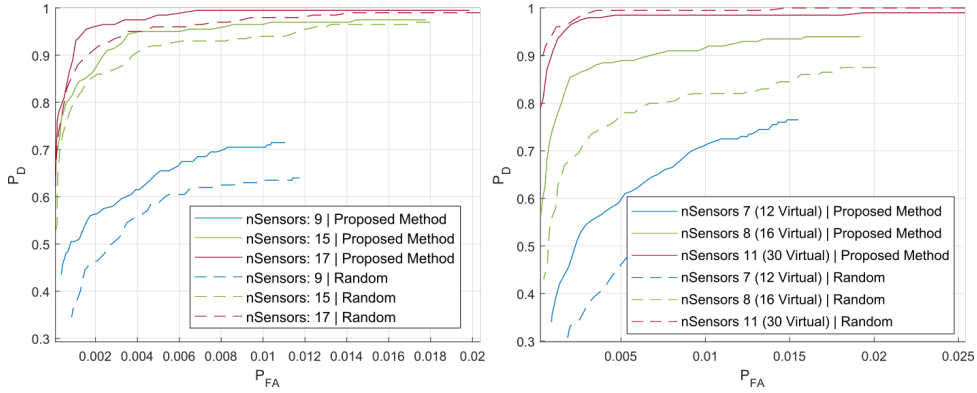

Figure 3.15: ROC curves for closely spaced targets in the testing simulations and an SNR of -20dB (+ 21dB FFT Gain). The solid lines represent the arrays generated by the proposed method, compared to the random ones shown by the dashed line. The physical ULA case is shown on the left and the MIMO case on the right.

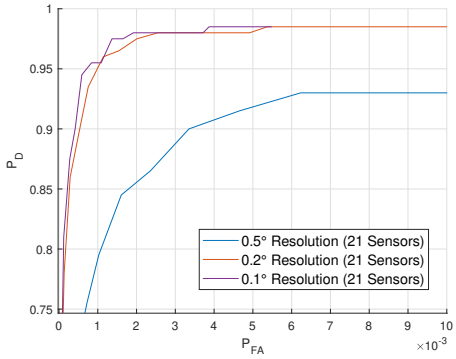

(a) ROC curves for different angular grid resolutions.

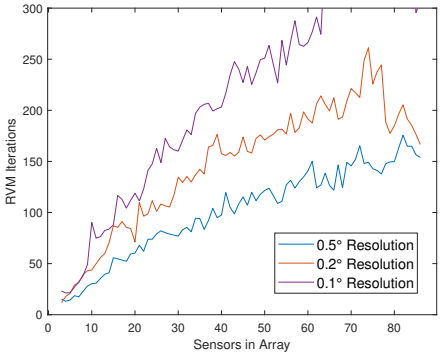

(b) Average (over 100 simulations) number of iterations needed by the BCS method to converge to the solution.

Figure 3.16: Effects of finer angular resolution in the angular grid used to create the steering matrix. The simulated scenes contain 2 targets with 1° angular separation. On the left side, the ROC curves are shown and on the right side the impact on the computation by the BCS method (the RVM) is shown.

in the peakfinding stage of the detector. Ultimately, the algorithm would not be able to distinguish the two targets, similar to the FFT beamformer. However, one strength of the BCS method is that this step size can be chosen smaller. To see this in effect, refer to figure 3.16a. Three different resolution sizes of 0.5°, 0.2° and 0.1° have been tested for a selected number of sensors in the array. Observe, in figure 3.16a, that the resolution capacity can potentially be improved by decreasing the angular step size used to create the steering matrix. It should be kept in mind, that this increases the dimension of the steering matrix and therefore the overall computation time, as it can be seen in figure 3.16b.

The resolution size plays an important role for the estimation error. Due to the discretization of the angular domain when creating the array steering matrix, there will be off-grid errors when the real target locations do not fall onto one of the discretized angular bins. It has been observed, in these cases, that the energy at that angular bin is sometimes split over the angular bins that surround the true target location (which lies off-grid). For this grid-based BCS method it is therefore intuitive, that a finer grid will also improve the estimation error. This has been observed in this experiment and is shown in figure 3.17. Furthermore, the splitting effect leads to false alarm detections. Therefore, the angular grid size does also have an effect on the detector metrics, as shown in 3.16a. Different methods to counteract these errors have been proposed in literature, but the study thereof is not subject for this thesis.

Another important parameter for the BCS method is the number of snapshots it can use in its inversion process. When using more than one snapshot, it is called "Multi-Task BCS" (MT-BCS) since each snapshot is treated as an inversion task, contributing to one common solution (this has been detailed in chapter 2). The experiments have been run with the same testing data as before, but comparing the output when the MT-BCS is used with 5 and 10 Snapshots. For this trial, the resolution has been kept fixed to 0.5°. In 3.18a it can be observed, that using more snapshots can, to a certain degree, improve

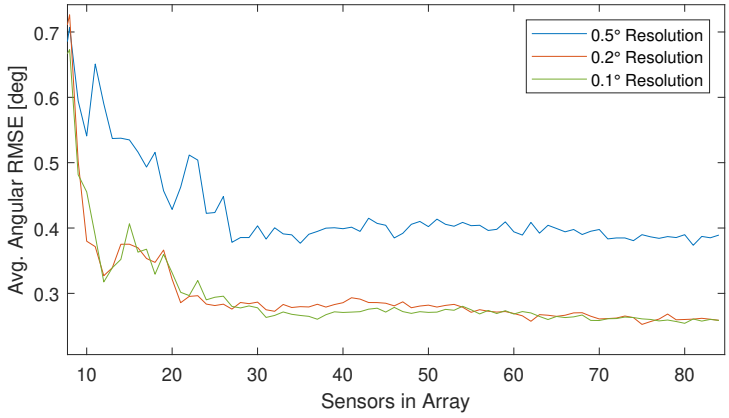

Figure 3.17: RMSE comparison for 0.5°, 0.2° and 0.1° grid resolutions when using the BCS method with one snapshot and data of around 4dB SNR

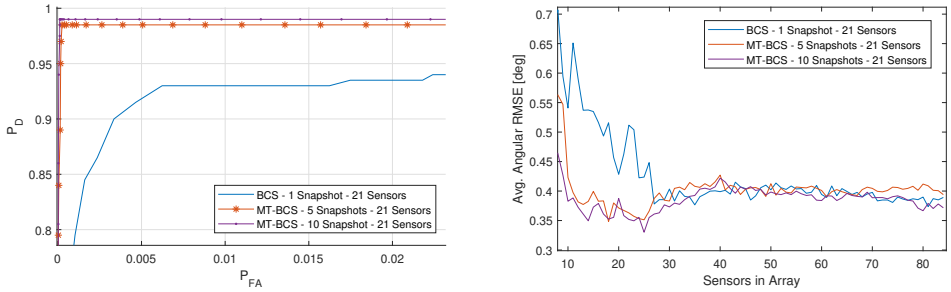

(a) ROC curves for different number of used snapshots.

(b) RMSE for different number of snapshots.

Figure 3.18: Influence of the number of used snapshots on the detection and estimation performance.

the detection performance. The two MT-BCS methods with 5 and 10 tasks (snapshots) show a performance increase from 0.93% to 0.99% probability of detection. This is still a much smaller amount of chirps that have to be utilized when compared to methods like MUSIC, where at least 86 chirps need to be used (corresponding to the amount of maximal antennas in the array for this thesis).

Finally, the performance of the BCS method is tested against the FFT beamformer and the Multiple Signal Classification (MUSIC) algorithm, a well established DoA estimation method that is able to resolve targets that are closer than the resolution limit [1]. The angular RMSE has been investigated for the BCS, MT-BCS and classic methods, which is shown in figure 3.19a. Since both the classic FFT beamformer method and the MUSIC method can only work with a ULA, and it would be an unfair comparison if the

[1] The MUSIC algorithm usually needs to know the number of frequencies [94]. To have a fairer comparison, an extended version of the MUSIC algorithm has been used, which estimates the number of targets using the Minimum Description Length (MDL)

aperture is changed, the metrics for these two methods have been computed only for the full array case (all 86 sensors included) and are shown as horizontal lines. It is very important to point out here, that the RMSE can only be calculated based on the estimations which have been paired to a true target. There might be cases where only one target has been detected with a good RMSE, but the false negative is not reflected in the RMSE plot shown in figure 3.19a. Therefore, when accessing the estimator performance, it is important not to look only at the RMSE but also at the detector metrics to see from which number of sensors onwards the correct number of targets can be detected. In the case of the FFT beamformer method, the targets cannot be discriminated, and it sees only one target. This has to be kept in mind when looking at the RMSE. It has to be viewed in conjunction with the detection metrics, which is shown in 3.19b. There it can be seen that the FFT method indeed is not able to detect the correct number of targets most of the time. With the focus still on the ROC curves in figure 3.19b, it is visible that the MUSIC method performs very well. This might be partly due to the fact, that the targets in the simulated scenes all have the same RCS and the simulated data is more ideal than real data. It should also be kept in mind, that the MUSIC method has to utilize all 86 virtual sensors and more than 86 snapshots to work. This, on the one hand, makes the direct comparison between the methods skewed, but on the other hand shows the potential of the BCS method, as it is not only able to work with heavily reduced, sparse sensor arrays but also with only one single snapshot. At a good detector threshold, the BCS method is able to resolve the closely spaced targets with only 17 sensors for the physical ULA.

Key-Observation: While the (MT-)BCS method can perform considerably well with as little as one single snapshot and a heavily sparse array, the MUSIC method is bound to a full ULA and at least as many snapshots as array elements, in this case 86.

3.7. CASE STUDY 3: 5 TARGETS WITH MIXED ANGULAR SEPARATION

The prior two case studies have looked at the performance of the generated, sparse antenna arrays for rather isolated cases. In practice, targets in one considered range bin may appear in angular domain very close together, further apart, or both in case of more than two targets. This section aims to investigate a scenario, with simulated scenes where 5 targets have been randomly placed in the same range bin with angular separations that are quite large, or below the Rayleigh resolution limit of 1.33°. An array has been generated based on this data using the proposed method and is again compared to a randomly generated array with the same sparsity. In addition, the performance of the generated arrays using other data has been tested for this scenario as well, to see how much the training data influences the performance when different data is present. During the testing, the BCS method is given a steering matrix with angular grid size of 0.5°, to provide the required angular resolution capabilities. The same grid size is given for the MUSIC method.

It is observed, that generally more sensor elements are required to reach good detec-

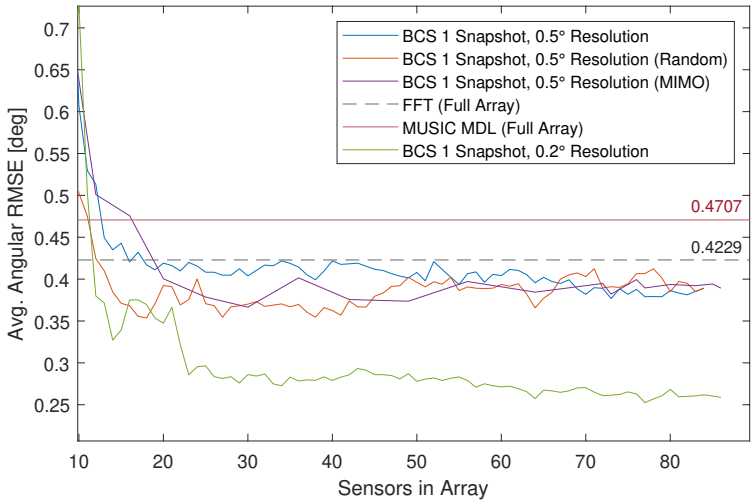

(a) RMSE of DoA estimation for different estimation methods.

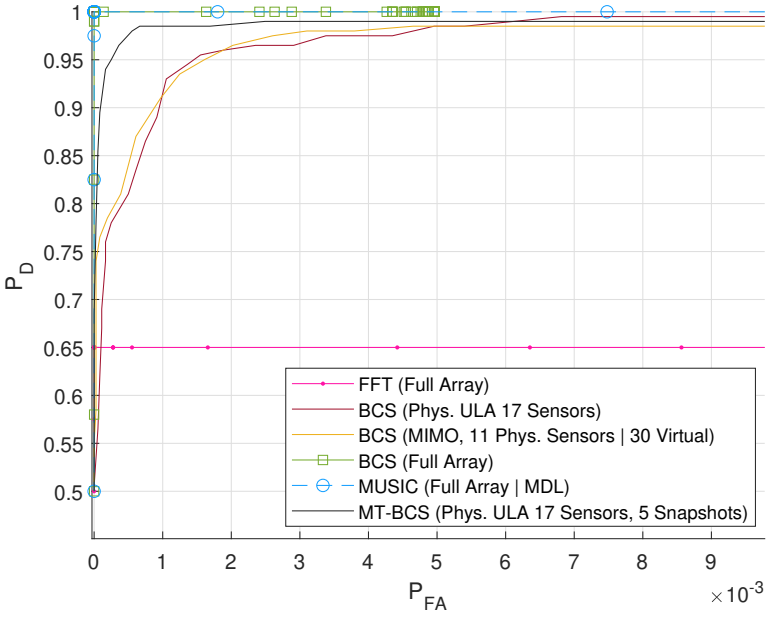

(b) ROC curves for different number of snapshots.

Figure 3.19: Comparison of the BCS method against different established estimation methods.

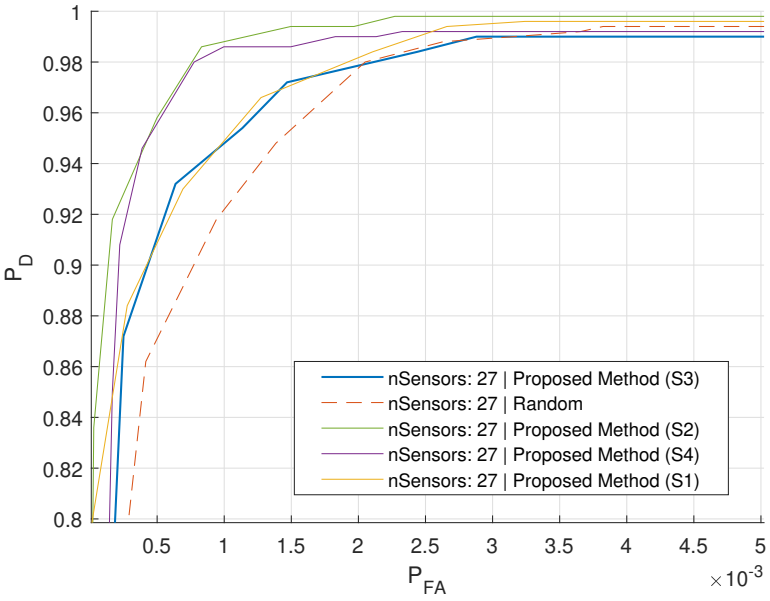

Figure 3.20: Exemplary view of the ROC curves for a selected number of array sparsity (27 sensors) and arrays of the physical ULA type.

tor performance in terms of the ROC curves. Moreover, in this scenario, the proposed entropy based method seem to have a harder time deciding on the most informative sensors to add. This has been revealed by the fact, that the randomly generated array is sometimes performing better than the one generated by the entropy method, at certain levels of array sparsity. However, another interesting observation has been made. Arrays that have been generated using the proposed method, but having been generated based on target scenes where all 5 targets have been well separated, seem to perform well with this data of mixed angular separations. This is illustrated by a view of the ROC curves in figure 3.20 for a selection of physical ULA arrays with 27 activated/included antennas. It can be observed, that the arrays generated based on simulated scenes with well separated targets (green and violet) achieve a better detection performance than the array trained for the same simulation (S3, blue curve). The different simulations S1-S4 are listed in table 3.2.

Figure 3.21 shows the RMSE for the same arrays.

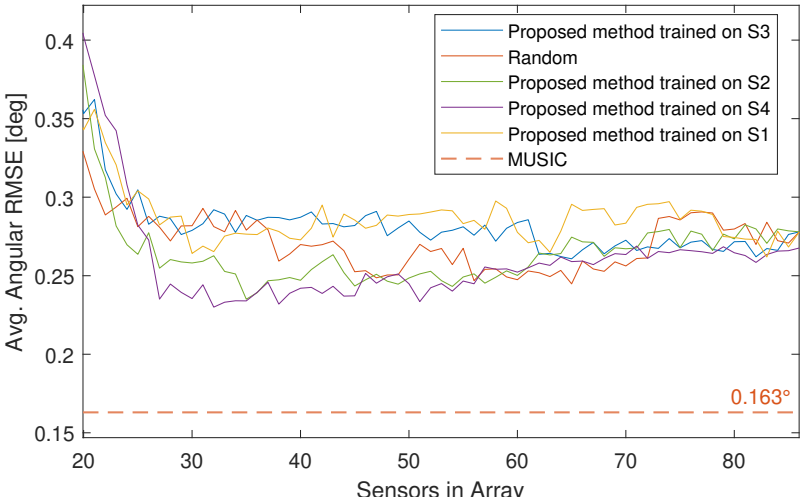

Figure 3.21: View of the RMSE with increasing number of sensors, different arrays of the physical ULA type. While the MUSIC method always needed more than 86 snapshots and all 86 antennas (hence the constant line) the BCS method has been used with only one snapshot.

4

TESTING WITH REAL RADAR DATA

As a final step in the assessment of the sparse arrays, they are tested with measured data. To this end, the Texas Instruments AWR2243 cascade evaluation board is used, which provides a total of 86 unique antennas for DoA estimation in azimuth when using the MIMO principle. A selection of different target scenarios have been set up to test the arrays in combination with the BCS DoA estimation method. Two measurement campaigns have been conducted at different locations, which are described in this chapter. The approximate point targets have been build with small-sized corner reflectors (described in 4.2 and 4.3), while two persons have been used as an extended target (shown in 4.4). The overall measurement setup and scenarios that have been captured will be described in section 4.1. To keep the chapter concise, it is described in the appendix C, how specific parameters for the BCS algorithm have been found and set specifically for the data and scenario at hand.

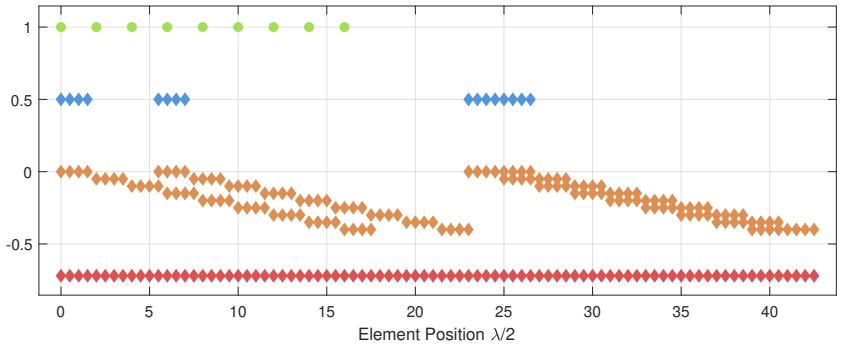

Figure 4.1: Sensor layout of the TI cascade evaluation board. The Tx sensors (green, spaced by 2λ) and the Rx sensors (blue) form a MIMO array with a lot of overlapping sensors. The final 86 unique sensor positions are marked in red.

THE final step in the performance analysis of BCS using sparse arrays is to test them with data that has been acquired through real measurements with the Texas Instruments AWR2243 Cascade evaluation board. This board features four single AWR2243 FMCW Transceiver chips which operate in the frequency band of 76 to 81 GHz [95], a typical frequency for state of the art automotive radar application [3]. Each single chip provides 3 transmit and 4 receive antennas, which brings a total of 12 transmit and 16 receive antennas to the cascade evaluation board [96]. By combining these antennas with the MIMO array principle described in chapter 2, a virtual array of 192 antennas can be obtained. However, due to the fixed printed antenna layout of the evaluation board design, many of these virtual antenna positions will be redundant, leaving a total of 86 unique virtual sensor positions which form a ULA. The array geometry is shown in figure 4.1. The virtual uniform array provides the basis for data acquisition and has also already been used as an exemplary case to apply the entropy based array generation which has been described in the previous chapters. The occurrences of overlapping antenna positions might even facilitate the MIMO version of the proposed sensor adding algorithm, as it reduces the repetition of sensor groups across the array aperture. For the physical ULA version of the proposed algorithm, only the resulting virtual elements are considered as unique sensor locations. Two measurement campaigns will be described in the following sections, where the generated arrays from chapter 3 are tested. To this end, data is always captured with the full number of antennas that the board can provide. In post-processing, only data from the sensors that are included into the generated, proposed sensor arrays is used.

4.1. MEASUREMENT SETUP

To take the real measurements, two measurement campaigns have been conducted. The TI cascade radar board has been mounted on a tripod roughly 1 meter above the ground at a feasible empty space outdoors. Corner reflectors have been placed at a constant distance of 5 and 10 meters, with varying angles to the line of sight of the radar. The dis-

Parameter	Value	Unit
Start frequency	77	GHz
Slope	5	MHz/μs
Ramp-End-Time	80	μs
Bandwidth	400	MHz
ADC samples	256	range samples
Rx Gain	48	dB
No. Chirps	128	-
No. Frames	4	-

Table 4.1: Parameters set and fixed between measurements in the TI cascade radar board.

tance has been chosen as it is feasible to walk back and forth during the measurement procedure and is acceptable for the far-field assumption. The far-field is computed considering the aperture of the physical receiver array, which is D =10.45 cm and results in a radial distance of $r = 2D^2/\lambda$ =5.6 m. Although the closest positioning of the targets is at 5 m, it is noted here that these conditions are rather soft thresholds, and it has been verified that the reasonable measurements are acquired. To obtain target measurements with varying RCS and possibly stronger reflections, multiple small corner reflectors have been attached to the poles in some cases (more detail is given in section 4.2).

The radar parameters for the measurement campaign have been set prior and kept constant to the values that are listed in table 4.1. Importantly, the maximum range has been set to about 108 meters in order to avoid too many target returns from outside the range of interest. Moreover, the range resolution has been set to a quite high value of 37.5 cm, such that in post-processing, the range bin where the targets are placed can be cut out and is less sensitive to the case when a target is not exactly at the expected distance. Since the available measurement equipment and the circumstances of the campaign did not allow for highly precise placement of the targets, this was a necessary step. Since the aperture of the radar is fixed and the number of unique, virtual receive antenna elements is N_{Rx} =86, the resulting angular resolution is obtained as

$$\Delta\theta = \frac{\lambda}{d \cdot N_{Rx} \cdot \cos\theta} \cdot \frac{180°}{\pi} \tag{4.1}$$

and can be calculated for a zero-degree view angle as $\Delta\theta_0$ =1.33°. It is noted here, that the settings presented in table 4.1 do not break the narrowband assumption, since 400MHz $\ll$ 77GHz (i.e. Bandwidth $\ll f_0$). Another important aspect to note is the actual distance between sensors in the receiver array, when a certain frequency and bandwidth combination is chosen for the TI board. With the parameters shown in 4.1 the centre frequency is f_0 =77.2GHz with wavelength $\lambda = c/f \approx$3.88 mm. In units of this wavelength, the spacing of the printed antenna on the TI board is $\Delta/\lambda = 0.5023$. It is only a small deviation from the theoretical half-lambda spacing, but it has shown to noticeably improve the DoA estimation accuracy.

Since no precise measurement equipment was available to place the corner reflectors at exactly the desired angles, the *law of cosines* has been utilised with fixed and known distance between target and radar, as well as the desired angular separation be-

tween targets (one of which has been used as a reference at 0°). The law of cosines to calculate the linear distance between two targets on the same radial distance from the radar is given as:

$$d_{meter} = \sqrt{2r^2(1-\cos\theta)} \tag{4.2}$$

where d_{meter} denotes the distance between two targets that lie on the same radial distance r from the radar and θ is the desired angular separation in degrees.

4.2. WELL SPACED TARGETS

The general overview of the first measurement site is given in figure 4.2. The red shaded area indicates the radar board's field of view and adjusted maximum FMCW range. The green shaded area marks the range resolution cell of about 37.5 cm, which has been extracted in the post-processing. The chosen site has been mostly flat soil. However, as can be suspected from figure 4.2, there is some ground clutter in the form of foliage and scree, which is clearly visible in the received data.

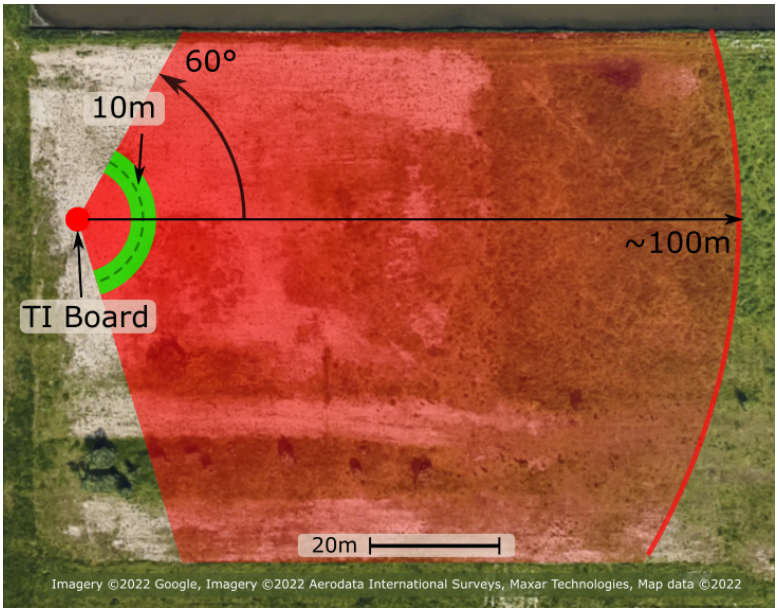

Figure 4.2: Overview of the measurement site close to the TU Delft campus (satellite image via Google Maps).

Different target arrangements have been captured during the first measurement campaign, which are listed in its full extent in table 4.2. For this thesis, only the measurements with all 5 targets present (as shown in figure 4.3, number 09 in table 4.2) have been used and are analysed in this section.

The BCS algorithm has been utilised and tested with the array proposed in chapter 3 for the 5 target scenes. It has been observed, that at around 37 included sensors for the physical ULA, the algorithm is able to detect the 5 targets quite well. Figure 4.4 shows

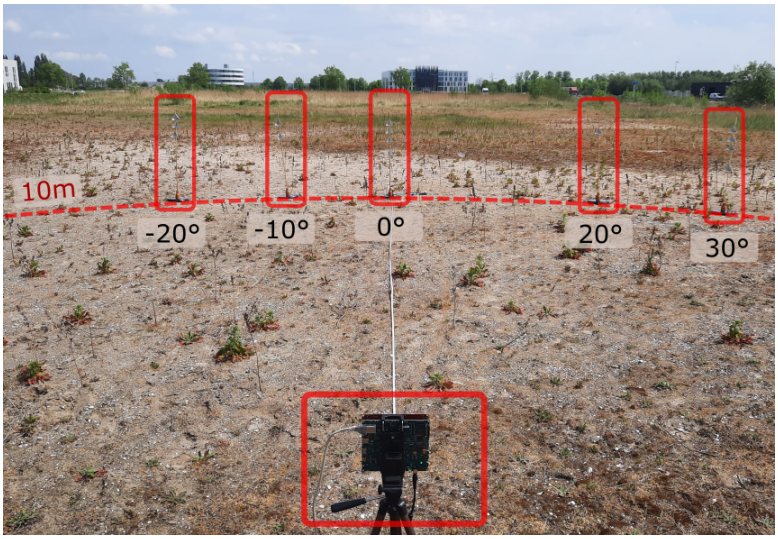

Figure 4.3: Measurement scene from the Radar point of view. All four maximally used targets have been placed at the 10m range from the radar at the angles -20°, -10°, 0°, 20° and 30°.

No.	No. Targets	Angles	Note
00	0	-	Empty reference scene
01	1	0°	5m distance for calibration matrix
02-06	1	-20°, -10°, 0°, 20°, 30°	Single measurement for each angle
07	2	0°, 30°	-
08	2	-10°, 0°	-
09	5	-20°, -10°, 0°, 20°, 30°	-
10	1	0°	Human target
11	2	-10°, 0°	Human targets

Table 4.2: Captured target arrangements during the first measurement campaign.

the BCS estimates using the sparse array compared to the classical FFT spectrum with the full 86-sensor array as a reference. Note that the used array has not been generated based on the measured data, but on simulated data.

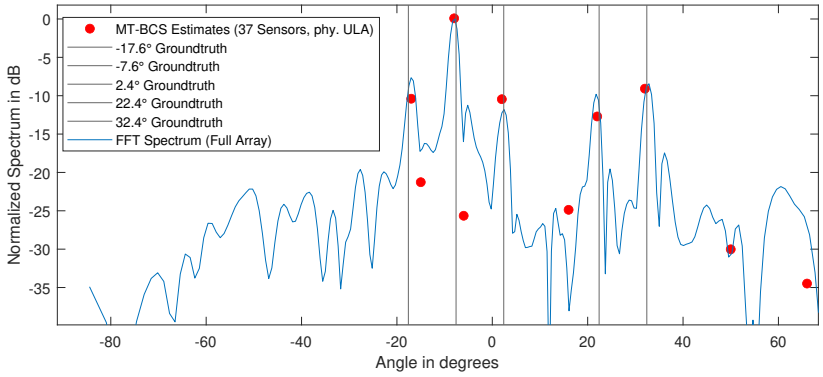

Figure 4.4: Example result of BCS-based DoA estimation for the 5 targets measured scene.

Figure 4.5 shows the RMSE for this measurement, using arrays with more and more sensor elements. The BCS method is compared to the MUSIC estimator and the FFT beamformer. Since both the MUSIC and the FFT method need a fully filled ULA, the RMSE values for these two methods have been displayed as a horizontal line. It can be observed, that the inclusion of more and more sensors does not decrease the RMSE, allowing for the conclusion that the usage of sparse arrays does not necessarily lead to a loss in estimation accuracy, which coincides with the observations from the simulated data. Figure 4.6 shows the ROC curves for the BCS method using 5 snapshots and a sparse array of 42 sensors with the physical ULA and 64 virtual sensors with the MIMO array. As an example, it is compared against a randomly generated array of 42 sensors in the physical ULA. The distinct difference in the physical ULA and MIMO based cases could be related to the different degrees of freedom in the MIMO array generation process. While the physical ULA based method has the freedom to place each physical receiver sensor according to the entropy update, in the MIMO array, such individual placement of the virtual receiver sensors is not possible.

The ROC curves displayed in figure 4.6 for this measurement show that in this real world measured case, more sensors are required to achieve good detection performances than have been promised by the simulated tests in chapter 3.4. A partial reason for this could be the strong clutter and the diverse RCS of the single targets. Moreover, it has been observed that over the number of multiple chirps, some targets fluctuate very strongly in terms of their RCS. In an attempt to improve the signal strength of the corner reflector targets against the surrounding clutter, to counteract possibly suboptimal orientation and design of the used corner reflectors, and to have some variance in their RCS multiple corner reflectors of the same size have been attached to the same pole. This is shown in figure 4.7. During the post-processing of the data, it has been observed that this has not led to the desired effect. Poles that had multiple corner reflectors attached some-

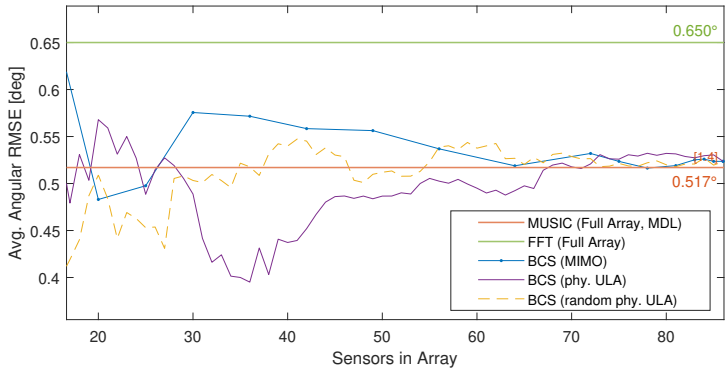

Figure 4.5: Comparison of BCS method against MUSIC with 86 snapshots and FFT DoA estimation.

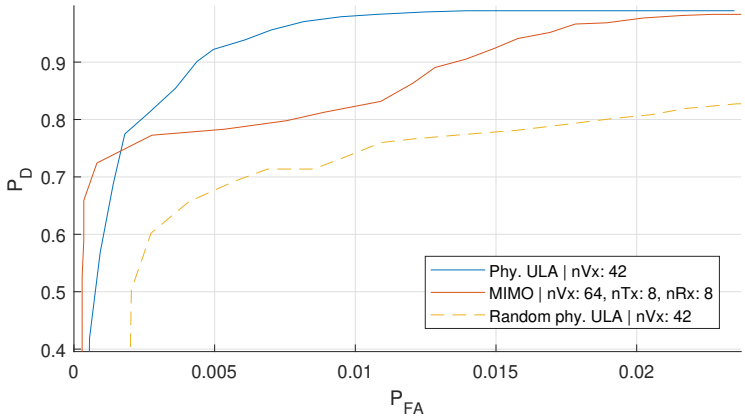

Figure 4.6: Comparison of BCS method against MUSIC and FFT DoA estimation.

times even showed a lower RCS in the spectrum compared to ones with fewer corner reflectors. Moreover, a strange behaviour has been observed, where the RCS of a target slowly diminished within one frame of 126 FMCW chirps. It is suspected, that the attachment of multiple corner reflectors might have led to deconstructive interference among them and did not benefit the operation. In the second measurement campaign, it has therefore not been repeated this way and the effect was not observed again. Anyhow, even with these effects and results which could also be viewed as realistic imperfections, the reduction of hardware could still entail the removal of one entire chip (3 transmitter- and 4 receiver antennas) while keeping good performance with respect to the detection of targets and estimation of their DoAs. In case a physical ULA is to be built, the results indicate a reduction of about 50% of the required antennas.

Figure 4.7: Composition of corner reflectors to achieve different target RCS values.

4.3. CLOSELY SPACED TARGETS

A second measurement campaign has been conducted to obtain measurements where two corner reflectors are very close together in angular domain, but again at the same radial distance from the radar. Since the clutter that has been present during the first measurement campaign was quite strong, the second round of measurements has been taken on a football field, offering a very homogeneous, clutter-free ground. Two corner reflectors have been mounted on a thin, horizontal, wooden pole, such that they can be shifted very close together. Starting from a distance of 1.4 cm from corner to corner (13 cm from centre to centre) the two corner reflectors have been shifted apart in steps of 3 cm (that corresponds to 0.3° at 5.6 m distance), until their separation has increased by 12 cm (corresponding to 1.22° at 5.6 m). The described setup is shown in figure 4.8.

No.	No. Targets	Angles	Note
12	0	-	Empty reference scene
13	1	0°	5 m distance for calibration matrix
14	2	0°, (1.33° to 2.56°)	Separation increase in steps of 3 cm/0.3°

Table 4.3: Captured target arrangements during the second measurement campaign.

Since for this type of real-world data captures, it was not feasible to acquire 100 different target locations, the presented results are not averaged over multiple trials. However, they are averaged over all recorded chirps (when the single snapshot BCS method is used) and might still offer valuable insight. First, the array generated with the proposed method for the physical ULA and 5-target training scenes has been tested for the captured data. The BCS method is given a steering matrix with angular discretisation of 0.5° steps, in order to give it enough resolution capabilities. It is compared against the FFT in

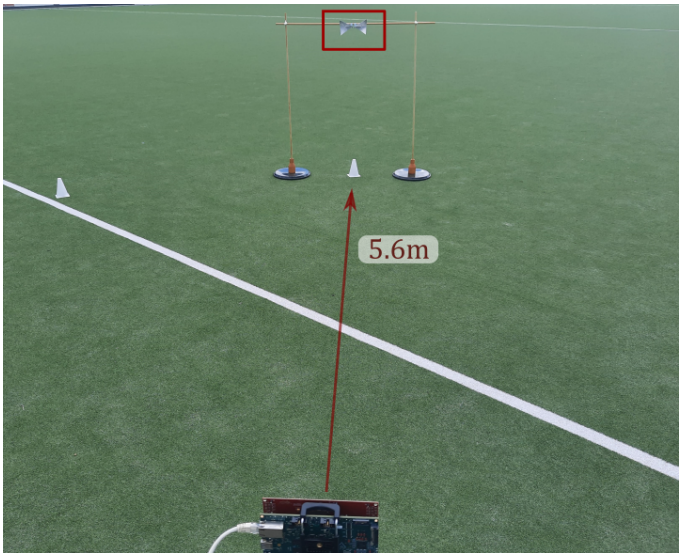

(a) Setup of the second capture, showing the radar in the front and the corner reflectors in the back.

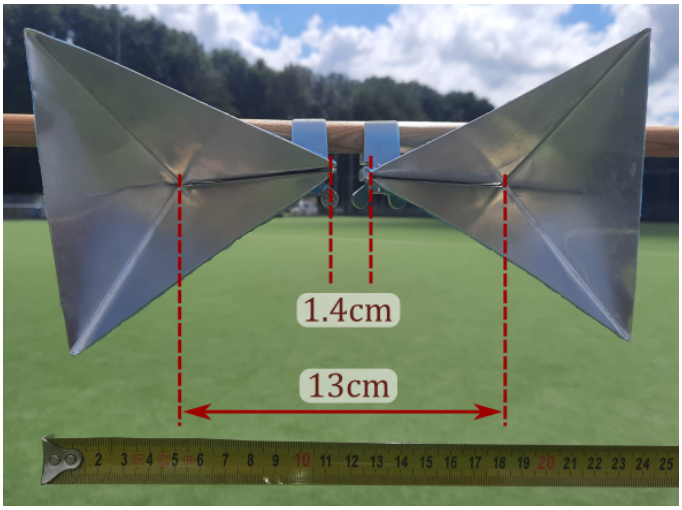

(b) Close-up photo of the two corner reflectors at their closest spacing of 13 cm (measured from their centres), corresponding to 1.33° angular separation.

Figure 4.8: Reference photographs for the second measurement campaign to capture very close corner reflectors.

this first examination. At the closest angular spacing of 1.33°, the FFT is not able to resolve the two corner reflectors, while the BCS method is. This is shown in figure 4.9. Note how the two BCS estimates (red dots) estimate the true angle values (black, horizontal lines) quite well and with around 15dB separation from the remaining false detections. The first secondary lobes left and right from the centre are roughly 13dB relative to the mainlobe and therefore might indeed be the secondary lobes of the array pattern (in case of the full array). This is, however, difficult to know for sure, since even the football field is not free from clutter or multipath echoes. Note also, that the shown estimate has been provided by the BCS using only one single snapshot (chirp). The same can be observed for the MIMO array, when a similar number of virtual sensors is included into the array.

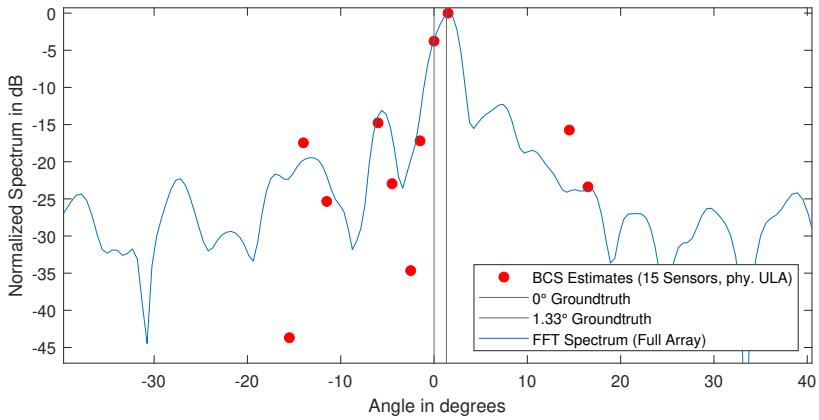

Figure 4.9: Angle estimation plot for the two corner reflectors at their closest spacing of 1.33°.

The number of sensors that seem to be enough for successful detection of the two targets can be best investigated by looking at the Jaccard maps as shown with the simulated data before. They are plotted for the physical ULA and the MIMO in figure 4.10.

When the two corner reflectors are separated by additionally $\approx 0.30°$, such that also the FFT method is able to distinguish them, the BCS method seems to need even fewer sensors. In this case, the BCS method is able to distinguish the two corner reflectors with as few as 5 sensor elements, compared to 15 sensors needed for the case before in figure 4.9. An exemplary plot for this is shown in figure 4.11.

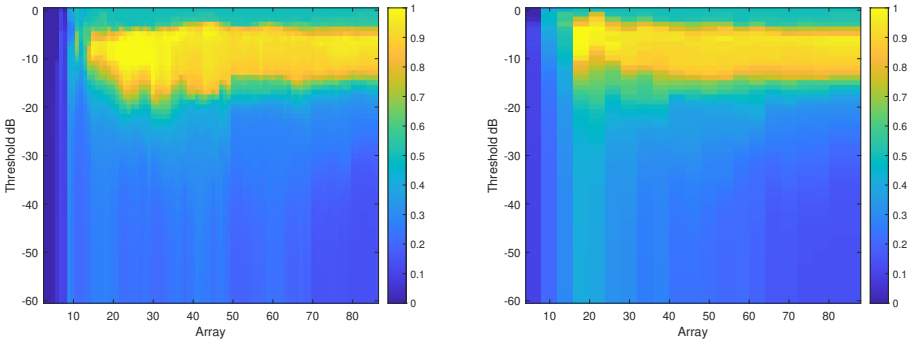

(a) Physical ULA

(b) MIMO Array

Figure 4.10: Jaccard index plotted over varying number of sensors and varying threshold for the two closely spaced targets using the BCS method.

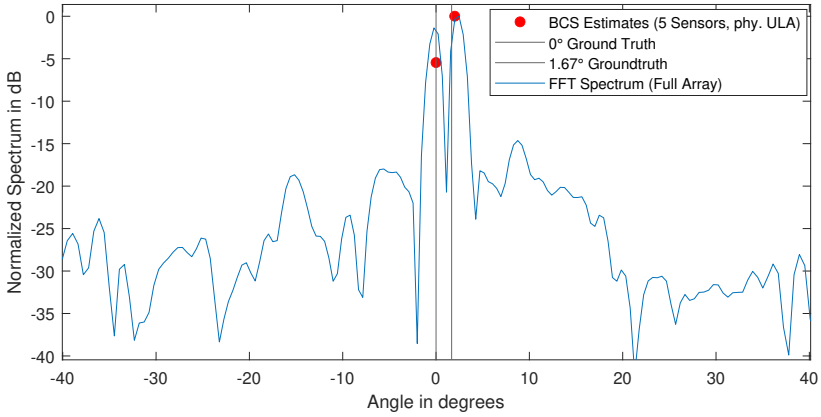

Figure 4.11: Angle estimation plot for the two corner reflectors at their second-to-closest spacing of 1.66°.

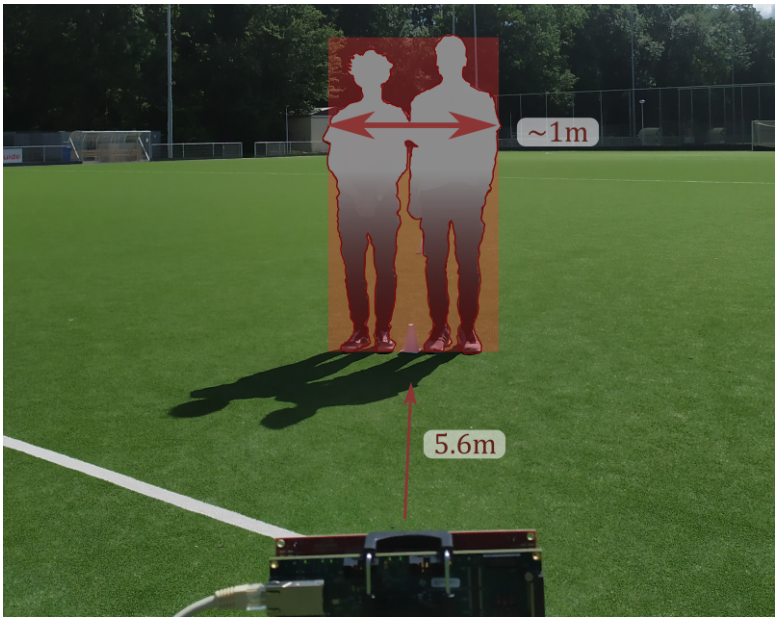

Figure 4.12: Measured scene of 2 persons standing closely together to form an extended target. The span from shoulder to shoulder is about 1 meter, corresponding to around 10° angular spread.

4.4. EXTENDED TARGET OF OPPORTUNITY

A final measurement has been taken to see how the BCS method behaves, when the reflecting target is not as pointlike as the corner reflectors. To test this, two people have been positioned shoulder to shoulder, to form an extended target with a span of about 1 m as shown in figure 4.12. This results in an angular span of about 10 degrees from shoulder to shoulder. As can be seen in figure 4.13, the estimated coefficient vector produced by the BCS has high non-zero values in the region where the extended target is placed. It seems to locate the DoA estimates at the points where also the FFT beamformer has its peaks. Those peaks could be related to the scattering centres of the extended target, which is not a smooth surface. Figure 4.13 shows two versions of estimates. The red dots show the output of the BCS method, when the parameter b is set to a rather low value of 25. This value has shown to be a good compromise between the sparsity of the estimated vector and the preservation of weaker target RCS for the data in this thesis, as it is discussed in more detail in the appendix C. Increasing this parameter to a value of 200 shows to eliminate almost all the estimates besides the ones corresponding to the extended target. These estimates are shown by the violet star markers. Moreover, it is visible that the magnitude estimate is not visibly degraded.

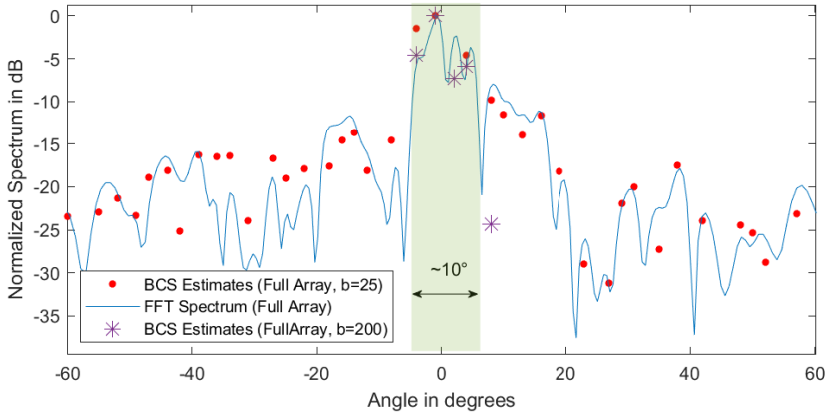

Figure 4.13: Example of the spatial spectrum estimation for the 2-Person extended target. Observe how a clear larger extent of spectral energy is present in the green marked region, corresponding to the target location. Note also, that changing the b-parameter of the BCS method can greatly reduce the number of secondary non-zero coefficients.

Finally, it has also been investigated how the sparse arrays are able to perform in this scenario. Again, the generated array from the previous sections is used, which is based on simulated data with 5 targets in the scene. For the physical ULA based array and this data capture, around 30 sensors seem to be sufficient such that the BCS algorithm obtains non-zero coefficients that cover the angular span of the extended target, which is shown in figure 4.14a. Similarly, the MIMO based generated sparse array with 30 virtual elements is able to recover those coefficients as well, which is displayed in figure 4.14b. In both cases, fewer than 50% of the sensors from the original, full (virtual) ULA of 86 sensors are needed. However, these conclusions are only tentative, as only one example capture of an extended target has been investigated.

Summarizing the insights of this chapter, it has been shown, that the BCS method is capable of performing well with measured data using the sparse arrays that have been generated purely based on simulated data. It is generally observed, that compared to the assessment based on simulated data, more sensor elements are needed when the captured data is used. Nevertheless, the measured data confirms that sensors could be removed while still being able to locate point targets that are further apart or below the Rayleigh resolution limit, as well as providing a point cloud of estimates for an extended target. The parameter that can be adjusted in the BCS method, which has been called b-parameter, could be used as either an addition or possibly even a substitute for a detector threshold, as it shows to suppress spectral energies caused by clutter while keeping the spectral energies corresponding to actual targets intact.

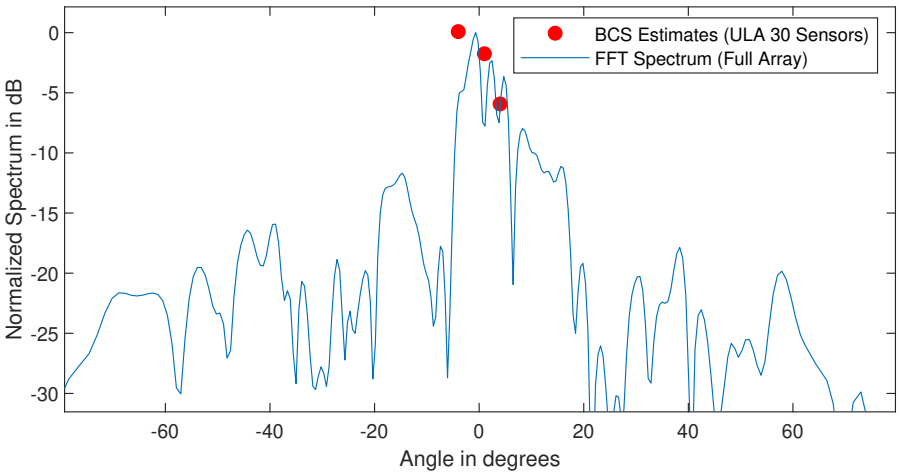

(a) BCS estimates using a physical ULA based sparse array with 37 sensors.

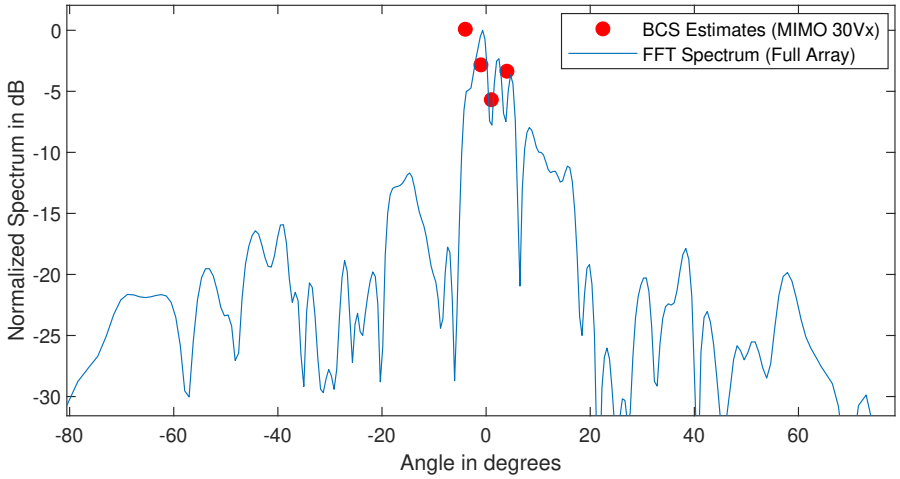

(b) BCS estimates using a MIMO based sparse array with 6 physical transmitters, 5 physical receivers and resulting 30 virtual receivers.

Figure 4.14: Example of the BCS estimates when an extended target is present, compared to the FFT beamformer spectrum for reference. The b-parameter for the BCS has been set to 200, to suppress the spurious estimates.

5

Conclusions and Future Work

RADAR technology has emerged as an important technology for countless modern technological solutions. Due to the progress made in chip manufacturing, it has found its way into more consumer based, civil applications. One of such applications is the use of radar systems in automotive vehicles, where it is aimed for more and more *intelligence* and automation. A key aspect of this and many other applications is often times the direction estimation of targets that are present in the observed scene. Improving the DoA estimation capabilities is generally a costly task, since the addition of more antennas and the increase in mechanical size entails an increase in hardware complexity, cost, energy consumption and difficulties due to spatial confinement in certain applications (the radar device has to fit somewhere on the car) [3].

A promising, emerging method that trades the described costs for better DoA estimation against computational demand is known under the term (Bayesian) compressive sensing [38]. It has found vast interest in literature, not only for DoA estimation. The DoA estimation problem is one application that is especially well suited for the use of BCS methods. When targets that are very confined in angular domain are assumed (e.g. point targets), the necessary sparsity condition is fulfilled and the CS framework can be applied. But besides offering a possible increase in resolution and the reduction of necessary snapshots, the CS framework offers the opportunity for sub-Nyquist sampling of the scene of interest. For DoA estimation, this amounts to a sparse spatial sampling of the scene, i.e. a sparse arrangement of antennas. Since the Bayesian CS framework also provides measures of confidence, Bayesian experimental design theory could be used to locate informative sensor positions, an opportunity that has not been extensively explored in radar based DoA estimation yet.

This thesis has made use of those intrinsic properties of the BCS DoA estimation framework (namely the provided uncertainty measures in the estimated signal vector), to devise a method that helps in the generation of sparse sensor arrays for one dimensional DoA estimation in the field of radar technology. Particularly, the entropy of the recovered signal (i.e. the uncertainty of the estimation) has been utilised, to fill up an empty grid of possible sensor positions by deciding at each step, which new sensor could

decrease the uncertainty the most. The method has been applied to generate arrays that can be implemented by a direct placement of physical antennas, or by means of a MIMO array configuration.

The proposed method is shown to decrease the estimated uncertainty faster, than if sensors would be added purely random. It is generally shown, that sparse arrays can be used in conjunction with the BCS DoA estimation method and can provide good estimation and detection results. When different sparsity levels are picked (i.e. the arrays are not filled up to a full ULA), it is shown that the generated arrays outperform randomly generated arrays in terms of the detection metrics, meaning that for certain scenarios the proposed arrays need fewer sensors than the random ones for similar detection performance. By the case study of 5 targets located within an FOV of $\pm 40°$ and good SNR conditions, the improvement for a sparsity level of 25 out of 86 sensors included (a factor of ≈ 0.3 times the full number of possible sensors) as compared to a randomly generated array with the same number of antennas lies at about 1.4-1.6%. It has been shown that the estimation performance shows to be more related to the angular grid that is used for the BCS estimation method and the entropy based arrays do not show consistent performance increase in terms of estimation accuracy measured by the RMSE.

Furthermore, the proposed arrays and generally sparse arrays have been tested with real captured measurements using a Texas Instruments evaluation board. It is shown, that even heavily sparse arrays can still detect and estimate the targets and their DoAs quite well, when compared to methods like MUSIC and the FFT beamformer. With the example study of the TI cascade evaluation board, and all the corresponding parameters that have been set accordingly, the proposed arrays could directly lead to a theoretical removal of entire transceiver chips on the board. Based on the measured data that has been captured, one single chip could be removed in the MIMO array case, while about 50% of the antennas in a physical ULA case could be removed. Ultimately, the proposed method is another step into the direction of reduced complexity, cost and energy consumption for one dimensional sensing systems, which in today's ecological world can be a small, but valuable contribution. On a broader scope, the idea this thesis is based on can be applied to other sensing systems as well, where spatial sampling is applied to measure sparse signals.

The proposed method for array generation, as well as the BCS algorithm that is used for DoA estimation, are influenced by numerous parameters. Many of those parameters have been reasonably fixed to certain values, based on empirical investigation or the given boundary conditions by the available hardware. However, it is noted that the proposed method is generally not confined to a grid of equally spaced candidate positions and could be expanded to either finer grids or even irregular positions.

5.1. FURTHER RESEARCH

- The proposed method has been confined to place sensors on a grid of possible locations, which is based on the virtual ULA provided by the TI cascade evaluation board. Further research could look into finer grids of possible sensor locations, or possibly even irregular or entirely grid-less options to place new sensors. Coupling effects between close sensor elements should probably be taken into account as well.

- The MIMO based approach for sensor placement has been observed to add many Tx sensors early on. Future algorithms could include techniques to either penalize the addition of transmitter elements, as they are generally more costly in terms of hardware and energy consumption. More over, abandoning the confinement to positions on a grid on $\lambda/2$ basis could offer more available search space and therefore more informative new sensor locations.
- To extend the study of practical feasibility, more dynamic scenarios could be measured. It has been hinted at in chapter 4.1 that strong clutter and a large variance in target RCS could impact the detection performance. This could be explored further for real world environments.
- Some subtopics have been covered only very simplistic here, to keep the scope of the thesis manageable. The detection algorithm, for example, is just based on a simple global thresholding. More elaborate detection methods could be employed to improve the overall detector performance. Furthermore, tracking algorithms could be appended to the pipeline to improve the robustness against false alarms and missed detections.

A

Array Generation Algorithms

A.1. Physical ULA Algorithm

Here, the mathematical steps that have been implemented in Matlab are described for the algorithm operating on a physical ULA are described. The following notation is introduced: The complex valued steering matrix is denoted as A and has the dimensions M rows corresponding to the sensors and G columns corresponding to the discretised steering angles. The expanded, real valued steering matrix is denoted as $A_{\mathbb{R}}$ and has doubled dimensions. The weights for each sensor, determining whether it is included or not, are denoted as w_i with $i = 1,\dots,M$ and can take values of either 0 or 1. The number of new candidate rows is denoted as C and represents the potential new rows in $A_{\mathbb{R}}$. Therefore, $C = 2M$ and in the case of the assumed example with 86 total sensors, $C = 2 \cdot 84 = 168$, since the two edge sensors have already been fixed. For each simulation $\delta h(\mathbf{r}_c)$ is computed according to equation 2.51 for each candidate c. This results in a matrix of C rows and I columns, which is then averaged over the I simulations for each candidate to obtain $\overline{\delta h}_{\mathbf{r}}$. Finally, as it has been shown in chapter 3, the expansion to real values has to be taken into account. To this end, the vector of $2M$ averaged candidate values is summed as shown in algorithm 1. For the calculation of the entropy update equation 2.51 an estimate for the noise variance $\alpha_0 = \sigma^2$ is required. This is calculated with the proposed re-estimate equation in [31], which uses the estimated covariance matrix $\hat{\Sigma}$ and the MSE of the reconstructed measurement vector $\hat{\mathbf{y}}$ as

$$\alpha_0 = \frac{\|\mathbf{y} - \hat{\mathbf{y}}\|^2}{M - 2G + \sum_m \alpha_m \hat{\Sigma}_{mm}} \tag{A.1}$$

where $\hat{\mathbf{y}} = A\hat{\mathbf{x}}$, $\mathbf{y}$ is the vector of CS measurements that is input to the BCS algorithm, M denotes the rows of the current basis (i.e. the number of antennas) and G is the number of basis vectors (i.e. the number of steering vectors in the steering matrix A. The subscripts m index the steering vectors that are currently included, meaning that $\hat{\Sigma}_{mm}$ denotes the m'th element on the diagonal of $\hat{\Sigma}$.

The set of sensor candidate rows has been denotes as R.

Algorithm 1 Sequential Sensor Adding: physical ULA

Require: Input example data for the BCS
$A \in \mathbb{C}^{M\times G} \Rightarrow A_{\mathbb{R}} \in \mathbb{R}^{2M\times 2G}$
$w_i \in \{w_i\}_{i=1,\dots,M} = \mathbf{0}$
$w_1 = w_M = 1$
Precompute steering matrix, $A_{\mathbb{R}}$
while candidates $\mathbf{r}_c$, $c = 1,\dots,C$ **do**
  for Training scene $i = 1,\dots,I$ **do**
    Run BCS to obtain $\hat{\Sigma}_i$
    Estimate α_0 via equation A.1
    Compute $\delta h_i(\mathbf{r}_c)$ for each candidate $\mathbf{r_c} \in R$
    $\delta H \in \mathbb{R}^{C\times I} \leftarrow \delta h_i(\mathbf{r}_c)$
  end for
  $\overline{\delta h}_{\mathbf{r}} = \frac{1}{I}\sum_i^I \delta H_{r,i}$
  $\widetilde{\delta h}_{\mathbf{r}} = \overline{\delta h}_{1:M} + \overline{\delta h}_{M+1:2M}$
  Set $w_i = 1$ for $\arg\max_{\mathbf{r}} \widetilde{\delta h}_{\mathbf{r}}$
  Recompute steering matrix
end while

A.2. MIMO-BASED ALGORITHM

The MIMO-based algorithm follows the same principle as the physical ULA one with the major difference that the new candidate at each iteration is sought for either a transmitter or receiver antenna, resulting in more than one new row in the steering matrix. In each iteration, the transmitter and receiver candidates are swept (individually), and the virtual array that results for each candidate is computed. Then the new resulting rows in the virtual array for each candidate are used in the entropy update equation given in 2.51. Again, to ensure the maximal array aperture is achieved, the border antennas are included. This has to be done for both the physical transmitter and receiver arrays. Two sets of candidate rows are generated for each iteration, denoted as R_{Vx}^{Tx} and R_{Vx}^{Rx} for the transmitter and receiver candidates, respectively. When the physical transmitter candidates are iterated, for each candidate the corresponding weight is set to 1 as $w_{Tx,c_{Tx}} = 1$ and the resulting weights for the virtual receiver array are calculated, denoted as $w_{Tx} \otimes w_{Rx} = w_{Vx}$ (the receiver weights are unchanged). The procedure for the physical receiver candidates follows analogous.

Algorithm 2 Sequential Sensor Adding: MIMO

Require: Border elements activated in Tx and Rx
Ensure: Reduction in Entropy per step
initialization;
$w_{Rx,i} \in \{w_{Rx,i}\}_{i=1,\dots,M} = \mathbf{0}$
$w_{Rx,1} = w_{Rx,M} = 1$
$w_{Tx,i} \in \{w_{Tx,i}\}_{i=1,\dots,M} = \mathbf{0}$
$w_{Tx,1} = w_{Tx,M} = 1$
Compute $A \in \mathbb{C}^{M\times G} \Rightarrow A_{\mathbb{R}} \in \mathbb{R}^{2M\times 2G}$
while candidates $\mathbf{r}_c$, $c = 1,\dots,C$ **do**
  for Training scene $i = 1,\dots,I$ **do**
    Run BCS to obtain $\hat{\Sigma}_i$
    Estimate α_0 via equation A.1
    for Tx Candidate c_{Tx} **do**
      $w_{Tx,c_{Tx}} = 1$
      $w_{Tx} \otimes w_{Rx} = w_{Vx}$
      $w_{Vx} \rightarrow \mathbf{r}_{Vx}$
      Compute $\delta h_i(\mathbf{r}_c)$ for each candidate $\mathbf{r_c} \in R_{Vx}^{Tx}$
      Store $\max_{\mathbf{r}_c} \delta h_i \rightarrow \delta h_i^{Tx}$
      $w_{Tx,c_{Tx}} = 0$
    end for
    for Rx Candidate c_{Rx} **do**
      $w_{Rx,c_{Rx}} = 1$
      $w_{Tx} \otimes w_{Rx} = w_{Vx}$
      $w_{Vx} \rightarrow \mathbf{r}_{Vx}$
      Compute $\delta h_i(\mathbf{r}_c)$ for each candidate $\mathbf{r_c} \in R_{Vx}^{Rx}$
      Store $\max_{\mathbf{r}_c} \delta h_i \rightarrow \delta h_i^{Rx}$
      $w_{Rx,c_{Rx}} = 0$
    end for
  end for
  $\overline{\delta h}_{Tx} = \frac{1}{I}\sum_i^I \delta H_{r,i}$
  $\overline{\delta h}_{Rx} = \frac{1}{I}\sum_i^I \delta H_{r,i}$
  if $\max_i \overline{\delta h}_{Tx} \geq \max_i \overline{\delta h}_{Rx}$ **then**
    $w_{Tx,i} = 1$ for $i = \arg\max_i \overline{\delta h}_{Tx}$
  else
    $w_{Rx,i} = 1$ for $i = \arg\max_i \overline{\delta h}_{Rx}$
  end if
end while

B

COMPUTING DETECTIONS AND THE DETECTOR/ESTIMATOR METRICS

The RVM estimator returns a vector of coefficients, which ideally has only non-zero coefficients at the indices corresponding to DoAs with targets present. In reality, however, there might be more than those coefficients non-zero. By empirical investigation it has been observed, that in some cases the returned vector constitutes a rather discontinuous function when plotted over the angular domain, while in other cases there are more smooth slopes towards the present targets. This seems to be dependent upon a multitude of factors, including the noise level, the sparsity of the utilised array, and the parameters (a and b) that are input to the BCS algorithm (the latter two are described in more detail in the appendix C).

In chapter 2 it has been described how the complex valued radar data is expanded using equation 2.10 to fit the real valued RVM model. Consequently, the vector returned by the RVM follows this expansion and has to be reduced to obtain the correct DoA estimates. This is done as

$$\hat{\mathbf{x}}_{cplx} = (\hat{x}_1, \ldots, \hat{x}_G) + j\,(\hat{x}_{G+1}, \ldots, \hat{x}_{2G}) \in \mathbb{C} \tag{B.1}$$

where $\hat{x}_i$ denotes the i'th coefficient in $\hat{\mathbf{x}} \in \mathbb{R}$, which is the real valued output vector of the RVM abiding to the expansion shown in equation 2.10. Depending on whether the multi-task or single-task BCS is utilized, the RVM returns a vector $\hat{\mathbf{x}}_l \in \mathbb{R}$ for each of the L tasks (snapshots/chirps). After applying equation B.1, each $i'th$ coefficient estimate is averaged individually over all L tasks and then normalised as

$$\bar{x}_i = \frac{1}{L}\sum_{l}^{L} |x_{i,l}| \cdot \frac{1}{\max \bar{\mathbf{x}}} \tag{B.2}$$

To pick out the peaks in the resulting vector, the MATLAB function *findpeaks* is used, yielding point estimates for potential target locations. However, since there can also be

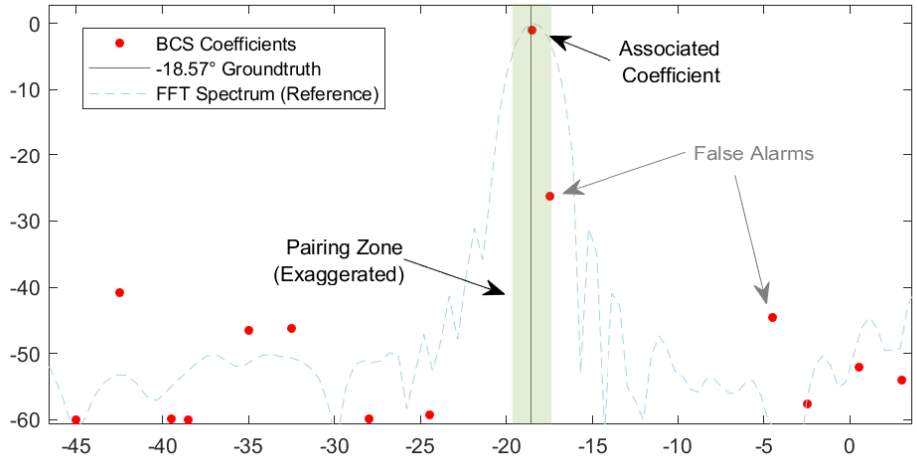

Figure B.1: Visualisation of the pairing radius around a ground truth. Note that the radius of this region is shown here as an exaggeration. In practice, it has been set to values of 1 and 2 degrees.

false non-zero coefficients, a thresholding must be applied. Finding the correct threshold can be a complicated task on its own. Therefore, an iterative procedure is applied, where a decreasing threshold is used and analysed via the Jaccard index and ROC curves (this is shown in detail in chapter 3). To obtain the metrics of true positives, false positives and false negatives, the known ground truth values are used. To this end, for each ground truth, a region of association is cut out from the estimates. This region can be defined as a user input. Within the cutout region, the estimate that is closest to the true value is paired with the ground truth and all others are retained for a possible next ground truth. At the end of the algorithm, all unpaired estimates are counted as false positives. Similarly, all ground truths for which no pairing estimate has been found in the defined region are counted as false negatives. This is shown with a visual example in figure B.1.

To calculate the RMSE of the angle estimate, only the paired estimates are used. This way it can happen, that the RMSE could be very good, while the detector performance is very bad (i.e. detecting only 1 out of 5 targets). It is therefore necessary to observe both the detection metrics and the RMSE (estimator metrics) when looking for a feasible level of array sparsity.

The equations used to compute the probability of detection, and the probability of false alarm are given as [97]:

$$P_D = \frac{TP}{TP+FN} \tag{B.3}$$

$$P_{FA} = \frac{FA}{FA+TN} \tag{B.4}$$

where TP is the number of true positives, FN the number of false negatives, FA the number of false alarms and TN the number of true negatives.

To access the estimation error in degrees, the Root Mean Square Error (RMSE) is computed for those estimates that have been paired to a ground truth (i.e. for valid true positives). Denoting the estimated target DoAs by the estimator $\hat{\theta}$ as $\hat{\theta}_i$, and the ground truth as θ_i, the RMSE is computed as:

$$\text{RMSE}(\hat{\theta}) = \sqrt{\text{MSE}(\hat{\theta})} = \sqrt{\frac{1}{TP}\sum_{i}^{TP}(\hat{\theta}_i - \theta_i)^2} \tag{B.5}$$

In the analysis of chapter 3, the RMSE metrics are shown for varying degrees of array sparsity on the x-axis. The computation of the RMSE at each array sparsity level, however, does not include the performance of detection in its calculation, leading to rather unusable RMSE values when only very few sensors are included in the array. This has to be kept in mind when looking at the RMSE.

C

RVM Parameter Selection

The multitask-BCS algorithm that has been proposed in [33] and is used in this thesis has two input parameters, besides the data and dictionary matrix. These parameters are related to the hyperparameters, which in turn control the hyperpriors in the algorithm (refer to chapter 2). For one of the hyperparameters, termed a, which is related to the signal variance, a data dependent expression is provided, and it can be set with knowledge of the standard deviation of the data [33]:

$$a = \frac{10^2}{\sigma^2_{data}} \tag{C.1}$$

However, this setting, as well as the b-parameter can also be set to zero, giving the algorithm no prior initialization and thus leading to so called *a priori ignorance* about the precisions of α [33]. Doing so, however, might result in coefficient vectors which have a lot of secondary coefficients with non-zero values. Increasing the b-parameter shows to suppress these other coefficients, leaving only the ones corresponding to the correct targets or highest energy. It has been observed in the case where only very few sensor elements are included in the utilised array, that initialising a with zero will cause the used BCS algorithm to not converge, and it will run for too many iterations. Therefore, although in theory no special initialisation for a and b should be needed, in the case of this thesis they have been initialised. In a practical array design application, the b-parameter could be fine-tuned to the selected level of array sparsity. For the a parameter, equation C.1 has been used.

For the b-parameter, however, there is no such direct equation provided. Therefore, an empirical search procedure has been conducted, which is described in the remainder of this section. Firstly, it is important to understand the influence this parameter has on the reconstruction algorithm. In the derivative steps of the algorithm in [33], the b-parameter is assigned to the *rate* parameter of the Gamma hyperprior, which is imposed on the hyperparameters α, representing the precision values of the zero-mean Gaussian prior imposed on the coefficients (the vector of DoA estimates, which should

be sparse). The rate parameter can be ascribed to the steepness of the Gamma distribution, relating it in a sense to the concentration of probability density. Increasing b leads to a more spiky Gamma distribution and, in turn, to the Gaussian prior being more concentrated around its mean for the corresponding α. From [31], this will let the algorithm remove the corresponding basis vector (i.e. the steering vector) from the model. In practice, it can be seen that when the parameter's value is increased, the non-zero coefficients which may contribute weaker to the reconstruction of the signal are more and more suppressed, leading to an increase in the sparsity of the resulting vector of weights (more coefficients are pushed to zero). To find a good value for the scenarios covered in this thesis, a sweep over a range of $b \in \{0, 1, \ldots, 50\} \equiv B$ has been computed. The MT-BCS algorithm has been run for different real-data target scenes for each value $b \in B$. As can be seen in figure C.1 in red, the RMSE of the reconstructed signal will increase as b is increased. This is according to the expectation, since also weaker coefficients have an influence to the total received signal by all antennas. However, as the interest lies not in the exact reconstruction of the signal that is received at the antennas, but rather in the main reflecting objects that correspond to the larger frequency coefficients, this loss might be tolerable. The RMSE is computed as the error between the original measurement vector y, and the reconstructed measurement vector $\hat{\mathbf{y}}$ using the estimate of the sparse coefficients vector $\hat{\mathbf{x}}$ as

$$\hat{\mathbf{y}} = A\hat{\mathbf{x}} \tag{C.2}$$

where A denotes the steering matrix (or generally the used basis matrix) and

$$\mathrm{RMSE}_y = \sqrt{\frac{\sum^N (\hat{y} - y)^2}{N}} \tag{C.3}$$

with N denoting the dimension of the signal vector $\mathbf{y}$, which is in this case the output of the sensor array at one range bin after the range FFT. The red plot in figure C.1 shows a factor of how sparse the vector of coefficients is, which is calculated as:

$$\mathrm{Sparsity} = \frac{card(\hat{\mathbf{x}})}{\dim \hat{\mathbf{x}}} \tag{C.4}$$

where $card(\hat{\mathbf{x}})$ denotes the cardinality of the coefficient-vector $\hat{\mathbf{x}}$ and $\dim \hat{\mathbf{x}}$ the dimension of $\hat{\mathbf{x}}$, i.e. the total number of coefficients.

By investigating different target scenes and different ranges of b, it has been found that often times the decrease in the sparsity factor becomes very small for larger b. Increasing b from there on does not seem to have a large influence on the algorithm's result. This is shown in figure C.2 for scenes with different numbers of targets present. Although both lines settle to a different value of sparsity, which is consistent with the expectation, as both depict different numbers of targets in the scene, they settle at their respective values at a similar b-value. It can be argued, that this parameter is able to influence the number of false alarms that will be present in the result of the BCS method. The higher this parameter is set, fewer coefficients besides the ones corresponding to the strongest targets will be non-zero, but the risk of eliminating weak targets is increased. It is therefore argued, that a non-zero value for this parameter can be desirable, but a too high value should be avoided as to not suppress real targets. Based on the study in this thesis and figure C.2, the b-Value is set to 25.

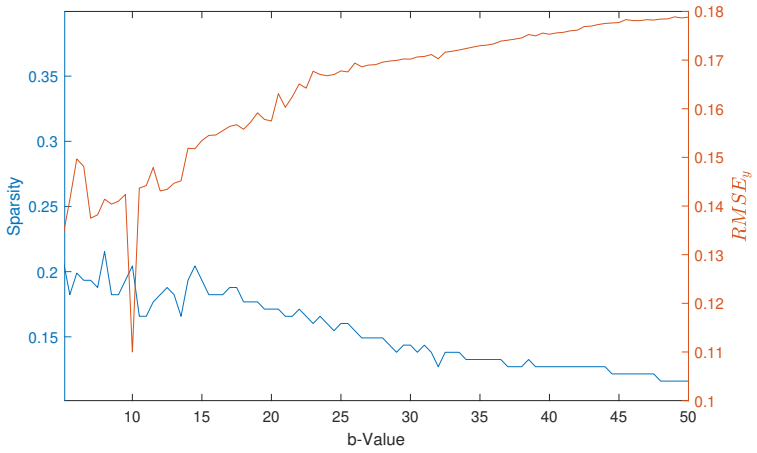

Figure C.1: Sparsity (blue) and reconstruction RMSE (red) for sweeping b-parameter.

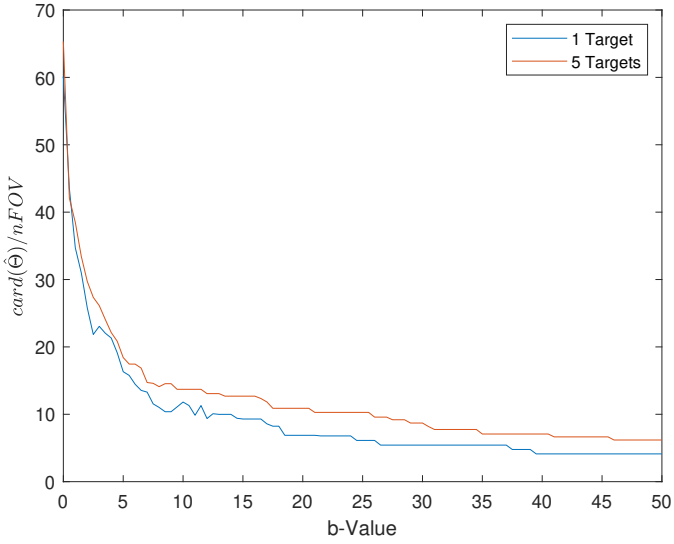

Figure C.2: Comparison of sparsity of the coefficients-vector with different target scenes

It has generally been observed, that the two parameters a and b have to be balanced against each other. Setting a very high initial value for a also requires higher values for b to suppress unwanted, non-zero coefficients and vice versa.

Based on the empirical study and the described considerations and effects of the discussed parameter, the value has been fixed to 25 for the processing of the measured data. This value appears to be a good setting that also works in cases where the utilised array is very sparse.

BIBLIOGRAPHY

[1] I. Bilik, O. Longman, S. Villeval, and J. Tabrikian, "The rise of radar for autonomous vehicles: Signal processing solutions and future research directions," *IEEE Signal Processing Magazine*, vol. 36, no. 5, pp. 20–31, 2019. DOI: 10.1109/MSP.2019.2926573.

[2] F. Engels, P. Heidenreich, A. M. Zoubir, F. K. Jondral, and M. Wintermantel, "Advances in automotive radar: A framework on computationally efficient high-resolution frequency estimation," *IEEE Signal Processing Magazine*, vol. 34, no. 2, pp. 36–46, 2017. DOI: 10.1109/MSP.2016.2637700.

[3] S. M. Patole, M. Torlak, D. Wang, and M. Ali, "Automotive radars: A review of signal processing techniques," *IEEE Signal Processing Magazine*, vol. 34, no. 2, pp. 22–35, 2017. DOI: 10.1109/MSP.2016.2628914.

[4] D. Malioutov, M. Çetin, and A. S. Willsky, "A sparse signal reconstruction perspective for source localization with sensor arrays," *IEEE Transactions on Signal Processing*, vol. 53, pp. 3010–3022, 8 2005, ISSN: 1053587X. DOI: 10.1109/TSP.2005.850882.

[5] M. Rossi, A. M. Haimovich, and Y. C. Eldar, "Spatial compressive sensing for mimo radar," *IEEE Transactions on Signal Processing*, vol. 62, pp. 419–430, 2 Jan. 2014, ISSN: 1053-587X. DOI: 10.1109/TSP.2013.2289875. [Online]. Available: http://ieeexplore.ieee.org/document/6657792/.

[6] S. Fortunati, R. Grasso, F. Gini, M. S. Greco, and K. LePage, "Single-snapshot doa estimation by using compressed sensing," *Eurasip Journal on Advances in Signal Processing*, vol. 2014, pp. 1–17, 1 2014, ISSN: 16876180. DOI: 10.1186/1687-6180-2014-120.

[7] V. K. Kukkala, J. Tunnell, S. Pasricha, and T. Bradley, "Advanced driver-assistance systems: A path toward autonomous vehicles," *IEEE Consumer Electronics Magazine*, vol. 7, no. 5, pp. 18–25, 2018. DOI: 10.1109/MCE.2018.2828440.

[8] H. Nyquist, "Certain topics in telegraph transmission theory," *Proceedings of the IEEE*, vol. 90, pp. 280–305, 2 2002, ISSN: 00189219. DOI: 10.1109/5.989875. [Online]. Available: http://ieeexplore.ieee.org/document/989875/.

[9] E. Candes and M. Wakin, "An introduction to compressive sampling," *IEEE Signal Processing Magazine*, vol. 25, pp. 21–30, 2 2008, ISSN: 1053-5888. DOI: 10.1109/msp.2007.914731.

[10] D. L. Donoho, "Compressed sensing," *IEEE Transactions on Information Theory*, vol. 52, pp. 1289–1306, 4 Apr. 2006, ISSN: 00189448. DOI: 10.1109/TIT.2006.871582.

[11] E. Candes, J. Romberg, and T. Tao, "Robust uncertainty principles: Exact signal reconstruction from highly incomplete frequency information," *IEEE Transactions on Information Theory*, vol. 52, pp. 489–509, 2 Feb. 2006, ISSN: 0018-9448. DOI: 10.1109/TIT.2005.862083. [Online]. Available: http://ieeexplore.ieee.org/document/1580791/.

[12] E. Candes and T. Tao, "Near optimal signal recovery from random projections: Universal encoding strategies?" 2006.

[13] D. L. Donoho and M. Elad, "Optimally sparse representation in general (nonorthogonal) dictionaries via l1 minimization," *Proceedings of the National Academy of Sciences of the United States of America*, vol. 100, pp. 2197–2202, 5 Mar. 2003, ISSN: 00278424. DOI: 10.1073/pnas.0437847100.

[14] "Chapter 11 - sparse methods for direction-of-arrival estimation," in *Academic Press Library in Signal Processing, Volume 7*, R. Chellappa and S. Theodoridis, Eds., Academic Press, 2018, pp. 509–581, ISBN: 978-0-12-811887-0. DOI: https://doi.org/10.1016/B978-0-12-811887-0.00011-0. [Online]. Available: https://www.sciencedirect.com/science/article/pii/B9780128118870000110.

[15] A. Massa, P. Rocca, and G. Oliveri, "Compressive sensing in electromagnetics - a review," *IEEE Antennas and Propagation Magazine*, vol. 57, pp. 224–238, 1 2015, ISSN: 10459243. DOI: 10.1109/MAP.2015.2397092.

[16] E. C. Marques, N. Maciel, L. Naviner, H. Cai, and J. Yang, "A review of sparse recovery algorithms," *IEEE Access*, vol. 7, pp. 1300–1322, 2019, ISSN: 21693536. DOI: 10.1109/ACCESS.2018.2886471.

[17] P. Rocca, M. A. Hannan, M. Salucci, and A. Massa, "Single-snapshot doa estimation in array antennas with mutual coupling through a multiscaling bcs strategy," *IEEE Transactions on Antennas and Propagation*, vol. 65, no. 6, pp. 3203–3213, 2017. DOI: 10.1109/TAP.2017.2684137.

[18] C.-Y. Chen and P. P. Vaidyanathan, "Compressed sensing in mimo radar," IEEE, Oct. 2008, pp. 41–44, ISBN: 978-1-4244-2940-0. DOI: 10.1109/ACSSC.2008.5074356.

[19] T. Strohmer and B. Friedlander, "Compressed sensing for mimo radar - algorithms and performance," IEEE, 2009, pp. 464–468, ISBN: 978-1-4244-5825-7. DOI: 10.1109/ACSSC.2009.5469862. [Online]. Available: http://ieeexplore.ieee.org/document/5469862/.

[20] M. Rossi, A. M. Haimovich, and Y. C. Eldar, "Global methods for compressive sensing in mimo radar with distributed sensors," 2011, pp. 1506–1510, ISBN: 9781467303231. DOI: 10.1109/ACSSC.2011.6190269.

[21] ——, "Spatial compressive sensing in mimo radar with random arrays," 2012, ISBN: 9781467331401. DOI: 10.1109/CISS.2012.6310839.

[22] J. Liu, C. Han, X. Yao, and F. Lian, "A novel coherence reduction method in compressed sensing for doa estimation," vol. 2013, pp. 1–9, 2013, ISSN: 1110-757X. DOI: 10.1155/2013/548979. [Online]. Available: http://www.hindawi.com/journals/jam/2013/548979/.

[23] S. Theodoridis, *Machine Learning: A Bayesian and Optimization Perspective*. May 2015, ISBN: 978-0128015223.

[24] D. J. C. MacKay, "Bayesian interpolation," *Neural Computation*, vol. 4, pp. 415–447, 3 1992, ISSN: 0899-7667. DOI: 10.1162/neco.1992.4.3.415.

[25] D. Wipf and S. Nagarajan, "A new view of automatic relevance determination," in *Advances in Neural Information Processing Systems*, J. Platt, D. Koller, Y. Singer, and S. Roweis, Eds., vol. 20, Curran Associates, Inc., 2007.

[26] M. E. Tipping, "The relevance vector machine," *Advances in Neural Information Processing Systems*, pp. 653–658, 2000, ISSN: 10495258.

[27] ——, "Sparse bayesian learning and the relevance vector machine," *Journal of Machine Learning Research*, vol. 1, pp. 211–244, 2001.

[28] S. Ji, Y. Xue, and L. Carin, "Bayesian compressive sensing," *IEEE Transactions on Signal Processing*, vol. 56, no. 6, pp. 2346–2356, 2008. DOI: 10.1109/TSP.2007.914345.

[29] S. D. Babacan, R. Molina, and A. K. Katsaggelos, "Bayesian compressive sensing using laplace priors," *IEEE Transactions on Image Processing*, vol. 19, pp. 53–63, 1 Jan. 2010, ISSN: 10577149. DOI: 10.1109/TIP.2009.2032894.

[30] A. Faul and T. Michael, "Analysis of sparse bayesian learning," Apr. 2002.

[31] M. E. Tipping, A. Faul, J. J. T. Avenue, and J. J. T. Avenue, "Fast marginal likelihood maximisation for sparse bayesian models," in *Proceedings of the Ninth International Workshop on Artificial Intelligence and Statistics*, 2003, pp. 3–6.

[32] M. Carlin and P. Rocca, "A bayesian compressive sensing strategy for direction-of-arrival estimation," in *2012 6th European Conference on Antennas and Propagation (EUCAP)*, 2012, pp. 1508–1509. DOI: 10.1109/EuCAP.2012.6206667.

[33] S. Ji, D. Dunson, and L. Carin, "Multitask compressive sensing," *IEEE Transactions on Signal Processing*, vol. 57, no. 1, pp. 92–106, 2009. DOI: 10.1109/TSP.2008.2005866.

[34] S. Ji and L. Carin, "Bayesian compressive sensing and projection optimization," *ACM International Conference Proceeding Series*, vol. 227, pp. 377–384, 1 2007. DOI: 10.1145/1273496.1273544.

[35] Q. Wu, Y. D. Zhang, M. G. Amin, and B. Himed, "Complex multitask bayesian compressive sensing," IEEE, May 2014, pp. 3375–3379, ISBN: 978-1-4799-2893-4. DOI: 10.1109/ICASSP.2014.6854226. [Online]. Available: http://ieeexplore.ieee.org/document/6854226/.

[36] S. Lei and W. Huali, "Direction-of-arrival estimation based on modified bayesian compressive sensing method," in *2011 International Conference on Wireless Communications and Signal Processing (WCSP)*, 2011, pp. 1–4. DOI: 10.1109/WCSP.2011.6096869.

[37] M. Carlin, P. Rocca, G. Oliveri, F. Viani, and A. Massa, "Directions-of-arrival estimation through bayesian compressive sensing strategies," *IEEE Transactions on Antennas and Propagation*, vol. 61, no. 7, pp. 3828–3838, 2013. DOI: 10.1109/TAP.2013.2256093.

C

[38] J. H. Ender, "On compressive sensing applied to radar," *Signal Processing*, vol. 90, pp. 1402–1414, 5 May 2010, ISSN: 01651684. DOI: 10.1016/j.sigpro.2009.11.009.

[39] M. Pastorino and A. Randazzo, "The svm-based smart antenna for estimation of the directions of arrival of electromagnetic waves," *IEEE Transactions on Instrumentation and Measurement*, vol. 55, pp. 1918–1925, 6 Dec. 2006, ISSN: 00189456. DOI: 10.1109/TIM.2006.884295.

[40] M. Carlin, P. Rocca, G. Oliveri, and A. Massa, "Multi-task bayesian compressive sensing for direction-of-arrival estimation," in *2012 IEEE International Conference on Wireless Information Technology and Systems (ICWITS)*, 2012, pp. 1–4. DOI: 10.1109/ICWITS.2012.6417819.

[41] Z. Yang, L. Xie, and C. Zhang, "Off-grid direction of arrival estimation using sparse bayesian inference," *IEEE Transactions on Signal Processing*, vol. 61, no. 1, pp. 38–43, 2013. DOI: 10.1109/TSP.2012.2222378.

[42] J. Dai, X. Bao, W. Xu, and C. Chang, "Root sparse bayesian learning for off-grid doa estimation," Aug. 2016. DOI: 10.1109/LSP.2016.2636319. [Online]. Available: http://arxiv.org/abs/1608.07188%20http://dx.doi.org/10.1109/LSP.2016.2636319.

[43] J. Dai and H. C. So, "Sparse bayesian learning approach for outlier-resistant direction-of-arrival estimation," *IEEE Transactions on Signal Processing*, vol. 66, pp. 744–756, 3 Feb. 2018, ISSN: 1053587X. DOI: 10.1109/TSP.2017.2773420.

[44] N. Hu, B. Sun, J. Wang, J. Dai, and C. Chang, "Source localization for sparse array using nonnegative sparse bayesian learning," *Signal Processing*, vol. 127, pp. 37–43, Oct. 2016, Proposed a nonnegative model as the weights are typically nonnegative, ISSN: 01651684. DOI: 10.1016/j.sigpro.2016.02.025.

[45] A. Moffet, "Minimum-redundancy linear arrays," *IEEE Transactions on Antennas and Propagation*, vol. 16, pp. 172–175, 2 Mar. 1968, ISSN: 0096-1973. DOI: 10.1109/TAP.1968.1139138. [Online]. Available: http://ieeexplore.ieee.org/document/1139138/.

[46] C.-Y. Chen and P. P. Vaidyanathan, "Minimum redundancy mimo radars," IEEE, May 2008, pp. 45–48, ISBN: 978-1-4244-1683-7. DOI: 10.1109/ISCAS.2008.4541350. [Online]. Available: http://ieeexplore.ieee.org/document/4541350/.

[47] P. P. Vaidyanathan and P. Pal, "Sparse sensing with co-prime samplers and arrays," *IEEE Transactions on Signal Processing*, vol. 59, pp. 573–586, 2 Feb. 2011, ISSN: 1053587X. DOI: 10.1109/TSP.2010.2089682.

[48] P. Pal and P. P. Vaidyanathan, "Nested arrays: A novel approach to array processing with enhanced degrees of freedom," *IEEE Transactions on Signal Processing*, vol. 58, pp. 4167–4181, 8 Aug. 2010, ISSN: 1053-587X. DOI: 10.1109/TSP.2010.2049264. [Online]. Available: http://ieeexplore.ieee.org/document/5456168/.

[49] A. Patwari, "Sparse linear antenna arrays: A review," *Antenna Systems [Working Title]*, Sep. 2021. DOI: 10.5772/intechopen.99444. [Online]. Available: https://www.intechopen.com/online-first/sparse-linear-antenna-arrays-a-review.

[50] S. Qin, Y. D. Zhang, and M. G. Amin, "Doa estimation of mixed coherent and uncorrelated targets exploiting coprime mimo radar," *Digital Signal Processing: A Review Journal*, vol. 61, pp. 26–34, Feb. 2017, ISSN: 10512004. DOI: 10.1016/j.dsp.2016.06.006.

[51] M. Wang and A. Nehorai, "Coarrays, music, and the cramér rao bound," May 2016. DOI: 10.1109/TSP.2016.2626255. [Online]. Available: http://arxiv.org/abs/1605.03620%20http://dx.doi.org/10.1109/TSP.2016.2626255.

[52] Y. Huang, G. Liao, J. Li, J. Li, and H. Wang, "Sum and difference coarray based mimo radar array optimization with its application for doa estimation," *Multidimensional Systems and Signal Processing*, vol. 28, pp. 1183–1202, 4 Oct. 2017, ISSN: 15730824. DOI: 10.1007/s11045-016-0387-2.

[53] S. Nannuru, P. Gerstoft, A. Koochakzadeh, and P. Pal, "Sparse bayesian learning for doa estimation using co-prime and nested arrays," vol. 2018-July, IEEE, Jul. 2018, pp. 519–523, ISBN: 978-1-5386-4752-3. DOI: 10.1109/SAM.2018.8448773. [Online]. Available: https://ieeexplore.ieee.org/document/8448773/.

[54] Q. Shen, W. Liu, W. Cui, and S. Wu, "Underdetermined doa estimation under the compressive sensing framework: A review," *IEEE Access*, vol. 4, pp. 8865–8878, 2016, ISSN: 21693536. DOI: 10.1109/ACCESS.2016.2628869.

[55] J. Yang, Y. Yang, G. Liao, and B. Lei, "A super-resolution direction of arrival estimation algorithm for coprime array via sparse bayesian learning inference," *Circuits, Systems, and Signal Processing*, vol. 37, pp. 1907–1934, 5 May 2018, ISSN: 15315878. DOI: 10.1007/s00034-017-0637-z.

[56] F. Chen, J. Dai, N. Hu, and Z. Ye, "Sparse bayesian learning for off-grid doa estimation with nested arrays," *Digital Signal Processing: A Review Journal*, vol. 82, pp. 187–193, Nov. 2018, ISSN: 10512004. DOI: 10.1016/j.dsp.2018.08.004.

[57] M. A. Hannan, N. Anselmi, G. Oliveri, and P. Rocca, "Joint doa and bandwidth estimation of unknown signals through single snapshot data and mt-bcs approach," in *2017 IEEE International Symposium on Antennas and Propagation USNC/URSI National Radio Science Meeting*, 2017, pp. 2389–2390. DOI: 10.1109/APUSNCURSINRSM.2017.8073237.

[58] M. A. Hannan, P. Rocca, and A. Massa, "Robust bcs-based direction-of-arrival and bandwidth estimation of unknown signals for cognitive radar," in *2018 IEEE International Symposium on Antennas and Propagation USNC/URSI National Radio Science Meeting*, 2018, pp. 625–626. DOI: 10.1109/APUSNCURSINRSM.2018.8608177.

[59] M. Carlin, P. Rocca, F. Viani, G. Oliveri, and A. Massa, "Multi-resolution bcs-based approach for doa estimation," in *2015 IEEE International Symposium on Antennas and Propagation USNC/URSI National Radio Science Meeting*, 2015, pp. 1074–1075. DOI: 10.1109/APS.2015.7304925.

C

[60] J. Liu, J. Wang, Z. Gao, and G. Hua, "Bayesian compressive sensing for target detection and parameter estimation using mimo radar," IEEE, Oct. 2017, pp. 1–3, ISBN: 978-1-5386-1608-6. DOI: 10.1109/APCAP.2017.8420652. [Online]. Available: https://ieeexplore.ieee.org/document/8420652/.

[61] B. Liu, B. Chen, M. Yang, and H. Xu, "Doa estimation using sparse bayesian learning for colocated mimo radar with dynamic waveforms," IEEE, Jun. 2020, pp. 1–4, ISBN: 978-1-7281-1946-5. DOI: 10.1109/SAM48682.2020.9104248. [Online]. Available: https://ieeexplore.ieee.org/document/9104248/.

[62] X. Wang, M. Huang, and G. Bi, "Sparse bayesian learning for doa estimation in mimo radar with unknown nonuniform noise," IEEE, Oct. 2016, pp. 1–5, ISBN: 978-1-5090-4828-1. DOI: 10.1109/RADAR.2016.8059247. [Online]. Available: http://ieeexplore.ieee.org/document/8059247/.

[63] T. Liu, F. Wen, L. Zhang, and K. Wang, "Off-grid doa estimation for colocated mimo radar via reduced-complexity sparse bayesian learning," *IEEE Access*, vol. 7, pp. 99 907–99 916, 2019, ISSN: 21693536. DOI: 10.1109/ACCESS.2019.2930531.

[64] J. Li, Y. He, L. He, and X. Zhang, "Dod and doa estimation for mimo radar based on combined music and sparse bayesian learning," IEEE, Aug. 2019, pp. 1–2, ISBN: 978-0-9960078-9-4. DOI: 10.23919/ACES48530.2019.9060555. [Online]. Available: https://ieeexplore.ieee.org/document/9060555/.

[65] Y. Arjoune, N. Kaabouch, H. E. Ghazi, and A. Tamtaoui, "A performance comparison of measurement matrices in compressive sensing," *International Journal of Communication Systems*, vol. 31, 10 Jul. 2018, ISSN: 10991131. DOI: 10.1002/dac.3576.

[66] L. Stankovic, D. P. Mandic, M. Dakovic, and I. Kisil, "Demystifying the coherence index in compressive sensing [lecture notes]," *IEEE Signal Processing Magazine*, vol. 37, pp. 152–162, 1 Jan. 2020, ISSN: 15580792. DOI: 10.1109/MSP.2019.2945080.

[67] M. Elad, "Optimized projections for compressed sensing," *IEEE Transactions on Signal Processing*, vol. 55, pp. 5695–5702, 12 Dec. 2007, ISSN: 1053587X. DOI: 10.1109/TSP.2007.900760.

[68] V. Abolghasemi, S. Ferdowsi, B. Makkiabadi, and S. Sanei, "On optimization of the measurement matrix for compressive sensing," 2010.

[69] T. Hong, X. Li, Z. Zhu, and Q. Li, "Optimized structured sparse sensing matrices for compressive sensing," Sep. 2017. [Online]. Available: http://arxiv.org/abs/1709.06895.

[70] K. Ardah, M. Pesavento, and M. Haardt, "A novel sensing matrix design for compressed sensing via mutual coherence minimization," Institute of Electrical and Electronics Engineers Inc., Dec. 2019, pp. 66–70, ISBN: 9781728155494. DOI: 10.1109/CAMSAP45676.2019.9022467.

[71] F. Roos, P. Hugler, L. L. T. Torres, *et al.*, "Compressed sensing based single snapshot doa estimation for sparse mimo radar arrays," IEEE, Mar. 2019, pp. 75–78, ISBN: 978-3-9812668-9-4. DOI: 10.23919/GEMIC.2019.8698136. [Online]. Available: https://ieeexplore.ieee.org/document/8698136/.

[72] A. Ajorloo, A. Amini, E. Tohidi, M. H. Bastani, and G. Leus, "Antenna placement in a compressive sensing-based colocated mimo radar," *IEEE Transactions on Aerospace and Electronic Systems*, vol. 56, pp. 4606–4614, 6 Dec. 2020, ISSN: 15579603. DOI: 10.1109/TAES.2020.2998196.

[73] M. F. Duarte and Y. C. Eldar, "Structured compressed sensing: From theory to applications," Jun. 2011. DOI: 10.1109/TSP.2011.2161982. [Online]. Available: http://arxiv.org/abs/1106.6224%20http://dx.doi.org/10.1109/TSP.2011.2161982.

[74] M. Courcoux-Caro, C. Vanwynsberghe, C. Herzet, and A. Baussard, "Sequential sensor placement using bayesian compressed sensing for source localization," IEEE, Jan. 2021, pp. 241–245, ISBN: 978-9-0827-9705-3. DOI: 10.23919/Eusipco47968.2020.9287709. [Online]. Available: https://ieeexplore.ieee.org/document/9287709/.

[75] M. W. Seeger, "Bayesian inference and optimal design for the sparse linear model," 2008, pp. 759–813.

[76] M. W. Seeger and H. Nickisch, "Compressed sensing and bayesian experimental design," ACM Press, 2008, pp. 912–919, ISBN: 9781605582054. DOI: 10.1145/1390156.1390271. [Online]. Available: http://portal.acm.org/citation.cfm?doid=1390156.1390271.

[77] P. Ren, Y. Xiao, X. Chang, *et al.*, "A survey of deep active learning," *ACM Comput. Surv.*, vol. 54, no. 9, Oct. 2021, ISSN: 0360-0300. DOI: 10.1145/3472291. [Online]. Available: https://doi.org/10.1145/3472291.

[78] K. Chaloner and I. Verdinelli, "Bayesian experimental design: A review," *Statistical Science*, vol. 10, 3 Aug. 1995, ISSN: 0883-4237. DOI: 10.1214/ss/1177009939. [Online]. Available: https://projecteuclid.org/journals/statistical-science/volume-10/issue-3/Bayesian-Experimental-Design-A-Review/10.1214/ss/1177009939.full.

[79] P.-J. Chung, M. Viberg, and J. Yu, "Chapter 14 - doa estimation methods and algorithms," in *Academic Press Library in Signal Processing: Volume 3*, ser. Academic Press Library in Signal Processing, A. M. Zoubir, M. Viberg, R. Chellappa, and S. Theodoridis, Eds., vol. 3, Elsevier, 2014, pp. 599–650. DOI: https://doi.org/10.1016/B978-0-12-411597-2.00014-X. [Online]. Available: https://www.sciencedirect.com/science/article/pii/B978012411597200014X.

[80] S. Sun, A. P. Petropulu, and H. V. Poor, "Mimo radar for advanced driver-assistance systems and autonomous driving: Advantages and challenges," *IEEE Signal Processing Magazine*, vol. 37, pp. 98–117, 4 Jul. 2020, ISSN: 15580792. DOI: 10.1109/MSP.2020.2978507.

[81] F. Ulaby, D. Long, W. Blackwell, *et al.*, *Microwave Radar and Radiometric Remote Sensing*. Jan. 2014, ISBN: 978-0-472-11935-6.

[82] M. Jankiraman, *FMCW Radar Design*, ser. Artech House radar library. Artech House, 2018, ISBN: 9781630815691. [Online]. Available: https://books.google.nl/books?id=cfF5DwAAQBAJ.

[83] S. Xu, "Joint parameters estimation using fmcw uwb waveform," 2020. DOI: https://doi.org/10.4233/uuid:f9ce79b1-7890-41b4-850b-134dcfbef52e.

[84] K. W. Forsythe and D. W. Bliss, "Mimo radar: Concepts, performance enhancements, and applications," in *MIMO Radar Signal Processing*. John Wiley & Sons, Ltd, 2008, ch. 2, pp. 65–121, ISBN: 9780470391488. DOI: https://doi.org/10.1002/9780470391488.ch2. eprint: https://onlinelibrary.wiley.com/doi/pdf/10.1002/9780470391488.ch2. [Online]. Available: https://onlinelibrary.wiley.com/doi/abs/10.1002/9780470391488.ch2.

[85] F. Robey, S. Coutts, D. Weikle, J. McHarg, and K. Cuomo, "Mimo radar theory and experimental results," in *Conference Record of the Thirty-Eighth Asilomar Conference on Signals, Systems and Computers, 2004.*, vol. 1, 2004, 300–304 Vol.1. DOI: 10.1109/ACSSC.2004.1399141.

[86] H. E. A. Laue, "Demystifying compressive sensing [lecture notes]," *IEEE Signal Processing Magazine*, vol. 34, pp. 171–176, 4 Jul. 2017, ISSN: 10535888. DOI: 10.1109/MSP.2017.2693649.

[87] R. G. Baraniuk, "Compressive sensing [lecture notes]," 2007.

[88] S. Foucart, "A note on guaranteed sparse recovery via l1-minimization," *Applied and Computational Harmonic Analysis*, vol. 29, pp. 97–103, 1 2010, ISSN: 1096603X. DOI: 10.1016/j.acha.2009.10.004.

[89] D. J. C. MacKay, "Bayesian interpolation," *Neural Computation*, vol. 4, pp. 415–447, 3 1992, ISSN: 0899-7667. DOI: 10.1162/neco.1992.4.3.415.

[90] T. M. Cover and J. A. Thomas, *Elements of Information Theory (Wiley Series in Telecommunications and Signal Processing)*. USA: Wiley-Interscience, 2006, ISBN: 0471241954.

[91] S. L. Brunton and J. N. Kutz, *Data-Driven Science and Engineering: Machine Learning, Dynamical Systems, and Control*, 1st. USA: Cambridge University Press, 2019, ISBN: 1108422098.

[92] D. Lay, L. S.R., and M. J.J., *Linear Algebra and Its Applications*. Pearson, 2016, ISBN: 9781292092232.

[93] D. J. C. MacKay, "Information-based objective functions for active data selection," *Neural Computation*, vol. 4, no. 4, pp. 590–604, 1992. DOI: 10.1162/neco.1992.4.4.590.

[94] M. H. Hayes, *Statistical Digital Signal Processing and Modeling*, 1st. USA: John Wiley; Sons, Inc., 1996, ISBN: 0471594318.

[95] *Awr2243 single-chip 76- to 81-ghz fmcw transceiver*, SWRS223B, Rev. 2021, Texas Instruments, Dec. 2020.

[96] *Awr2243 cascade*, SWRA574B, Rev. 2020, Texas Instruments, Oct. 2014.

[97] A. Géron, *Hands-on machine learning with Scikit-Learn and TensorFlow : concepts, tools, and techniques to build intelligent systems.* Sebastopol, CA: O'Reilly Media, 2017, ISBN: 978-1491962299.